ABSTRACT

Title of Document: AN OPTOFLUIDIC SURFACE ENHANCED RAMAN SPECTROSCOPY MICROSYSTEM FOR SENSITIVE DETECTION OF CHEMICAL AND BIOLOGICAL MOLECULES

Soroush Hossein Yazdi, Doctor of Philosophy, 2013

Directed By: Professor Ian M. White, Fischell Department of Bioengineering

As the human population grows, there is an increasing demand for early detection of a variety of analytes in different fields. This demand mainly includes early and sensitive detection of pathogens, disease biomarkers, pesticides, food contaminants, and explosives. To address this, lab-on-a-chip (LOC) technology has emerged as a tool to improve portability, automation and sensitivity of sensors by taking advantage of integrated laboratory functions on a miniaturized chip. It is agreed that LOC has the potential to make various sensing modules practical for real-world applications.

In this work, we have developed a highly sensitive, portable, and automated optofluidic surface enhanced Raman spectroscopy (SERS) microsystem for chemical and biological detection. SERS is a powerful molecular identification technique that combines laser spectroscopy with optical properties of metal nanoparticles. Optofluidic SERS is defined as the synergistic use of microfluidic functions to

improve the performance of SERS. By leveraging microfluidic functions, the optofluidic SERS microsystem mixes and concentrates the sample and nanoparticles resulting in an improved performance as compared to conventional open microfluidic SERS systems. The device requires low sample volume and has multiplexed detection capabilities. Moreover, it is suitable for on-site detection of analytes in the field because of its improved automation and portability due to the integrated fiber optics.

The final device consists of two regions of packed silica beads inside microchannels for biomolecular interaction as well as sample concentration for SERS measurements. Additionally, an on-chip micromixer and fiber optics are integrated into the device. Optical fibers aligned to the detection zone make the biosensor alignment-free, which greatly improves automation. Practical applications for the detection of real-world analytes (e.g., pesticides, fungicides, food contaminants, and DNA sequences) are demonstrated utilizing our optofluidic SERS microsystem. Detection of biological samples could be extended to proteins and proteolytic enzymes through displacement assays.

Consequently, the integration of microfluidic functions, including a microporous reaction zone, a nanoparticle concentration zone, and a micromixer, combined with the use of integrated fiber optics and portable spectrometers, make our microsystem suitable for on-site detection of analytes at trace levels.

AN OPTOFLUIDIC SURFACE ENHANCED RAMAN SPECTROSCOPY MICROSYSTEM FOR SENSITIVE DETECTION OF CHEMICAL AND BIOLOGICAL MOLECULES

By

Soroush Hossein Yazdi

Dissertation submitted to the Faculty of the Graduate School of the
University of Maryland, College Park, in partial fulfillment
of the requirements for the degree of
Doctor of Philosophy
2013

Advisory Committee:
Professor Ian White, Chair
Professor Yu Chen
Professor Don DeVoe
Professor Peter Kofinas
Professor Miao Yu

Dedication

I dedicate my dissertation to my parents and sister.

Acknowledgements

I would like to express my deepest appreciation to my advisor, Dr. Ian White, for his excellent guidance, motivation, and knowledge. I could not have imagined having a better advisor and mentor for my Ph.D. study.

I would like to thank my committee members for their kind guidance and insightful feedbacks.

Many thanks to my labmates at Photonics Biosensing lab for all the helps and good times.

I would like to thank all my friends at Maryland, Washington DC, and Virginia for the good memories during the last four years.

Last but not the least, I would like to thank my family for always being there for me.

Table of Contents

DEDICATION II

ACKNOWLEDGEMENTS III

LIST OF FIGURES VI

CHAPTER 1: INTRODUCTION 1
1.1 MOTIVATION: NEED FOR A SENSITIVE, PORTABLE, AND AUTOMATED SENSING PLATFORM 1

CHAPTER 2: CURRENT TRENDS IN RAMAN SPECTROSCOPY: FROM RAMAN SCATTERING TO OPTOFLUIDIC SERS 5
2.1 RAMAN SCATTERING 5
2.2 SURFACE ENHANCED RAMAN SPECTROSCOPY (SERS) 8
2.3 SURFACE ENHANCED RESONANCE RAMAN SCATTERING (SERRS) 12
2.4 OPTOFLUIDIC MICROSYSTEMS FOR DETECTION OF CHEMICAL AND BIOLOGICAL MOLECULES 14
2.5 OPTOFLUIDIC SERS: SYNERGIZING SERS AND MICROFLUIDICS FOR CHEMICAL AND BIOLOGICAL ANALYSIS 19
2.6 IMPROVING THE PERFORMANCE OF SERS MICROSYSTEMS WITH OPTOFLUIDICS 26
2.6.1 Photonic Crystal Waveguides for Optofluidic SERS 26
2.6.2 Concentration with Active Microfluidic Techniques 28
2.6.3 Concentration with Passive Micro/Nanofluidic Techniques 31
2.6.4 Three-dimensional Micro/Nanofluidic SERS Substrates 32
2.6.5 SERS Excitation by Optofluidic Resonators 35
2.7 SUMMARY 36

CHAPTER 3: A POROUS OPTOFLUIDIC MICROSYSTEM FOR HIGHLY SENSITIVE AND REPEATABLE SERS DETECTION 38
3.1 INTRODUCTION 38
3.2 EXPERIMENTAL SECTION 40
3.2.1 Materials 40
3.2.2 Preparation of Silver Colloid 41
3.2.3 Fabrication of the Optofluidic Device 42
3.2.4 Scanning Electron Microscopy 44
3.2.5 SERS Measurements 44
3.3 RESULTS AND DISCUSSION 45
3.4 CONCLUSION 51

CHAPTER 4: MULTIPLEXED DETECTION OF AQUACULTURE FUNGICIDES USING A PUMP-FREE OPTOFLUIDIC SERS MICROSYSTEM 52
4.1 INTRODUCTION 52
4.2 EXPERIMENTAL 54
4.2.1 Device Fabrication 54
4.2.2 Silver Nanoparticle Synthesis 55
4.2.3 SERS Measurements 55
4.3 RESULTS 56
4.4 CONCLUSION 60

CHAPTER 5: AN OPTOFLUIDIC SURFACE ENHANCED RAMAN SPECTROSCOPY MICROSYSTEM INTEGRATED WITH AN ON-CHIP MICROMIXER 62
5.1 INTRODUCTION 62
5.2 EXPERIMENTAL SECTION 68
5.2.1 Preparation of Silver Nanoparticles 68
5.2.2 Micromixer Design and Simulation 68
5.2.3 Thiol-Modification of Silica Microspheres 69
5.2.4 Fabrication of the Optofluidic Device 69
5.2.5 SERS Measurements 71
5.3 RESULTS 72
5.4 CONCLUSION 80

CHAPTER 6: MULTIPLEXED DETECTION OF DNA SEQUENCES USING A COMPETITIVE DISPLACEMENT ASSAY IN AN OPTOFLUIDIC SERRS-BASED MICROSYSTEM 82
6.1 INTRODUCTION 82
6.2 EXPERIMENTAL SECTION 89
6.2.1 Preparation of Silver Colloid 89
6.2.2 Preparation of DNA-functionalized Chitosan-silica Beads 89
6.2.3 Verification of DNA Hybridization and Competitive Displacement 93
6.2.4 Optimizing the Number of Matching Bases Between DNA Probe and DNA Reporter 93
6.2.5 Fabrication of the Optofluidic Device 94
6.2.6 Thiol-Modification of Silica Beads 95
6.2.7 SERRS Measurements 96
6.2.8 Multiplexed Detection using SERRS and Competitive Displacement 96
6.3 RESULTS 97
6.3.1 Analysis of DNA Competitive Displacement 97
6.3.2 Optofluidic SERRS Detection with Competitive Displacement 100
6.3.3 Multiplexed Detection with the Competitive Displacement SERRS Assay 102
6.4 CONCLUSION 104

CHAPTER 7: CONCLUSION 106
7.1 SUMMARY 106
7.2 CONTRIBUTIONS TO THE FIELD 108
7.3 FUTURE WORK 110

BIBLIOGRAPHY 112

List of Figures

Figure 1.1 The schematic of the final optofluidic SERS microsystem for biological molecules detection 3

Figure 2.1 When incident photons hit a molecule, the majority of the scattered photons stay in the same wavelength, however, a very small portion undergo shift in their energy and wavelength which is called Raman scattering 5

Figure 2.2 The scattered photon has no exchange of energy in case of Rayleigh scattering, while in Raman scattering molecule either gains or loses energy to photons. 6

Figure 2.3 (a) Excitation of surface plasmons on metal nanoparticles due to electric field excitation (b) SEM image of aggregated silver nanoparticles. 9

Figure 2.4 Effect of spacing between two silver nanospheres forming a dimer on the magnitude of the electric field as a ratio of the incident electric field. Evaluations were carried out using FDTD simulations and Analytical Calculations using the multipole expansion method. Reproduced from Dhawan et al.[18] with permission from The Optical Society of America 10

Figure 2.5 SERS spectrum of Rhodamine 6G molecule 12

Figuire 2.6 (a) SEM image of an optofluidic ring-resonator (OFRR) cross section with an outer radius of 50 μm. (b) The experimental setup of the OFRR and a tapered fiber optic of 4μm in diameter. Reproduced from White et al.[82] with permission from the Optical Society of America 16

Figure 2.7 (A) Optofluidic device and experimental setup schematic for virus detection. Arrows represent direction of excitation and emission inside the ARROW waveguides; (B) solid-core ARROW waveguide; (C) liquid-core waveguide; (D) photograph of the ARROW biosensor. Reproduced from Rudenko et al.[94] with permission from Elsevier 18

Figure 2.8 (a) In conventional SERS, a sample droplet is dried onto a SERS-active substrate; target analyte molecules are concentrated onto the substrate after drying. (b) In one form of microfluidic SERS, analyte molecules are mixed with a solution of nanoparticles and passed through a microfluidic channel under laser illumination. (c) In another form of microfluidic SERS, a SERS-active substrate is incorporated as the bottom of a microfluidic channel. In b and c, the density of target analyte molecules adsorbed at SERS-active locations within the SERS detection region is much lower compared with conventional SERS techniques 23

Figure 2.9 Increasing N (Eq. 1) by extending the detection volume. (a) Photonic crystal structures can be used to confine and guide light along a microfluidic channel. (b) Excitation light guided along with the sample in the hollow core of a PCF, as in Yang et al. 2010. (c) Excitation light guided in the solid core of a PCF, such that the evanescent field interacts with the sample, as in Khaing Oo et al. 2010 27

Figure 2.10 Increasing N (Eq. 1) by concentrating the number of analyte molecules adsorbed to SERS-active hot spots in the detection volume. (a) Electro-active concentration of analyte molecules at a SERS-active surface, as in Cho et al. 2009. (b) Concentration of silver nanoparticles and analyte molecules using a nanofluidic channel. Reprinted from Wang et al. 2009. (c) Microhole array for "flow-through" optofluidic SERS. Reprinted with permission from Guo et al.[122], Copyright 2012, American Chemical Society 29

Figure 3.1 Nanofluidic trapping vs. open-channel microfluidics. (a) In an open channel, nanoparticles are poorly concentrated. (b) A nanochannel traps silver nanoparticles (Ag NPs) into the detection volume. (c) Packed silica spheres form a nanofluidic matrix, which is capable of trapping a high number of Ag NPs into a relatively large detection volume without clogging. An optical fiber can be aligned to the nanoporous matrix. 39

Figure 3.2 (a) Micrograph showing packed microspheres and integrated fiber optic cables. (b) Silver nanoparticles (AgNPs) are trapped in the silica microsphere matrix. (c) Excitation and collection is performed by integrated fiber optic cables. (d) Experimental setup: the sample is loaded with a syringe pump. The fiber optic cables are connected to a diode laser and a Raman spectrometer. 43

Figure 3.3 SEM micrograph of the silica microspheres packed into the microfluidic channel after running silver nanoclusters through the channel. The bright spots on the silica spheres are silver nanoclusters that became trapped in the matrix. 45

Figure 3.4 Time-dependent accumulation of SERS signal as silver nanoparticles with adsorbed R6G are trapped and concentrated within the nanofluidic matrix. R6G concentration in colloid=100 nM. Spectra are shifted vertically for visual clarity. 46

Figure 3.5 Within the nanoporous matrix, the SERS signal is greater than 250 times more intense as compared to the open channel. R6G concentration in colloid=100nM. 47

Figure 3.6 (a) Mean intensity of the 1509 cm^{-1} Raman peak for various R6G concentrations. Error bars represent standard deviation, N=3. (b) Measured SERS signal after 4 µl of 100 pM R6G (400 attomoles) is loaded into the microchannel. 48

Figure 3.7 Recorded SERS spectra for greater than 145 ppm malathion in water (the solubility limit) in an open microfluidic channel and for 12 ppb malathion in water in the 3D nanofluidic channel. Arrows indicate the Raman peaks for malathion. The background signal is also shown to enable the clear identification of the malathion Raman peaks. 50

Figure 4.1 Concept of the pump-free optofluidic SERS device. Negative pressure from a pipette draws the sample into the channel. Packed silica microspheres trap and concentrate AgNPs and adsorbed analytes. Integrated fiber optic cables eliminate the need for a microscope. 53

Figure 4.2 Representative SERS spectra acquired when loading R6G samples either by pipette or syringe pump. Error bars represent the standard deviation of the intensity of the peaks. Spectra are shifted vertically for clarity. 57

Figure 4.3 SERS spectra of (a) 50 ppb malachite green, (b) 10 ppm methyl parathion, (c) 50 ppb thiram. 58

Figure 4.4 Multiplexed SERS spectrum of 0.1 ppb malachite green oxalate (■), 5 ppm methyl parathion (△), and 5 ppb thiram 60

Figure 5.1 Optofluidic SERS microsystem with packed microspheres for passive concentration, an integrated micromixer to promote adsorption of the target analyte, and integrated fiber optic cables for optical excitation and collection. 64

Figure 5.2 (a) Schematic of optofluidic SERS microsystem. (b) Photo of optofluidic SERS microsystem. (c) Micrograph of packed microspheres and integrated fiber optic cables. 70

Figure 5.3 COMSOL simulation results, demonstrating that AgNPs are completely mixed throughout the microfluidic mixer within 8 mm, while for a straight channel mixing of the AgNPs does not occur. 73

Figure 5.4 Micrograph verifying the mixing of AgNPs with the sample. At the inlet (1), the discrete separation of the two flows is evident, while at (4), after 8 mm in the channel, the AgNPs are mixed throughout the channel. 74

Figure 5.5 Comparison of the SERS signal acquired for R6G when off-chip mixing and on-chip mixing are used. 75

Figure 5.6 Detection of melamine in the optofluidic SERS microsystem. (a) Acquired SERS spectra for 125, 12.5, and 1.25 ppm melamine. (b) Acquired spectra for 125 ppb melamine. (c) Height of the 690 cm^{-1} Raman peak vs melamine concentration. Data points represent the average of three trials while the error bars represent the standard deviation. 76

Figure 5.7 Comparison of melamine detection in an open channel (12.5 ppm) and in the packed silica microsphere (125 ppb) detection region. The passive concentration improves the detection limit by 2 orders of magnitude. 77

Figure 5.8 Detection of thiram in the optofluidic SERS microsystem. (a) Acquired SERS spectra for 1 ppm, 100 ppb, 10 ppb, and 1 ppb thiram. (b) Acquired spectra for 1 ppb thiram. (c) Height of the 1380 cm^{-1} Raman peak vs thiram concentration. Data points represent the average of three trials while the error bars represent the standard deviation. 79

Figure 5.9 SERS spectrum of 8 ppb thiram recorded with a portable spectrometer 80

Figure 6.1 Competitive displacement assay concept. Probes hybridized to reporter molecules (with an attached Raman label) are immobilized onto the substrate. The reporter is designed to hybridize to the probe, but with lower affinity than the target, thus enabling the target to displace the reporter. The displaced reporter sequence then flows to the SER(R)S detection region. 86

Figure 6.2 Optofluidic SERRS microsystem with integrated competitive displacement for DNA sequence detection. Silica microspheres functionalized with DNA probe-reporter pairs (inset) are packed against a frit. When the target sequence is introduced at the inlet, Raman-labeled reporter oligos are displaced. As they flow along the channel, they are mixed with metal nanoclusters and trapped in the optofluidic SERRS detection region 87

Figure 6.3 (A) Au colloid (pH=3.5) (B) Au colloid after adding CS-silica beads (pH=3.5) (C) Au colloid after adjusting pH to 9 and then adding CS-silica beads 91

Figure 6.4 Effect of DNA probe concentration on DNA reporter hybridization (DNA reporter concentration = 10 μM). DNA probe concentration; (A) 0 μM (B) 1 μM (C) 10 μM (D) 50 μM (E) 100 μM. 92

Figure 6.5 Fluorescence microscopy images of probe-functionalized microspheres to analyze the competitive displacement for varying probe-reporter affinities. Higher fluorescence in the left column indicates increased hybridization between probe and reporter; lower fluorescence in the right column indicates higher displacement of reporter by the target sequence 98

Figure 6.6 Quantified fluorescence from microspheres for the three probe-reporter-target systems. The use of Probe 2, which has a 12-base match with the reporter and a 17-base match with the target, generates the highest contrast due to displacement while also exhibiting strong probe-reporter hybridization. Thus, Probe 2 is selected for the SERRS measurements. 99

Figure 6.7 Addition of nitric acid promotes interaction between the TAMRA-labeled reporter and the metal nanostructures, enabling the SERS spectrum of TAMRA to be observed. 100

Figure 6.8 (A) Net intensity of the 1650 cm^{-1} SERRS peak for various DNA target sequence concentrations. Error bars represent the standard deviation of three trials. The data is fit to a Langmuir isotherm. (B) The TAMRA SERRS signal is easily observed, even with only 100 pM target DNA. When adding 100 nM non-matching DNA, no signal is observed. 101

Figure 6.9 Multiplexed detection of target DNA sequences using competitive displacement in the optofluidic SERRS microsystem when 100 nM of each target sequence is added. Triangle = TAMRA; Plus = R6G. 103

Chapter 1: Introduction

1.1 Motivation: Need for a Sensitive, Portable, and Automated Sensing Platform

Point-of-care and point-of-sample systems are needed for fast, multiplexed and highly sensitive detection of analytes in different fields. Rapid detection of contaminants and biomarkers permits fast and proper treatment of patients, limits the transmission of disease and contamination in the population, and minimizes the waste of public resources on ineffective treatments. Lab-on-a-chip systems allow miniaturization and integration of complex laboratory functions, which could move sophisticated diagnostic tools out of the laboratory. These systems result in fast, sensitive, reliable, and simple-to-operate diagnostic sensors. LOC systems can be used to analyze small volumes of complex fluids, and without the need for an expert operator.[1,2]

Current solutions for molecular diagnosis are mainly based on immunoassay (e.g., ELISA) and nucleic acid techniques (PCR). While highly sensitive, these methods are laborious, time-consuming, and require trained experts and sophisticated lab settings; hence, they are not appropriate for fast and on-site detection. Moreover, multiplexed detection of analytes, which is usually required for accurate and complete diagnosis, is limited due to the detection mechanism and the need for complicated optical settings. However, surface enhanced Raman spectroscopy (SERS) allows highly sensitive detection of biological molecules with detection limits comparable to fluorescence detection. At the same time, multiplexed detection of the analytes can be achieved using a single laser source and filter set.

In addition, although mass spectrometry-based detection systems are highly sensitive for multiplexed detection of small molecules, they have limitations in terms of portability, cost, and the need for trained staff. SERS-based detection techniques have the potential to become miniaturized and portable while retaining the ease of use, high sensitivity, and multiplexing capabilities of SERS.

Surface enhanced Raman spectroscopy is an excellent alternative to ELISA and mass spectrometry as the sensing mechanism. SERS is a chemical sensing technique that offers sensitivity comparable to that of fluorescence detection. At the same time, it is highly specific to molecular vibrations and chemical bonds within an analyte molecule and can uniquely identify the molecule in a sample.

Herein, we have developed a porous optofluidic SERS-based sensor to perform portable, automated, multiplexed, and highly sensitive detection of various types of analytes. Our device's capability to perform sensitive and on-site detection is enabled by the integration of microfluidic functions as well as surface enhanced Raman spectroscopy (SERS). The SERS detection mechanism is well-known for its high sensitivity and specificity and has the potential to be made practical by integrating it with on-chip lab functions and portable detection equipment. Another interesting advantage of SERS is its capability of performing multiplexed detection with a simple optical configuration as opposed to fluorescence-based detection.

Our final device consists of three major on-chip lab functions integrated onto a chip of a few square centimeters in area as it shown in Figure 1.1: 1) 3D porous matrix for biological reactions, 2) on-chip micromixer for mixing analytes and metal nanoparticles, and 3) 3D porous detection zone for improved SERS signal collection.

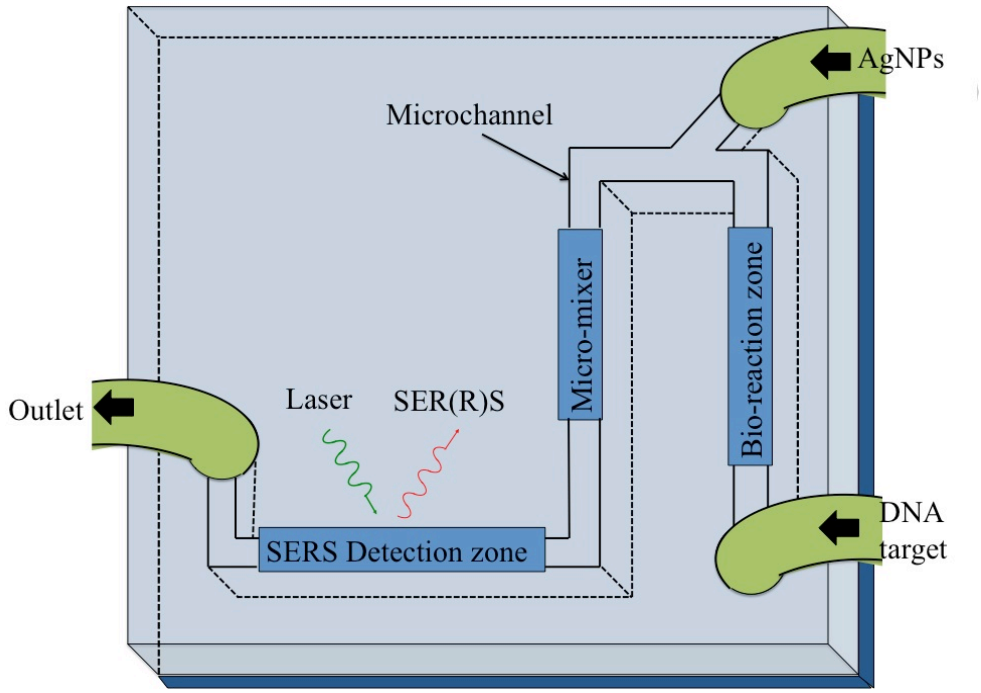

Figure 1.1 The schematic of the final optofluidic SERS microsystem for biological molecules detection

Detection of several chemicals and biological samples is presented in this work. Our optofluidic SERS microsystem is capable of performing sensitive detection of a variety of pesticides, fungicides, and food contaminants. Biomolecule detection is achieved thorough a competitive displacement assay. To demonstrate this concept, we have utilized the optofluidic SERS sensor to detect target DNA sequences through competitive displacement hybridization. Additionally, the device has the potential to perform multiplexed detection of proteins and proteolytic enzymes.

The combination of the optofluidic SERS device with a portable laser diode and spectrometer could lead to the development of a sensitive system for on-site detection.

The results of this dissertation to develop a sensitive, portable, and automated optofluidic SERS sensor are categorized in the following chapters; In chapter 2, an

overview on Raman scattering, SERS, resonance SERS (SERRS), and optofluidic SERS is presented. In chapter 3, we demonstrate the use of the porous optofluidic SERS device for sensitive detection of a variety of analytes. In chapter 4, the concept of a pump-less optofluidic SERS device is presented by multiplexed detection of aquaculture fungicides. A more automated porous optofluidic microsystem utilizing an integrated on-chip micromixer is examined in chapter 5. In chapter 6, biological sample detection is presented through competitive displacement assay by adding a bio-reaction zone to the device. Finally, chapter 7 discusses conclusions, contributions to the field and the future work.

Chapter 2: Current Trends in Raman Spectroscopy: from Raman Scattering to Optofluidic SERS

In this chapter, we will overview Raman scattering and how metal nanoparticles/nanostructures enhance the scattering to generate a SERS signal. Resonance SERS will be also described. Finally, recent developments in optofluidic SERS will be discussed.

2.1 Raman Scattering

As shown in Figure 2.1, when photons from a laser source with a specific frequency hit a molecule, the majority of light scatters at the same wavelength as the incident light, which is called *Rayleigh scattering*.

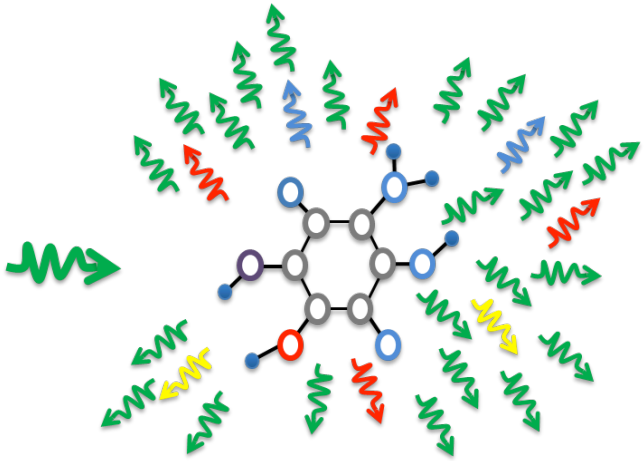

Figure 2.1 When incident photons hit a molecule, the majority of the scattered photons stay in the same wavelength, however, a very small portion undergo shift in their energy and wavelength which is called Raman scattering

However, a very small portion of the scattered photons undergo a change in their energy and consequently shift in wavelength due to inelastic energy exchange with

the scattering molecule which was discovered by Dr. C. V. Raman in 1928. This phenomenon is known as *Raman scattering*.

Upon photon impingement, the incident photon excites the molecule from an energy state (either the ground state or an excited energy state) to a higher virtual energy state which is not associated with any transitions in electron levels (Figure 2.2). Then the molecule emits a photon when it relaxes. If the molecule relaxes to a different vibrational state than the initial energy state, there would be a change in photon energy resulting in Raman scattering. The shift in wavelength can be an increase (Stokes) or a decrease (Anti-Stokes) depending on whether photons interacted with a molecule in the ground state or an excited vibrational state. At room temperature, based on Boltzman statistics, the initial state of the molecule is more likely to be the ground state; therefore, Stokes Raman is more common to happen than anti-Stokes Raman.[3]

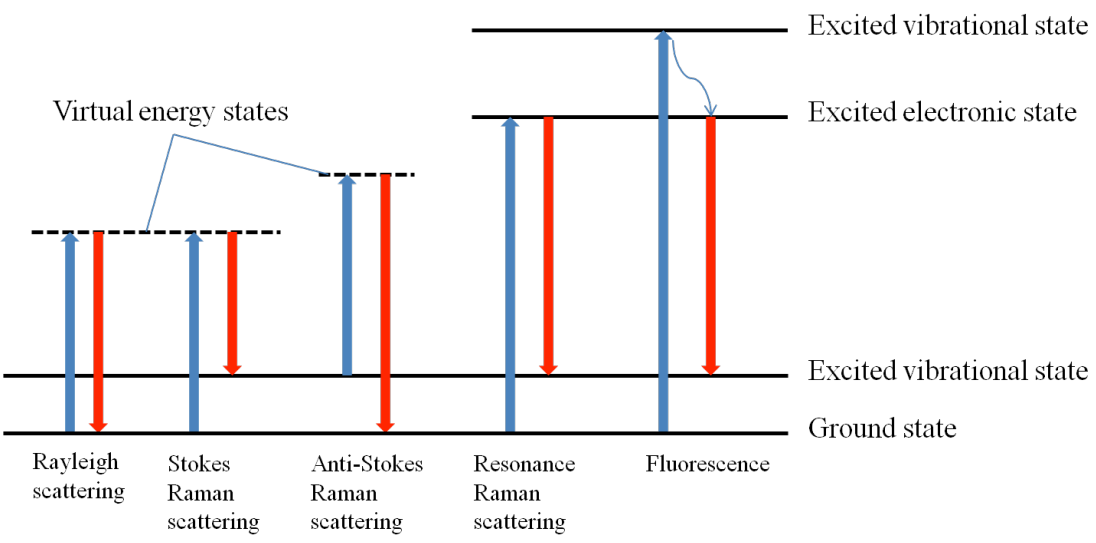

Figure 2.2 The scattered photon has no exchange of energy in case of Rayleigh scattering, while in Raman scattering molecule either gains or loses energy to photons.

The shift in Raman scattered photons is related to the vibrational energy states specific to each molecule, and hence the measured wavelength shifts uniquely identify the analyte molecule. Moreover, the intensity of Raman scatterings is proportional to the number of molecules, which allows analyte quantification.

Since the molecule is excited to a virtual energy state, there is no limitation on the frequency of the incident photon, allowing the use of a wide range of laser sources (UV, visible, and IR). Raman intensity is proportional to υ^4, where υ is the frequency of the excitation laser.[4] This means that much higher Raman signal can be achieved by using a UV laser rather than an IR source; however, many samples show strong fluorescence in UV region which can swamp the Raman signal. Therefore, the excitation laser wavelength should be selected based on the application. In case of using IR laser; the lower Raman intensity can be compensated by using higher laser power as well as longer integration times.

There are two benefits of Raman scattering over fluorescence emission; 1) Raman scattering happens faster (roughly 20 femtoseconds) than fluorescence (hundreds of picoseconds to nanoseconds)[4], and 2) Raman shows much smaller line widths (couple of cm^{-1}) as compared to fluorescence (couple of hundreds cm^{-1}), which results in higher multiplexing capabilities for Raman spectroscopy.

The Raman spectrum of each molecule is presented by photon counts versus the Raman shift. The Raman shift has cm^{-1} unit and it does not depend on the excitation laser ($\Delta\upsilon=\upsilon_0-(\upsilon_0-\upsilon_1)=\upsilon_1$). Therefore, regardless of the wavelength of the laser source, each molecule has its unique Raman shifts in the Raman spectrum.

2.2 Surface Enhanced Raman Spectroscopy (SERS)

Unfortunately, Raman scattering is a weak effect since it only happens for a small portion of scattered photons. Thus, in its conventional form, it cannot be applied to detection of trace quantities of analytes in low concentrations due to the extremely small cross section of each molecule. The Raman scattering cross sections are about 14 orders of magnitude smaller than of those of fluorescent dyes.[5,6]

Enhancement in Raman scattering on a roughened silver substrate was first observed, though not recognized, by Fleischman et al.[7] in 1974. Three years later Jeanmaire and Van Duyne[8], and Albrecht and Creighton[9], discovered that the reason of Raman scattering enhancement is the optical and chemical enhancements from metal nanostructures and nanoparticles. This phenomenon was called *surface enhanced Raman scattering (SERS)*. SERS can provide a huge enhancement, up to 11 orders of magnitude, to the Raman signal, making it comparable to fluorescence in terms of sensitivity.[6,10]

SERS is the result of the combination of the electromagnetic enhancement provided by the localized surface plasmon resonances at the metal nanostructure surface[5,11–13] and a chemical effect due to the metal.[14]

Basically, localized surface plasmons (LSPs) are electron oscillations localized at the surface of metallic nanoparticles and nanostructures. LSPs are excited by an electromagnetic field (light) at an incident resonance wavelength and result in strong light scattering of the molecule adsorbed onto the surface of the nanoparticle.

The enhanced light scattering is due to the generation of high intensity local electromagnetic fields close to the surface due to the LSP excitation. For

enhancement to occur, the surface needs to be roughened to give a perpendicular component to the plasmon.[15] Figure 2.3a shows excitation of surface plasmons at the surface of a metal nanoparticle. The resonant frequency of the particles depends on the type of metal, particle size/shape, and aggregation state.[12] Figure 2.3b illustrates aggregated silver nanoparticles.

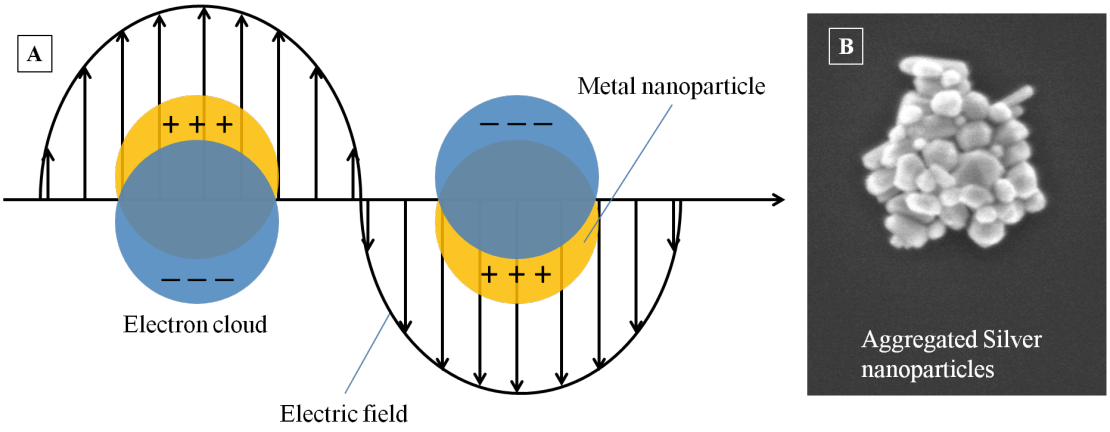

Figure 2.3 (a) Excitation of surface plasmons on metal nanoparticles due to electric field excitation (b) SEM image of aggregated silver nanoparticles.

Another enhancement mechanism called the chemical enhancement is due to the charge transfer between the adsorbed analyte and the nanoparticle. In this case, the exciting radiation interacts with the metal to form an electron–hole pair and energy is transferred to the analyte through the metal to the bonds of the molecule. It is commonly agreed that the dominant factor between the two mechanisms is electromagnetic enhancement which shows eight orders of magnitude higher enhancement.[15,16]

The most common types of metal nanoparticles for SERS enhancement are gold and silver. Both of these materials display resonance in visible and IR frequency, which is desirable, and results in high enhancement in Raman scattering. Regarding

the size of the particles, it can be tuned to show resonance with different laser wavelengths based on their size. The typical size of nanoparticles is in the range of 10-200 nm and the resonance peak is shifted by changing their size.

Another important factor to gain high SERS enhancement is to have an optimized aggregation state within the metal nanoparticles. An extremely high intensity electromagnetic field is generated between the gaps of aggregated metal nanoparticles. The increased intensity is due to coupling of surface plasmons of close nanoparticles (<~2 nm distance).[17] These high intensity EM field gaps are called *"hot spots"*.

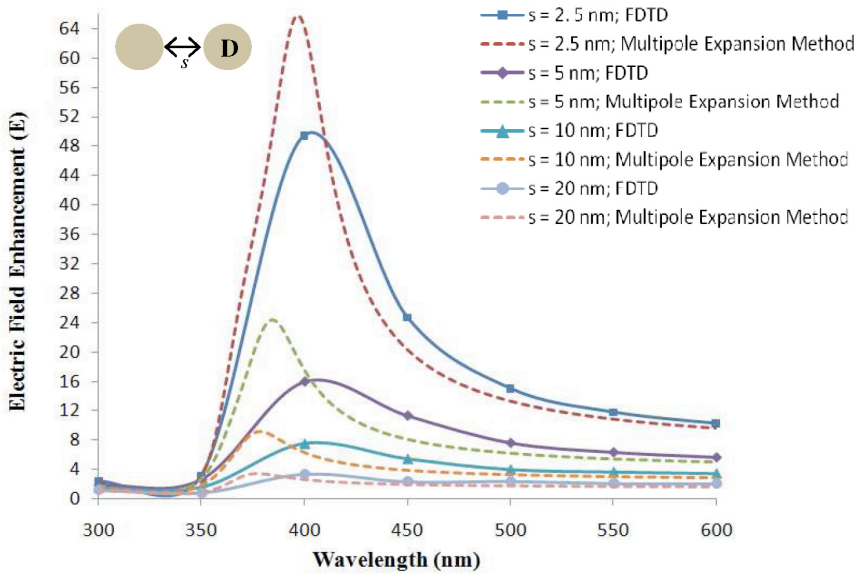

Figure 2.4 Effect of spacing between two silver nanospheres forming a dimer on the magnitude of the electric field as a ratio of the incident electric field. Evaluations were carried out using FDTD simulations and Analytical Calculations using the multipole expansion method. Reproduced from Dhawan et al.[18] with permission from The Optical Society of America.

Figure 2.4 shows the effect of spacing between two silver nanoparticles forming a dimer on the electric field magnitude.[18] Salts, like NaCl, Tris-HCl and

other aggregating agents can be added to the metal nanoparticle colloid to induce the formation of hotspots. The hotspots generate an intensive localized electromagnetic field allowing the detection of low concentration analytes.

In addition to hot spots, high intensity electromagnetic fields are generated at sharp features of metal nanoparticles too. Nanoparticles containing sharp edges and corners result in increased electromagnetic fields. This effect is called the *"lightening rod effect"*.[19]

SERS is a distance dependent effect since the electromagnetic field strength decreases with distance. Therefore the maximum Raman enhancement occurs if the molecule is adsorbed to the metal surface and it would drop by $(r/(r+d))^{12}$ dependency as it is located further from the surface, where r is the nanoparticle radius and d is the distance of the molecule from the surface.[11,16]

In addition to high sensitivity of this technique, the narrowband spectral SERS fingerprint enables detection of multiple analytes with a single laser source and filter set, which is generally not easily feasible using fluorescence detection. Also, the intensity of the SERS peaks corresponds directly to the concentration of the scattering molecules, enabling the quantification of the scattering molecule.

Figure 2.5 represents the SERS spectrum of Rhodamine 6G molecule, a commonly used dye in SERS and fluorescence spectroscopy. The SERS peaks identified with arrows are specific to the R6G molecule and identify it within a sample.

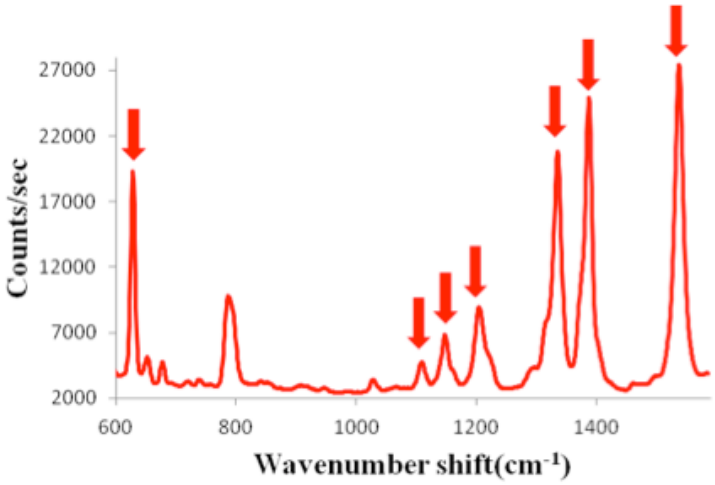

Figure 2.5 SERS spectrum of Rhodamine 6G molecule

SERS has been studied widely for a number of sensing applications over the recent decades. SERS detection has been reported for various applications including detection of food and water contaminants such as pesticides[20–25] for environmental monitoring, or in the area of safety and security such as detection of explosives[26–29], or in healthcare for detection of toxins[30,31], drugs[32,33], metabolites[34–36], DNA sequences[37–42], proteins[43–47], virus and bacteria.[48–53]

2.3 Surface Enhanced Resonance Raman Scattering (SERRS)

The *Resonance Raman effect* occurs when a molecule is excited by excitation radiation with a frequency that matches an electronic transition of the molecule. This effect may result in up to six orders of magnitude enhancement in Raman scattering allowing the detection of much lower analyte concentration. In this case, high fluorescence is observed too. Since the cross-section of resonance Raman is six orders of magnitude smaller than the cross-section of fluorescence, Raman scattered photons are masked by fluorescence signal in many cases. One way to improve

resonance Raman photons collection and suppress the fluorescence is to use an ultrafast Kerr shutter to separate resonance Raman scattering from fluorescence emission based on their different time dependences which was explained earlier.[4]

Resonance Raman scattering is usually observed with analytes that have a chromophore. This effect has been widely used on biological chromophores, such as heme and chlorophylls molecules. By changing the excitation wavelength, different resonance Raman spectrum of the same molecule can be recorded. If the excitation frequency matches the absorption of a specific bond of the molecule, then the Raman spectrum associated with this part is selectively enhanced and separated from the rest of the molecule.

When the molecular resonance effect is combined with SERS, it results in a very intense Raman scattering which is called *surface enhanced resonance Raman scattering (SERRS)*.[54] Signal enhancement up to 14 orders of magnitude has been reported using SERRS.[55] A major benefit of SERRS is that fluorescence is efficiently quenched by the metal surface which effectively prevents the Raman scattering from being masked by fluorescence signal.[56]

In SERRS, the bands associated with the chromophore dominate in the SERRS spectrum. When a chromophore with a resonance frequency in the red region is mixed with metal nanoparticles with plasmon resonance frequency in blue region, the strongest SERRS signal is achieved when the sample is excited with an excitation frequency close to the molecular resonance. This shows the significant effect of the molecular resonance in Raman scattering enhancement in SERRS.[55]

SERRS has been widely used for detection of biological samples.[39,57–59] The common practical approach for sensitive and specific detection of biomacromolecules, is to employ SE(R)RS in a labeled immunoassay or DNA hybridization format. The labels, which are often fluorophores or other strong Raman scatterers, are referred to as Raman labels. As opposed to fluorescence-based transduction, however, the Raman labels each generate a unique and narrowband Raman spectral fingerprint upon laser excitation, which enables an increase in multiplexing density as compared to fluorescence while utilizing only a single laser and a single filter set.

In spite of the tremendous power and the reported success of SE(R)RS, it has had a limited impact outside of research labs due to the bulky and costly laboratory equipment and SERS-active substrates that have been used for high sensitivity SE(R)RS detection. One potential way to take advantage of SE(R)RS in practical applications is to integrate it with microfluidic functions which will be explained in the optofluidic SERS section.

The next section will give a brief overview on advantages of optofluidic sensors over conventional detection tools. Moreover, common optical sensing mechanisms that have been integrated with microfluidic systems will be described.

2.4 Optofluidic Microsystems for Detection of Chemical and Biological Molecules

Recent years have seen the emergence of optofluidics as a toolkit to combine optical sensing mechanisms with microfluidic functions.[60–65] Optofluidic microsystems enable small sample consumption, improved portability, automation,

and reduced cost as compared to traditional bulky systems, such as flow cytometers. Laminar flows in microfluidic systems can effectively transport analytes and nanostructures with desirable optical properties into targeted regions of a photonic sensing platform.

These microdevices have been recently built with polydimethylsiloxane (PDMS), polymethylmethacrylate (PMMA), or cyclic olefin copolymer (COC), which are cheaper than silicon-based microsystems. Attractive properties of PDMS such as optical transparency and a biocompatible surface chemistry along with the ease of fabrication have made it a good choice for fast and cheap microdevice prototyping. Different microfluidic functions, such as micro-valves[66], microchannels, micro-pumps[67], and microfluidic mixers[68] have been integrated into PDMS-based microsystems. Integration of these microfluidic functions allows performing the required laboratory functions faster, easier, and more automated.

Optofluidic microsystems are suitable for detection of biological and chemical samples. Integration of sample preparation, sample delivery, and anlayte detection allows the use of small sample volumes which is required in many detection assays.[61,65]

In optofluidic sensors, the sensing signal is often generated from refractive index (RI), fluorescence, or surface enhanced Raman spectroscopy (SERS). These optical sensing mechanisms can be combined with microfluidic functions such as mixing, chromatography, on-chip nanoparticle synthesis, and electrophoresis to improve their performance for chemical and biological detection.

One way to detect chemical and biological samples via optofluidic microsystems is by measuring the refractive index (RI) of the sample. In this label-free technique, the RI of the solution changes due to the presence of the analytes. RI detection requires a small sample volume, which makes it suitable for detection of chemical and biological targets.

In many optofluidic RI sensors, the electric field can be confined to a small volume, thus enabling a small number of molecules to be detected. Various optofluidic designs have been explored in order to confine the electromagnetic field to a small volume to perform more practical detection. These designs include metallic nanohole-array-based plasmonics[69–73], photonic crystal fibers (PCFs)[74–77], ring resonators[78–82], Fabry–Pérot cavities[83–85], and Mach–Zehnder interferometers.[86]

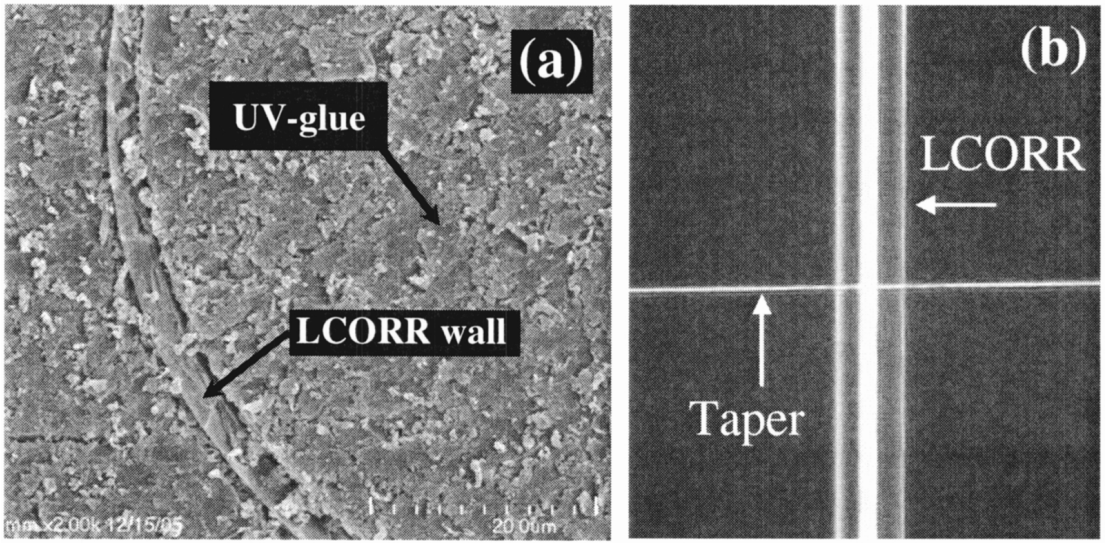

Figure 2.6 (a) SEM image of an optofluidic ring-resonator (OFRR) cross section with an outer radius of 50 μm. (b) The experimental setup of the OFRR and a tapered fiber optic of 4μm in diameter. Reproduced from White et al.[82] with permission from the Optical Society of America

One example of RI-based optofluidic systems is the optofluidic ring resonator (OFRR).[78–82] In the OFRR, ring resonators are integrated with microfluidic functions

to improve sample delivery while retaining their high sensitivity. The detection limit of 10^{-7} RIU for small molecules has been reported using this technique.[80] Figure 2.6 shows an example of an OFRR device in which the light is coupled on the surface of a silica capillary via a tapered fiber optic cable. The output signal is changed due to the change in the refractive index of the sample introduced into the capillary as the concentration of target analytes increases.[82]

Although label-free RI sensing is attractive due to the reduced number of steps in the assay and the real-time readout, fluorescence-based detection has its own benefits, including better sensitivity and higher multiplexing capabilities in many applications. Like RI-based sensing, many different designs have been developed to improve light-matter interaction in optofluidic fluorescence-based detection to improve the sensitivity. These designs include liquid-core waveguides[87,88] and photonic crystal structures[89–93] to improve fluorescence collection efficiency.

The antiresonant reflecting optical waveguide (ARROW) design is an example of optofluidic fluorescence detection[94–96]. ARROW is capable to confine light to a core with a refractive index lower than either of the surrounding cladding layers. Single molecule detection has been demonstrated with a very small sample volume using this technique. Figure 2.7 is an example of an optofluidic ARROW microsystem. The device demonstrated excellent sensitivity for virus detection.[94]

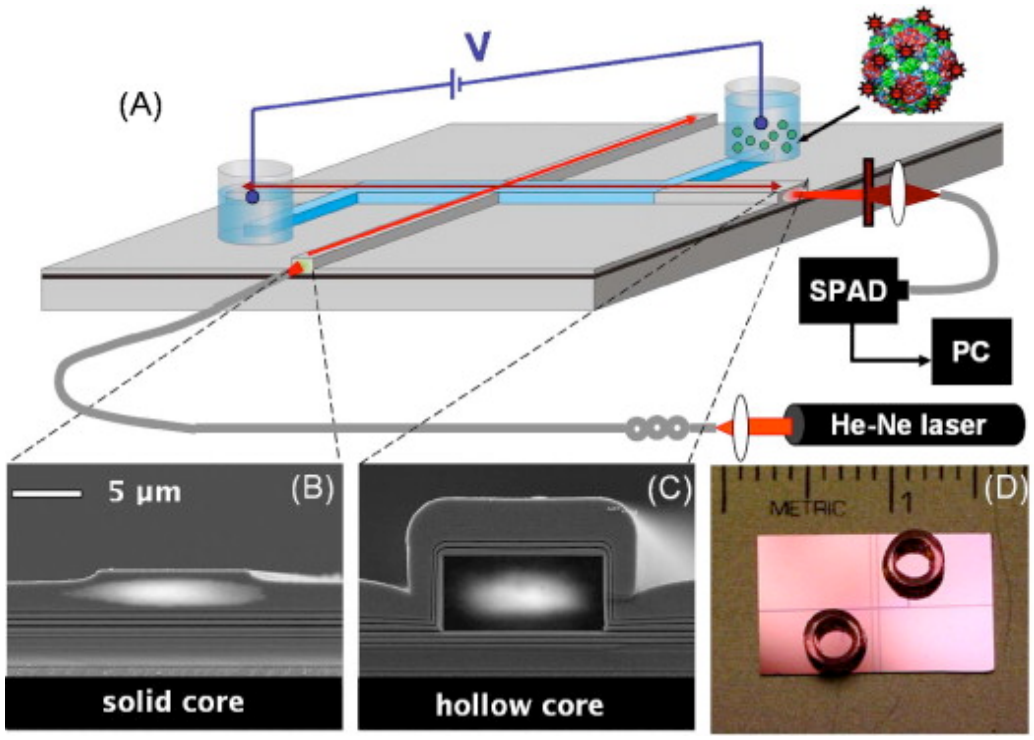

Figure 2.7 (A) Optofluidic device and experimental setup schematic for virus detection. Arrows represent direction of excitation and emission inside the ARROW waveguides; (B) solid-core ARROW waveguide; (C) liquid-core waveguide; (D) photograph of the ARROW biosensor. Reproduced from Rudenko et al.[94] with permission from Elsevier.

Another approach for optofluidic sensing is based on SERS. Optofluidic SERS has the advantage of label free detection of RI-based detection as well as high sensitivity of fluorescence-based detection. Additionally, optofluidic SERS offers much higher multiplexing capabilities. These benefits make optofluidic SERS an excellent candidate for sensitive detection of analyte for practical applications.

An important issue to consider is that combination of SERS detection and a simple microfluidic system can be detrimental to the detection limit due to the limited sample volume and diffusion-based transport, however, optofluidic techniques has the potential to improve the detection limit by utilizing microfluidic functions and make

the sensing platform suitable for real-world applications. A detailed overview on optofluidic SERS will be presented in the next section.

2.5 Optofluidic SERS: Synergizing SERS and Microfluidics for Chemical and Biological Analysis[1]

As explained earlier, SERS leverages the specificity of Raman scattering and the sensitivity provided by localized plasmonic effects for applications in chemical and biomolecular detection. However, nearly four decades after the first report of SERS, practical uses of the technique remain limited. Optofluidic SERS—the synergistic use of microfluidics to improve the performance of SERS—may finally lead to practical devices for chemical and biomolecular detection.

In this section, we describe recent advances in optofluidic SERS microsystems that have been developed to improve the performance and applicability of SERS. These techniques include designs that improve the light–analyte interaction, that perform active or passive concentration of metal nanoparticles and/or analyte molecules, and that utilize microfluidic techniques to improve functionality.

Photonic-based biological and chemical sensing techniques are often categorized either as label-free (e.g., refractive index transduction) or as labeled (e.g., using fluorophore-conjugated biorecognition molecules). It is commonly accepted that label-free techniques enable direct detection with fewer steps while fluorescent-based techniques provide improved detection limit. Surface enhanced Raman spectroscopy (SERS) has continued to gain in popularity as an alternative

---

[1] This section is adapted from: Ian M. White, Soroush H. Yazdi, and Wei W. Yu, Optofluidic SERS: synergizing photonics and microfluidics for chemical and biological analysis, *Microfluidics and Nanofluidics*, 12, 205-216, 2012

transduction method. In many implementations, SERS can offer the simplicity of label-free detection while providing the sensitivity of fluorescent-labeled techniques. When utilized in a labeled detection paradigm, such as when biorecognition molecules are conjugated to plasmonic nanostructures, SERS can offer significantly denser multiplexing as compared with fluorescence detection while requiring a simpler optical system.

Raman spectroscopy enables these advantages because of the specificity of the acquired signal. Upon laser light excitation, Raman-scattered photons from a molecule reveal the landscape of vibrational energy states of the molecule, which are unique to any molecule. Thus, detection of the Raman scattered photons provides a unique spectral fingerprint that can be used to identify the molecule and its characteristics. Unfortunately, Raman scattering is an extremely weak effect and thus it cannot generally be applied to detection of trace quantities of analytes in its conventional form. Nearly 40 years ago, however, it was discovered that noble metal nanostructures provide a boost of many orders of magnitude to the Raman signal for molecules interacting at the surface.[7–9]

This effect, surface enhanced Raman scattering, is the result of the combination of an electromagnetic enhancement provided by the localized surface plasmon resonances at the metal nanostructure surface[5,13,97] as well as by a less understood chemical effect at the metal surface.[14] The power of the SERS technique was realized 15 years ago with the demonstration of single molecule identification using SERS.[6,10,14,98]

In general, SERS is capable of performing label-free detection on small molecules, as the spectral bands can easily be identified and distinguished. For macromolecules, such as large protein and DNA molecules, it is more common to employ SERS in a labeled immunoassay[45,46,57,99] or hybridization format.[39,42,53,57,58,100–102]

The labels, which are often fluorophores or other strong Raman scatterers, are referred to as Raman reporter probes (RRPs). As opposed to fluorescence-based transduction, however, the RRPs each generate a unique Raman spectral fingerprint upon laser excitation, which enables much denser multiplexing than fluorescence while utilizing only a single laser and a single filter set.[37,103] These conceptual advantages make SERS an intriguing potential choice for a number of translational applications in molecular detection.

Despite years of research and a mounting number of published reports, SERS has had a relatively small impact outside of the research laboratory. Meanwhile, over the past decade a trend has emerged in photonic biosensing in which the detection head is integrated with microfluidic functions into a microsystem; this is generally thought to improve the practical use of the photonic device. Implementing SERS in a microfluidic environment provides the advantage of functional integration of automated sample processing and delivery. For example, a number of reports have shown on-chip mixing of metal nanoparticles and target analytes in a microfluidic channel immediately before SERS detection within the channel.[30,59,104,105] In addition, one report demonstrated the capability to synthesize SERS-active metal nanostructures within a microfluidic channel[106], while another report leveraged

optical tweezers within a microfluidic channel to construct metal nanoparticle aggregates to increase SERS activity.[107]

While the integration of these and other microfluidic functions is an advantage, the performance of SERS can be limited when conducted within a microfluidic environment. Figure 2.8 compares a conventional SERS detection method with microfluidic-based SERS. Today, SERS measurements are commonly performed by fabricating a gold or silver nanostructured substrate and drying the sample onto the substrate (Fig. 2.8a). When SERS was initially implemented in microfluidics, two common approaches were utilized: mixing the sample with a silver colloid in a microfluidic channel (Fig. 2.8b), or passing the sample through a microfluidic channel that has a silver or gold nanostructured substrate at the bottom of the channel (Fig. 2.8c). When performing SERS detection with a colloid, the acquired Raman signal intensity can be reduced as compared with conventional SERS detection because there are fewer analyte molecules that have adsorbed onto or become bound to SERS-active surfaces within the detection volume (Fig. 2.8b vs. a). Likewise, when using a 2D SERS substrate at the bottom of a microfluidic channel, the acquired signal intensity is often worse because under laminar flow the analyte is transported to the SERS substrate only by diffusion, which is less effective than drying the sample onto the SERS-active surface (Fig. 2.8 c vs. a).

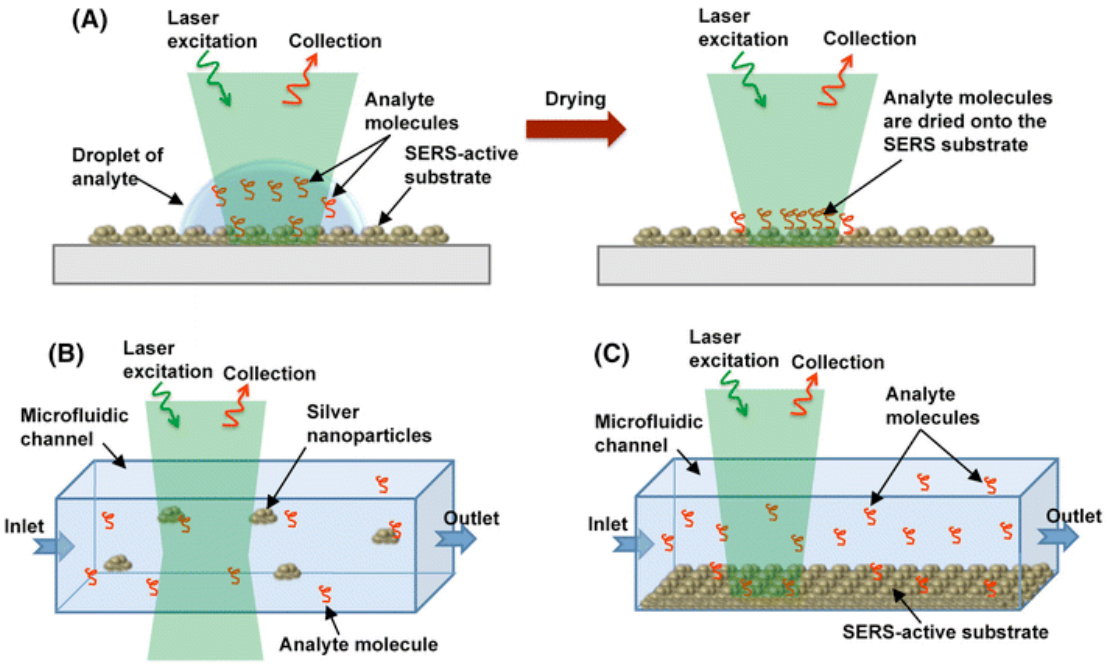

Figure 2.8 (a) In conventional SERS, a sample droplet is dried onto a SERS-active substrate; target analyte molecules are concentrated onto the substrate after drying. (b) In one form of microfluidic SERS, analyte molecules are mixed with a solution of nanoparticles and passed through a microfluidic channel under laser illumination. (c) In another form of microfluidic SERS, a SERS-active substrate is incorporated as the bottom of a microfluidic channel. In b and c, the density of target analyte molecules adsorbed at SERS-active locations within the SERS detection region is much lower compared with conventional SERS techniques

Over the past few years, some in the SERS community have drawn upon optofluidics techniques to improve upon the performance of and add functionality to SERS microsystems. Optofluidics has emerged recently out of the emphasis on the integration of photonics into microsystems.[60–63,65,108]

We define optofluidics to imply a synergistic relationship between photonics and microfluidics in which microfluidics improves the function or performance of the photonics and/or photonics improves the function or performance of the microfluidics.

Numerous examples of optofluidics-based molecular detection have been reported recently. In label-free refractive-index-based detection, the concept of micro/nanofluidic flow-through devices is replacing planar biosensors.[69,71,109] In these microsystems, the sample is passed through micro/nanochannels within the sensor head [e.g., nanohole arrays[69,71] or Fabry–Perot cavities with nanochannels[109], as opposed to being passed over the top of the sensor head, thus eliminating the strong dependence on diffusion and dramatically improving performance. One recently reported example of optofluidic-based fluorescence detection is the use of a capillary-based microfluidic channel in which the cross-section acts as a ring resonator (the optofluidic ring resonator, or OFRR). This device has been used in conjunction with Förster resonance energy transfer (FRET) to detect DNA hybridization.[110]

To understand how optofluidic concepts can be applied to SERS microsystems to improve the performance, we consider the parameters related to the measured power of a Raman signal:

$$P_{Raman} \alpha \quad I \times \sigma \times N \tag{1}$$

where I is the laser excitation intensity in the detection volume, σ is the Raman scattering cross-section, and N is the number of analyte molecules within the detection volume. When considering SERS, N becomes the number of analyte molecules interacting with the metal nanostructures within the detection volume, while σ includes the enhancement (electromagnetic and chemical) provided by the metal nanostructures (in reality, the electromagnetic enhancement is locally increasing the intensity I, but for convenience, we group the enhancement into the cross-section term). For the special case of surface enhanced resonance Raman

spectroscopy (SERRS), in which the excitation laser wavelength matches the optical absorption of the target molecule, the Raman scattering cross-section σ is further increased.[54] Taken together, Eq. 1 demonstrates that to maximize the measured SERS signal, a system should aim to maximize the intensity in the detection volume, the enhancement provided by the metal nanostructures, and the number of target molecules that interact with the nanostructures within the detection volume.

Herein, we evaluate how the concepts of optofluidics can be applied to improve the performance of SERS microsystems. Most reports published to date are focused on improving SERS performance by increasing the parameter N. We will first present three categories of optofluidic SERS techniques that aim to increase detection performance:

(i) Photonic structures that expand the detection volume, and thus increase N.

(ii) Active techniques that increase target analytes and their interaction with metal nanostructures, thereby increasing N.

(iii) Passive techniques that increase nanoparticle-analyte conjugates in the detection volume, and thus increase N.

We will then discuss the possibility for increasing the detection performance of SERS microsystems by incorporating optically resonant structures into the detection volume, which can increase the parameter I from Eq. 1.

2.6 Improving the Performance of SERS Microsystems with Optofluidics

2.6.1 Photonic Crystal Waveguides for Optofluidic SERS

Photonic crystal fiber (PCF) utilizes an array of longitudinal holes along the optical cable to impart special transmission properties, such as particular spectral characteristics or tolerance to nonlinearities. Recently, the air cavities in PCF have been assigned the additional function of microfluidic sample containment. Thus, for a properly designed PCF, light propagates along the fiber, interacting with the sample, which is contained throughout the entire length of the channel. In the case of SERS, the excitation light acts as a Raman pump along the fiber, and Raman-scattered photons are also guided along the fiber to the detector (Fig.2.9 a). As a result, the detection volume extends along the entire length of the PCF, as opposed to comprising only a small spot on a SERS-active substrate or a small volume in a cuvette at which the excitation laser is focused. This extension of the detection volume increases the number of analyte-nanostructure conjugates (N in Eq. 1), and thus improves the detection performance of SERS.

A number of published reports have demonstrated the concept of using PCF for optofluidic SERS.[111–113] In general, there are two parallel approaches to form a SERS detection system from PCF. In work by Yang et al. the core of a hollow-core fiber is filled with the sample in a silver colloid, and thus the excitation light propagates directly along with the sample (Fig. 2.9b). A detection limit of 100 pM for Rhodamine 6G (R6G) was achieved.

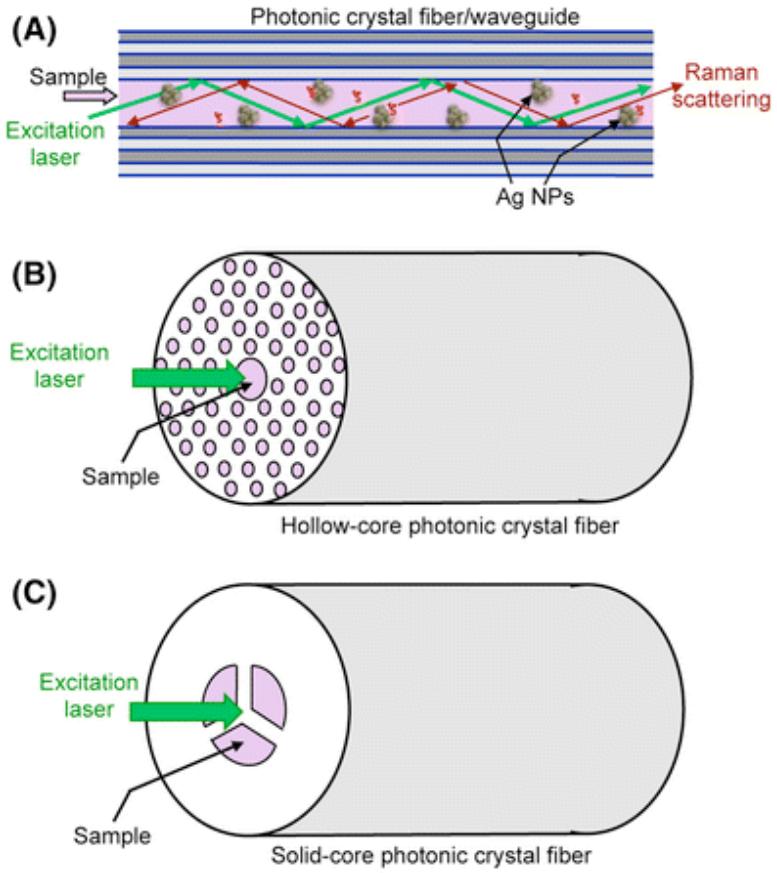

Figure 2.9 Increasing N (Eq. 1) by extending the detection volume. (a) Photonic crystal structures can be used to confine and guide light along a microfluidic channel. (b) Excitation light guided along with the sample in the hollow core of a PCF, as in Yang et al. 2010. (c) Excitation light guided in the solid core of a PCF, such that the evanescent field interacts with the sample, as in Khaing Oo et al. 2010

In an alternative approach, Khiang Oo et al. utilized a solid core fiber and loaded the sample into the hollow channels that form the cladding (Fig.2.9c). In that work, metal nanoparticles were first immobilized onto the surface of the hollow channels, and then the sample was loaded. Because the fiber cable has a solid core, the evanescent field of the guided mode serves to excite the Raman scattered photons. A detection limit of 100 pM for R6G was also achieved with this structure.

The optofluidic concept of extending the sample volume along a liquid light-guiding structure has also been demonstrated on-chip. Measor et al. utilized an anti-resonant reflecting optical waveguide (ARROW) structure to create a liquid core waveguide on a chip.[114] Light is coupled into the ARROW structure via an adjacent on-chip waveguide, while the liquid sample is also loaded into the ARROW structure from an on-chip microfluidic channel. While the on-chip nature of this structure limits the length of the detection volume as compared with the PCF, the on-chip implementation may have practical advantages when considering the benefits of system integration.

2.6.2 Concentration with Active Microfluidic Techniques

For decades, a simple trick has been used to increase the parameter N when performing SERS in a bulk environment; the sample is dried onto a surface. Clearly, this is difficult to do within a microfluidic channel. However, alternative techniques have been developed to transport a large number of the target analyte molecules from the bulk solution to the detection volume. In one example, Cho et al. leveraged the conductive properties of a nanostructured SERS-active surface at the bottom of a microfluidic channel; it is used as an electrode to attract charged analyte molecules from the bulk solution, as illustrated in Fig. 2.10a. Using this approach, the authors were able to detect the Raman signal for 10 fM adenine, an improvement of eight orders of magnitude over the non-concentrated case in which diffusion is the only mass transfer mechanism to deliver the analyte molecules to the SERS substrate.[115]

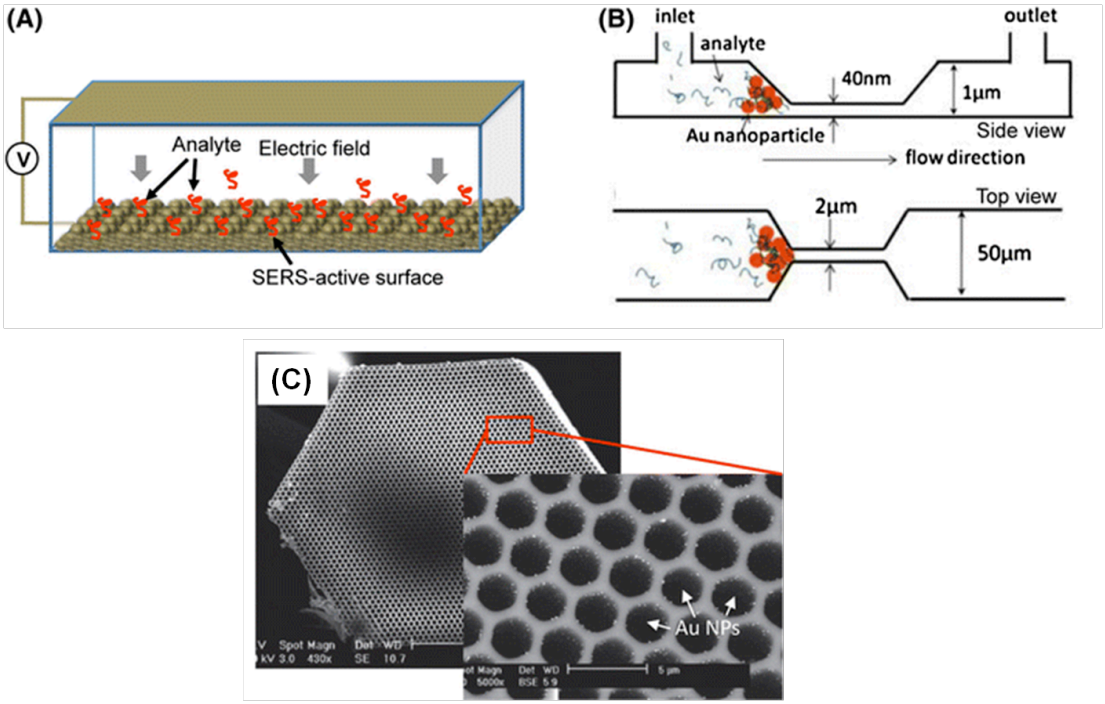

Figure 2.10 Increasing N (Eq. 1) by concentrating the number of analyte molecules adsorbed to SERS-active hot spots in the detection volume. (a) Electro-active concentration of analyte molecules at a SERS-active surface, as in Cho et al. 2009. (b) Concentration of silver nanoparticles and analyte molecules using a nanofluidic channel. Reprinted from Wang et al. 2009. (c) Microhole array for "flow-through" optofluidic SERS. Reprinted with permission from Guo et al.[122], Copyright 2012, American Chemical Society

Active forces have also been used to concentrate analyte molecules bound to silver nanostructures into the detection volume as a method to improve the SERS detection performance. Huh et al. fabricated electro-active microwells into a microfluidic chip in which opposing electrodes were located at the top and bottom of the well.[57] Oligo-modified nanoparticles were loaded into the chip and electrokinetic forces between electrodes cycled the nanoparticles in the microwell, causing them to mix with the sample, which contained the target oligo sequence. After mixing, the nanoparticles were then driven to one of the electrodes and concentrated within the

detection volume. Using this method, the authors have reported a number of biologically significant results. In the initial demonstration, the authors were able to detect 30 pM TAMRA-labeled oligonucleotide sequences of the Dengue virus.[57] Later, the same research group utilized this optofluidic microsystem to detect single-nucleotide polymorphisms (SNPs) in DNA sequences using the ligase detection reaction to link the reporter molecule with the metal nanostructure in the case of an SNP.[102]

Furthermore, the multiplexing capabilities of SERS were demonstrated in this work, as three K-Ras oncogene alleles were detected simultaneously at a concentration of 10 pM. Importantly, while many optofluidic SERS techniques presented to date use purified small molecules for characterization, the work presented for the electro-active microwell chip demonstrates biologically significant applications of SERS.

Similar to the electro-active microwell system, Hwang et al. recently reported the electrokinetic concentration of metal nanoparticles and adsorbed analyte molecules in a liquid sample sandwiched between two electrode plates.[116] However, unlike other electrokinetic SERS devices, in this report one of the electrodes is formed from a photoconductive layer. As a result, when the excitation laser is focused onto the photoconductive plane and an AC voltage is applied across the electrodes, charged particles are concentrated at the activated location of the photoconductive plane (i.e., the exact location of the excitation laser focusing spot). As a result, nanoparticles and adsorbed analytes can be concentrated and analyzed at any desired location within the fluidic microcell. The authors have termed this technique

as optoelectrofluidic SERS. While the initial report of optoelectrofluidic SERS presents a poor detection limit (50 μM adenine), we expect that optimization of the technique will lead to detection limits closer to that achieved by the electro-active microwell concentration device reported by Huh et al., described above.

In addition to electrokinetic forces, magnetic forces provide another mechanism for actively concentrating analyte molecules into the SERS detection volume, which again increases the term N in Eq. 1. Han et al. utilized magnetic beads coated with silver nanostructures as a SERS-active substrate.[117] Whereas conventional SERS techniques may use a static substrate, in this case mobile magnetic beads that can mix throughout the sample serve as the substrate; this provides an advantage in terms of mass transport of target analyte molecules to the SERS substrate. After mixing these mobile SERS-active substrates with the sample, a magnetic field concentrates the beads into a small detection volume. Malachite green was detected down to 10 ppb using this technique.

2.6.3 Concentration with Passive Micro/Nanofluidic Techniques

While active concentration of analytes at the SERS-active substrate is an effective optofluidic technique to increase the SERS signal, this improvement may come at the cost of increased fabrication steps to incorporate the active control elements. Therefore, it is also useful to consider the passive concentration of analyte-nanoparticle conjugates within nanofluidic elements. This concept was first reported by Wang et al. who formed a channel 40 nm in height in a glass substrate that bridged two microfluidic channels.[118] Gold nanoparticles loaded into the microchannel become trapped at the inlet of the nanochannel, forming a high-enhancement

detection zone (Fig. 2.10b). As the sample is driven through the channel, the analyte molecules are captured at the surfaces of the nanoparticles that are lodged at the channel inlet. The authors reported a detection limit of 10 pM adenine in these experiments. In later work, the same group used this concept to detect β-amyloid protein[119] and subsequently to obtain structural information from BSA and insulin proteins.[44] While these reports make clear the advantage of using a nanofluidic channel to trap and concentrate nanoparticles and adsorbed analyte molecules, the nanofabrication of microchannels into glass substrates can be difficult, and thus may not provide significant advantages as compared with integrating active control components.

More recently, Park et al. demonstrated the fabrication of a nanofluidic channel using the controlled collapse of polydimethylsiloxane (PDMS), the most popular material for soft-lithography microfabrication.[120] Oligo-labeled gold nanoparticles, which had been reacted with 3 nM of TAMRA-labeled complementary target, were loaded electrophoretically. As expected, the Raman signal for TAMRA increased significantly during the first minute of loading, showing that the nanoparticles and bound target molecules were being concentrated into the detection volume. In comparing the two aforementioned approaches, the PDMS device appears to be simpler to fabricate, but the hydrophobic nature of PDMS makes it difficult to load; as a result, electrophoretic pumping is required.

2.6.4 Three-dimensional Micro/Nanofluidic SERS Substrates

Figure 2.8c above illustrated a conventional technique for a SERS microsystem in which the sample is passed across a two-dimensional SERS-active

substrate. The performance is limited by diffusion of analyte molecules to the substrate. Recently, Liu et al. have extended the microfluidic SERS-active substrate into three dimensions by trapping metal nanoparticles throughout a porous polymer monolith in a microfluidic channel.[121] The nanoparticle-functionalized monolith presents a tortuous path through which the sample passes, creating nearly continuous opportunities for analyte molecules to adsorb to a metal nanoparticle. Thus, as opposed to relying on diffusion to deliver the analyte molecules to the SERS-active substrate, the analyte molecules are essentially passing through the SERS substrate. With this monolith-based three-dimensional SERS substrate, the authors reported a detection limit of 220 femtomoles of R6G.

In a similar but more ordered approach, Guo et al. created a three-dimensional SERS-active surface by fabricating a multihole capillary; the 190-μm glass capillary has nearly 3,000 "holes" (2.1 μm each) in the cross-section, which serve as a microfluidic array (Fig. 2.10c).[122] Gold nanoparticles are attached to the walls of each channel, creating a three-dimensional SERS-active structure. A detection limit of <1 pM R6G is reported. This approach builds upon the new optofluidic trend of "flow-through" sensing, in which the sample flows through a nanofluidic biosensor instead of flowing over a planar sensor.[69,71,109] Just as with the monolith, the flow-through optofluidic device dramatically reduces the mass transport limitations of conventional open microfluidic channels.

In Fig. 2.8, we illustrated the challenges involved when translating SERS to microfluidic devices; compared with conventional sample application techniques, typical microfluidic techniques are hindered by poor interaction between target

molecules and the metal colloid or nanostructured surface. Previous sections present two optofluidic paradigms (active and passive) to promote interaction between target molecules and the SERS-active materials. Both classes of optofluidic devices are able to overcome the challenges of microfluidic SERS devices. While it is premature to predict which technique will ultimately have a commercial impact, it is nonetheless instructional to compare the active and passive optofluidic SERS methodologies.

In general, the active techniques promote interactions between target molecules and the SERS-active nanostructures and concentrate the target molecules within the detection volume through the use of forces, such as electrokinetic forces. Thus, the devices require the incorporation of the active elements, such as electrodes and control circuitry in the case of electrokinetic devices. On the other hand, although the passive devices do not require the fabrication of the active elements, the nanofluidic devices may require complicated fabrication or additional fabrication steps to create the passive concentration elements. Furthermore, the devices based on single nanofluidic channels presented above may be more prone to clogging, are limited in sample throughput, and may have poor repeatability due to variations in aggregation at the nanofluidic channel.

The three-dimensional nanofluidic device presented above was shown to be repeatable, had good sample throughput, and were not prone to clogging.[121] However, they have not yet been evaluated with complex biological samples, which are believed to cause problems in channels with small dimensions. Assuming that the passive optofluidic devices can overcome the issues with sample throughput and clogging, we believe that ultimately the technology that leads to the devices with the

lowest cost per chip will have the greatest impact in commercial applications, including environmental testing, defense, and clinical assays.

2.6.5 SERS Excitation by Optofluidic Resonators

In the optofluidic approaches described above, the SERS detection performance is improved by increasing the number of analyte molecules in the SERS-active detection volume, either through the use of photonic crystal structures to extend the detection volume, or through microfluidic techniques that concentrate analyte molecules into the detection volume. However, returning to Eq. 1, we see that an alternative approach to improving the SERS performance is to increase the optical intensity that excites the sample. One method to increase the optical intensity within the detection volume is to leverage optically resonant structures. Examples of optical microresonators include microspheres, waveguide ring resonators, microtoroids, Fabry–Perot cavities, and photonic crystal structures.[109,123–128] Optically resonant structures serve as photon traps, which leads to a dramatic increase in the optical intensity within the resonator as compared with the intensity that is incident upon the resonator. For example, using the well-established coupling theory of optical ring resonators[129], it can be shown that a ring resonator with a Q-factor of 10^6 can have an optical enhancement of two to three orders of magnitude when operated at critical coupling.[128]

The first demonstration of the use of an optical resonator integrated into a microfluidic channel for SERS excitation was based on the optofluidic ring resonator (OFRR)[128]; the cross-section of the capillary serves as a ring resonator while the sample is delivered through the microfluidic capillary.

More recently, planar photonic crystal structures have been utilized as an optically resonant substrate for SERS excitation.[130–132] In each of these examples, the resonators create a high-intensity optical field at the surface of the resonator.

We expect that the true value of using optical resonators as a substrate for high-intensity SERS excitation will be realized when the resonant structures are combined with the analyte-nanoparticle pre-concentration approaches described in previous sections. While the pre-concentration methods are able to increase the number of analytes (N in Eq. 1) in the SERS-active detection volume by many orders of magnitude, the optically resonant structures promise to increase the optical intensity (I in Eq. 1) by two to three orders of magnitude. Thus, as the optofluidic SERS approaches reported in this chapter exhibit detection limits on the order of picomolar to femtomolar concentrations, the synergistic combination of optical resonators with micro/nanofluidic concentration is expected to push the detection limits into the attomolar range.

2.7 Summary

While the dramatic signal enhancement of SERS was discovered nearly 40 years ago, today there are still only a small number of practical implementations for biological and chemical analytics. Microfluidic integration is often thought to be a common road to practical implementations for optical sensing technologies, but in the case of SERS, a simple microfluidic translation can be detrimental to the detection performance. However, the new paradigm of optofluidics, in which synergy between photonics and microfluidics increases performance and functionality, is enabling dramatic progress in SERS-based microsystems. A number of recent reports were

reviewed here that demonstrate the use of optofluidic techniques to improve the detection performance of SERS by several orders of magnitude, thus matching or exceeding the performance of traditional SERS measurements while retaining the benefits of integrated microsystems.

As SERS becomes more familiar as an option for biological and chemical analytics, and as the cost of microsystem fabrication drops, we expect that the advantages of SERS, discovered decades ago, will finally be utilized in practical applications. In the next chapter, we will present a highly sensitive, portable, and automated porous optofluidic SERS microsystem. This easy-to-fabricate device enhances Raman scattering by passively concentrate the sample. Sensitive detection of a variety of analytes is presented

Chapter 3: A Porous Optofluidic Microsystem for Highly Sensitive and Repeatable SERS Detection[2]

3.1 Introduction

As already stated in the previous chapter, a simpler optofluidic SERS approach is to employ a fluidic design that passively concentrates analyte-nanoparticle conjugates into the detection volume. Nanoparticles and adsorbed/bound analyte in the sample are concentrated as they flow into the channel; there is no need for additional active components in the device to concentrate the sample. Figure 3.1b illustrates this concentration effect at the nanofluidic channel inlet; this effect is contrasted with an open microfluidic channel in Fig. 3.1a, in which no concentration occurs and thus the number of SERS-active regions in the detection volume at any given moment is relatively low. Passive concentration has been accomplished by fabricating a single nanofluidic channel to accumulate nanoparticle-analyte conjugates.[118–120] These reports show excellent detection performance.

However, transport through a single nanochannel potentially limits the throughput and creates opportunities for clogging the channel. Moreover, fabrication of a single nanochannel is complex and may not be as repeatable as typical microfabrication.

---

[2] **This chapter is adapted from: Soroush H. Yazdi and Ian M. White, A nanoporous optofluidic microsystem for highly sensitive and repeatable SERS detection, *Biomicrofluidics*, 6, 014105, 2012. (selected for publication in the Virtual Journal of Nanoscale Science and Technology and the Virtual Journal of Biological Physics Research)**

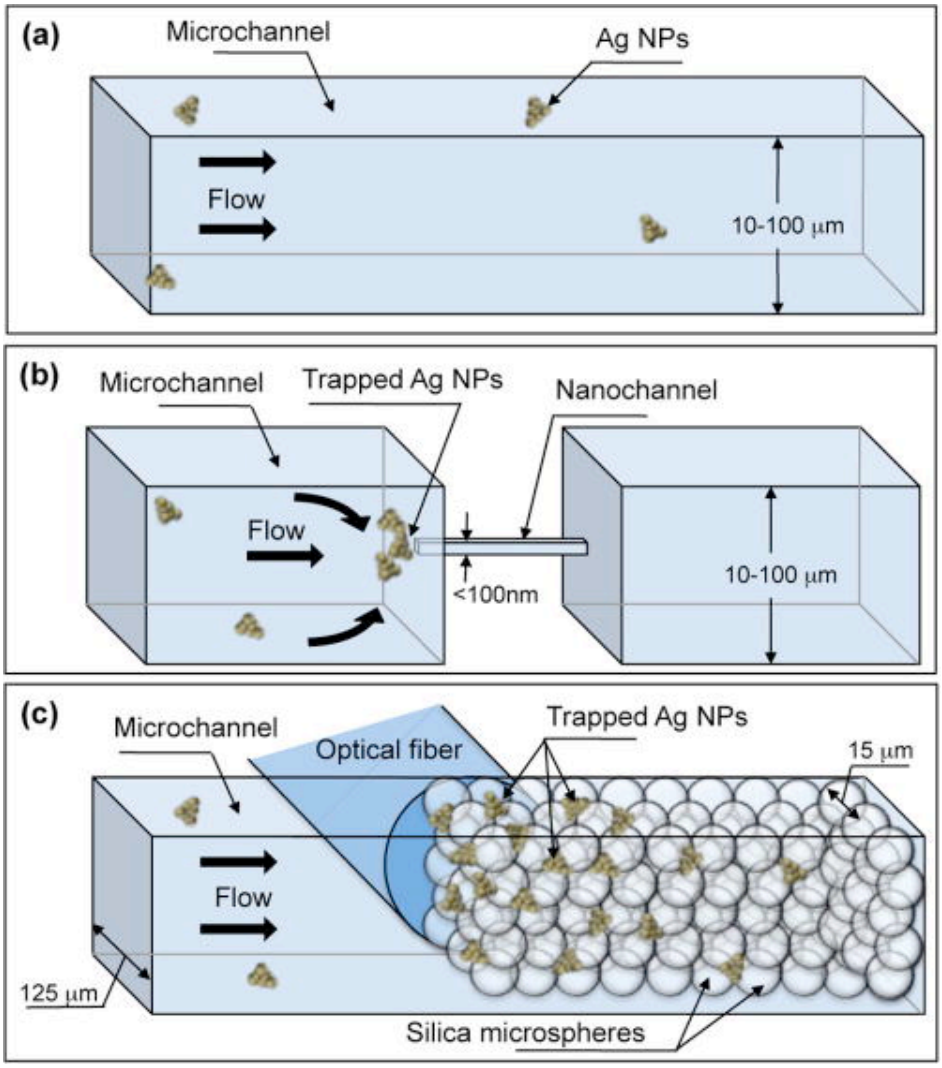

Figure 3.1 Nanofluidic trapping vs. open-channel microfluidics. (a) In an open channel, nanoparticles are poorly concentrated. (b) A nanochannel traps silver nanoparticles (Ag NPs) into the detection volume. (c) Packed silica spheres form a porous matrix, which is capable of trapping a high number of Ag NPs into a relatively large detection volume without clogging. An optical fiber can be aligned to the porous matrix.

In this work, we utilize a three-dimensional porous matrix to concentrate silver nanoparticles with adsorbed analyte molecules for SERS detection. The concept is illustrated in Fig. 3.1c. This device is simpler and more robust to create, as nanofabrication is not required. A microchannel is partially packed by porous silica

microspheres against a narrowing section of the microfluidic channel. As the sample is loaded through the porous matrix, analyte-nanoparticle conjugates are trapped, leading to an increase in the number of SERS-active hot spots and analyte molecules in the detection volume (Fig. 3.1c), which results in an increased Raman signal. Numerous porous channels, inherently created within the matrix of packed silica microspheres, enable high throughput and reduced sample-loading time as compared to a single nanochannel. Moreover, the 3D porous matrix is less prone to clogging due to the high number of available channels within the matrix. Additionally, our design incorporates integrated fiber optic cables. Two channels are created for locating the fiber optic cables into the device, aligned to the detection volume. By using large-core multimode fiber optic cables, we create a relatively large detection volume as compared to typical microfluidic SERS devices. This greatly improves the chip-to-chip detection repeatability of the device because a large number of nanoclusters are concentrated into the detection volume, which decreases the randomness that is historically associated with SERS-based sensors that rely on a small detection volume. Furthermore, as a result of integrating fiber optic cables, the device requires no optical alignment, which can lead to portable applications and on-site detection.

3.2 Experimental Section

3.2.1 Materials

Silicon wafers were purchased from University Wafer (South Boston, MA). AZ 4620 photoresist from AZ electronic materials (Branchbug, NJ) was used to

pattern and mask the wafer for deep reactive ion etching (DRIE). Sylgard 184 was acquired from Dow Coring (Midland, MI) and used to create polydimethylsiloxane (PDMS) devices in the standard 10:1 ratio. Tridecafluoro-1,1,2,2-tetrahydrooctyl-1-trichlorosilane was purchased from Pflatz and Bauer (Waterbury, CT). Porous silica microspheres (15 μm diameter, 6 nm pore size) were obtained from Kisker Biotech GmbH & Co. (Steinfurt, Germany) to form the porous matrix. Silver nitrate, sodium citrate, and trizma base were obtained from Sigma-Aldrich (St. Louis, MO). Rhodamine 590 chloride, also known as Rhodamine 6G (R6G), was purchased from Exciton (Dayton, OH). Malathion was purchased from Cerilliant (Round rock, TX). All materials were used as received.

3.2.2 Preparation of Silver Colloid

Silver nanoparticles were synthesized by the commonly used method of Lee and Meisel.[133] Briefly, 90 mg of silver nitrate was added to 500 ml of deionized water. The solution was heated in a flask while stirring. Upon boiling, sodium citrate (100 mg) was added, and the solution was boiled for 10 min. After the color of the solution became greenish brown, it was removed from heat. 10 mM Tris-HCl (pH 8.2) was added to the silver nanoparticle solution to promote aggregation before running each experiment. To determine the nanoparticle size and clustering density, the colloid was dried onto a wafer and imaged with a scanning electron microscope (SEM). According to the images, the typical silver nanoparticle size is 50 nm, and typical clusters contain tens of nanoparticles.

3.2.3 Fabrication of the Optofluidic Device

The PDMS microfluidic device was fabricated with typical soft lithography methods. PDMS is selected for the optofluidic device because of its optical transparency and low auto-fluorescence.[134,135] A silicon wafer was patterned using standard photolithography and channels were etched by DRIE to a depth of 125 μm. AZ 4620 photoresist was selected as the mask during DRIE because of its relatively high thickness. The channel height is set to be 125 μm to match the standard size of fiber optic cables. PDMS was cast onto the silicon wafer following vapor-phase silanization with fluoro-silane. After casting PDMS, vacuum was applied to remove air bubbles; the PDMS was then cured at 60°C for 4h. Finally, the PDMS channels were sealed onto a piranha-cleaned glass substrate through corona treatment and stored overnight at 60°C.

Micrographs of the assembled device are presented in Fig. 3.2. To trap silica spheres, a frit structure is designed into the channel. The 125 μm channel narrows to a width of 7 μm at the frit (this is thinner than necessary; we designed it as thin as possible to enable us to attempt a range of silica sphere sizes). The 15 μm silica microspheres were diluted in deionized water to 5 mg/ml. A 1 μl droplet of silica microspheres was placed at the channel inlet and the vacuum was applied from the outlet. This volume has been selected because it packs the microspheres just within the detection volume, as shown in Fig. 3.2. Chips were used within 1 day of assembly.

Two multimode fiber optic cables (Thorlabs, Newton, NJ) were inserted into the device through channels created for this purpose. The fiber optic cables have a

105 µm core diameter and a 125 µm cladding diameter; the ends of the fibers were cleaved (Fujikura CT-04B fiber optic cleaver) to minimize light scattering. The distance from the fiber optic tips to the detection zone in the microfluidic channel was set to be 80 µm; this is the minimum distance that can prevent sample leakage from the microfluidic channel into the fiber optic channels.

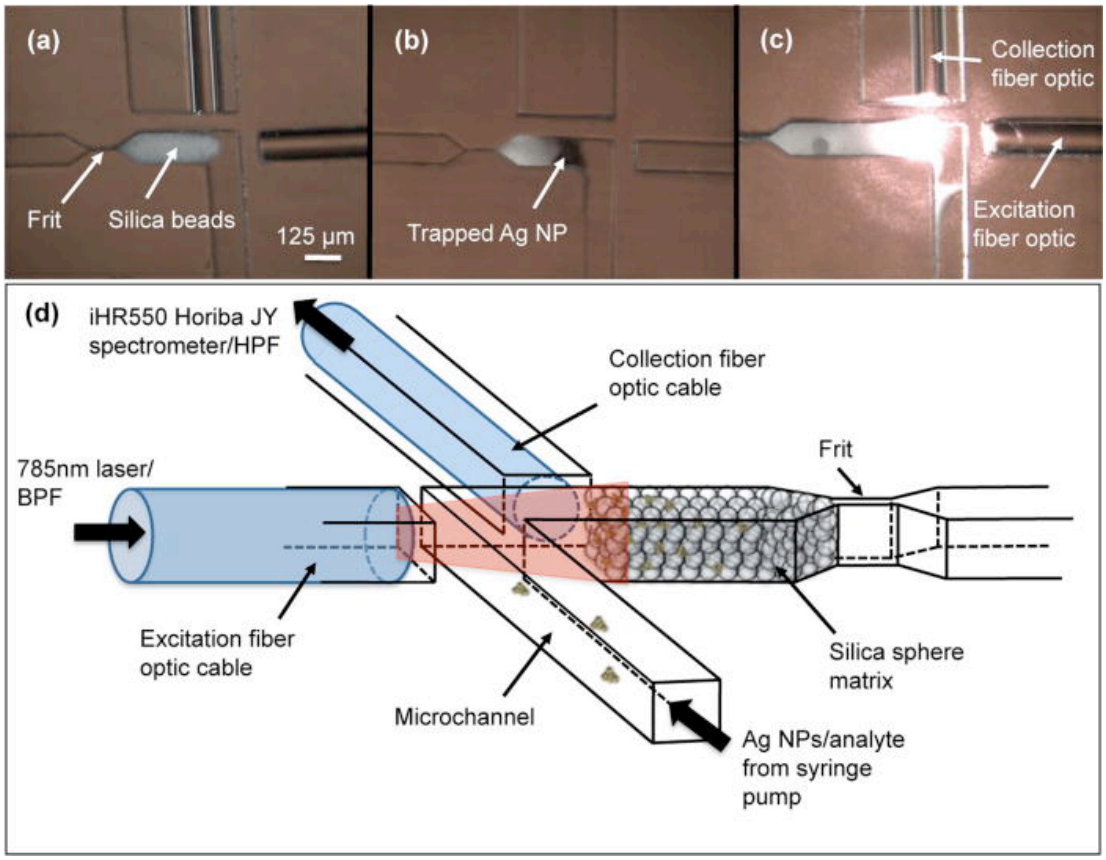

Figure 3.2 (a) Micrograph showing packed microspheres and integrated fiber optic cables. (b) Silver nanoparticles (AgNPs) are trapped in the silica microsphere matrix. (c) Excitation and collection is performed by integrated fiber optic cables. (d) Experimental setup: the sample is loaded with a syringe pump. The fiber optic cables are connected to a diode laser and a Raman spectrometer.

3.2.4 Scanning Electron Microscopy

We recorded SEM images of silver nanoparticles in the matrix of silica microspheres. Silica microspheres were packed into the microfluidic channel and then the silver colloid (described above) was loaded into the channel. The PDMS was then peeled from the glass base; the packed microspheres remained in the channel. Carbon was sputtered onto the device, including the exposed beads in the channel.

3.2.5 SERS Measurements

One of the integrated fiber optic cables carries excitation light from a diode laser (785 nm, 15 mW, Ocean Optics, Dunedin, FL), while the other collects the Raman-scattered photons (Fig. 3.2). Different angles between the two fiber optic cables (from 0° to 180°) were investigated using various device designs to optimize the collection of Raman photons; 90° proved to be the most efficient angle, which is in agreement with a previous report by Ashok et al.[136] As illustrated in Fig. 3.2, excitation and collection fiber optics were connected, respectively, to the 785nm diode laser and the Raman spectrometer (iHR550 Horiba JY). A band pass filter and a high pass filter (Omega Optical, Brattleboro, VT) used to reduce the optical background were located at the excitation and collection, respectively. For each experiment, the aggregated silver nanoparticles were mixed with selected concentrations of R6G for 15 min. The solution was then introduced into the channel at a flow rate of 2 μl/min for 2 min (consuming 4 μl) using a digital syringe pump (Fischer Scientific, Inc.). R6G concentrations of 100 pM, 1 nM, 10 nM, and 100 nM were each tested on three devices. A 1-s exposure time was used for 10 nM and 100

nM R6G. For the two lower concentrations, a 5-s exposure time was used. In all cases, the software automatically translated the measured optical intensity to counts/second. SERS measurements were also performed in the microsystem using the organophosphate malathion. Malathion was diluted in silver colloid solution down to 12 ppb and introduced into the channel at a flow rate of 2 µl/min for 5 min. A 5-s exposure time was used to collect Raman scattered photons.

3.3 Results and Discussion

A micrograph of the trapped microspheres within the microfluidic channel is shown in Fig. 3.2a. The packed porous silica microspheres act as a three-dimensional porous matrix to concentrate silver nanoparticles and adsorbed analyte molecules. Figure 3.2b shows the silica matrix after loading silver nanoparticles into the channel; the darkened region is the trapped nanoparticles. Scattered light from the microsphere matrix due to the excitation light from the fiber optic cable is shown in Fig. 3.2c.

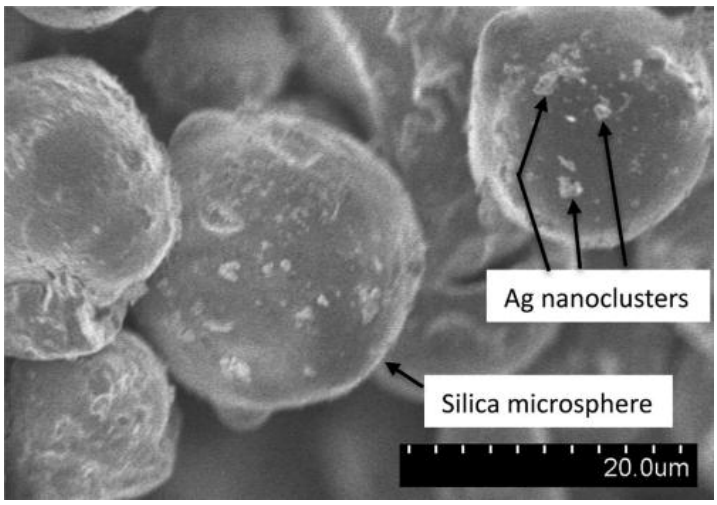

Figure 3.3 SEM micrograph of the silica microspheres packed into the microfluidic channel after running silver nanoclusters through the channel. The bright spots on the silica spheres are silver nanoclusters that became trapped in the matrix.

An SEM of the silica microsphere matrix inside the channel is presented in Fig. 3.3. As shown in the micrograph, silver nanoclusters are coating the surface of the silica beads with relatively high density. The clusters range in size from a few nanoparticles to a few tens of nanoparticles or on the order of 100 nm–1 μm. It is clear from this image that a relatively large number of SERS-active hot spots exist within the detection region as compared to the case of an open-channel system (i.e., Fig. 3.1c versus Fig. 3.1a).

To illustrate the capability of the device to effectively concentrate silver nanoparticles and adsorbed analyte, we recorded the Raman spectra at 20-s time intervals while loading the sample (Fig. 3.4). The well known Raman peaks of R6G at 1310, 1363, and 1509 cm^{-1} are visible after only a few seconds of loading; within 2 min, the R6G spectral bands increase dramatically.

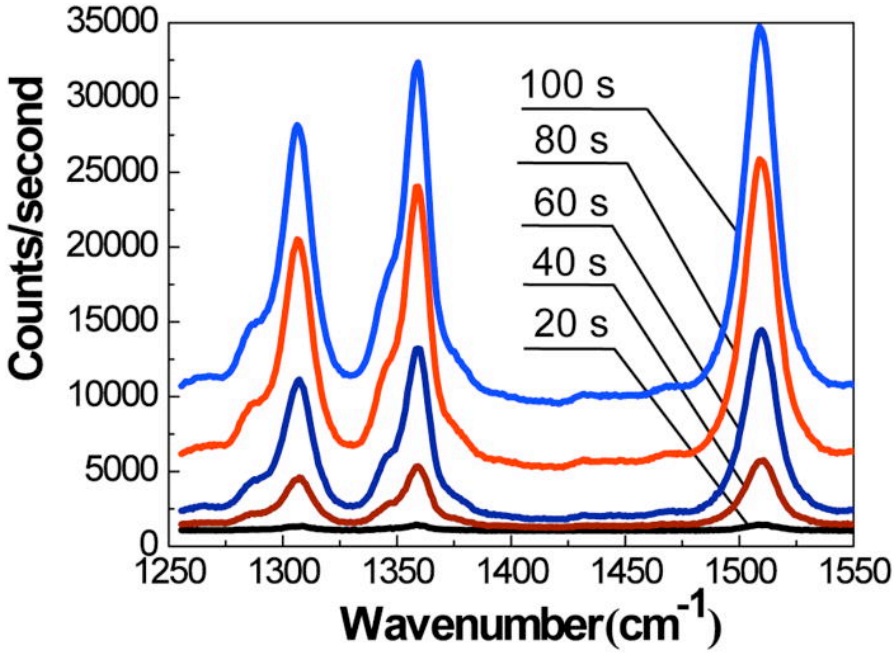

Figure 3.4 Time-dependent accumulation of SERS signal as silver nanoparticles with adsorbed R6G are trapped and concentrated within the porous matrix. R6G concentration in colloid=100 nM. Spectra are shifted vertically for visual clarity.

After 2 min of sample loading time, the signal exhibits saturation; even after 15 min of sample loading, the signal did not increase further. Thus, 2 min was determined to be the optimal sample loading time for the parameters used here. In all subsequent experiments with R6G, the sample is loaded for 2 min before the measurements are taken.

Intuitively, the trapping of silver nanoparticles with adsorbed R6G molecules provides a performance improvement as compared to an open microfluidic channel because of the increase in the number of analyte molecules in SERS-active hot spots within the detection volume.

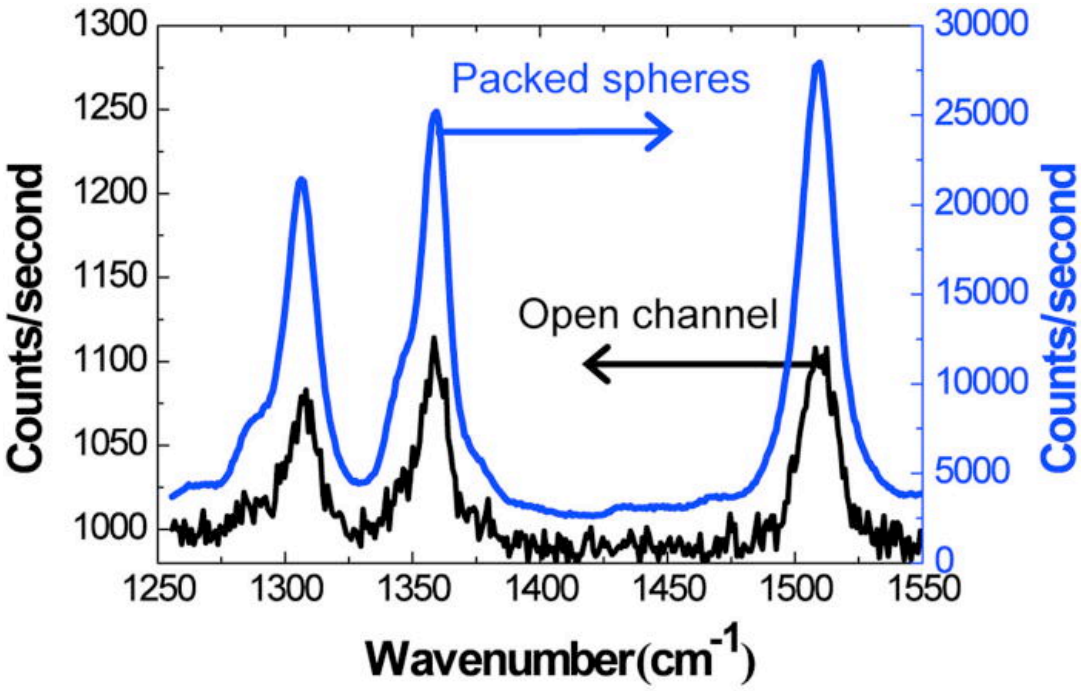

Figure 3.5 Within the porous matrix, the SERS signal is greater than 250 times more intense as compared to the open channel. R6G concentration in colloid=100nM.

To quantify the performance increase as compared to open-channel microfluidic SERS, the respective spectra of 100 nM R6G in silver colloid were measured in an open microfluidic channel and in the packed-microsphere matrix. In

both cases, the sample was loaded for 2 min at 2 µl/min. As shown in Fig. 3.5, the signal is more than 250 times stronger when using the packed microsphere matrix due to accumulation of analyte molecules and the additional formation of hot spots.

To determine the detection limit, the chip-to-chip repeatability, and the quantitative capabilities of the SERS device, we loaded various concentrations of R6G (100 pM–100 nM) in silver colloid into packed-microsphere matrices for 2 min. Each concentration test was performed on three separate chips. Figure 3.6 displays the mean intensity and standard deviation of the 1509 cm^{-1} Raman peak for each concentration of R6G. The Raman intensity is linearly proportional to the R6G concentration as depicted in Fig. 3.6a.

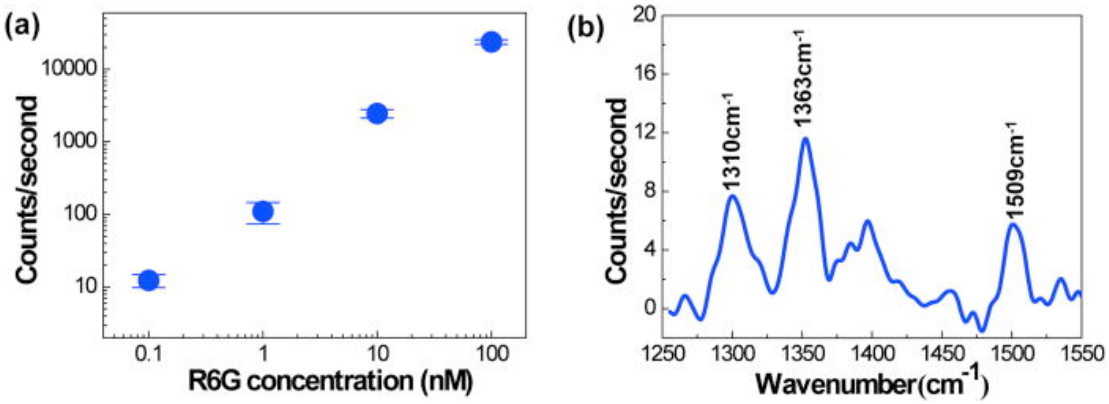

Figure 3.6 (a) Mean intensity of the 1509cm^{-1} Raman peak for various R6G concentrations. Error bars represent standard deviation, N=3. (b) Measured SERS signal after 4 µl of 100 pM R6G (400 attomoles) is loaded into the microchannel.

The linear trend and the low standard deviation demonstrate that this optofluidic SERS device is repeatable and can be utilized for quantitative detection of analytes. The high chip-to-chip repeatability is likely a result of the use of integrated multimode fiber optic cables. A high number of silver nanoclusters are concentrated into the relatively large detection volume defined by the fiber optic cables, which

reduces the statistical variation that is common for SERS techniques that use a small detection area or volume. Furthermore, the integrated fiber optic cables ensure that the detection volume is exactly the same from chip to chip and measurement to measurement; this may not be the case for measurements with typical Raman microscopes, which require manual focusing and alignment.

The recorded Raman spectrum for a concentration of 100 pM R6G is presented in Fig. 3.6b. The sample was loaded at 2 μl/min for 2 min, which implies that only 400 attomoles of R6G molecules were loaded into the device. Nonetheless, the 1310, 1363, and 1509 cm^{-1} Raman peaks are clearly visible in the recorded spectra. Thus, we can conclude that the use of the porous channel results in a detection limit of 400 attomoles of R6G in silver colloid solution.

Although R6G is a common model analyte for characterizing the performance of SERS analytical devices, it may not be representative of typical analytes that must be detected in practical measurements. R6G is positively charged in water, causing it to readily adsorb to negatively charged silver nanostructures; additionally, it has a large Raman scattering cross section. To demonstrate the use of the porous device studied in this work for practical samples, we detected the pesticide malathion in water. Malathion is a widely used organophosphate insecticide that can contaminate waterways after application in agricultural areas.

Figure 3.7 presents the malathion detection results in the microsystem. For an open microfluidic channel, we had to exceed the solubility of malathion in water (145 ppm) before we could detect a SERS signal (i.e., no signal was detected for less than 145 ppm). This is a drastic reduction in performance as compared to the result for

R6G in an open microfluidic channel (Fig. 3.5), in which less than 100 nM (47 ppb) can be detected. This difference in detection performance is due to malathion's lower affinity for the silver nanocluster surfaces and its decreased Raman cross-section.

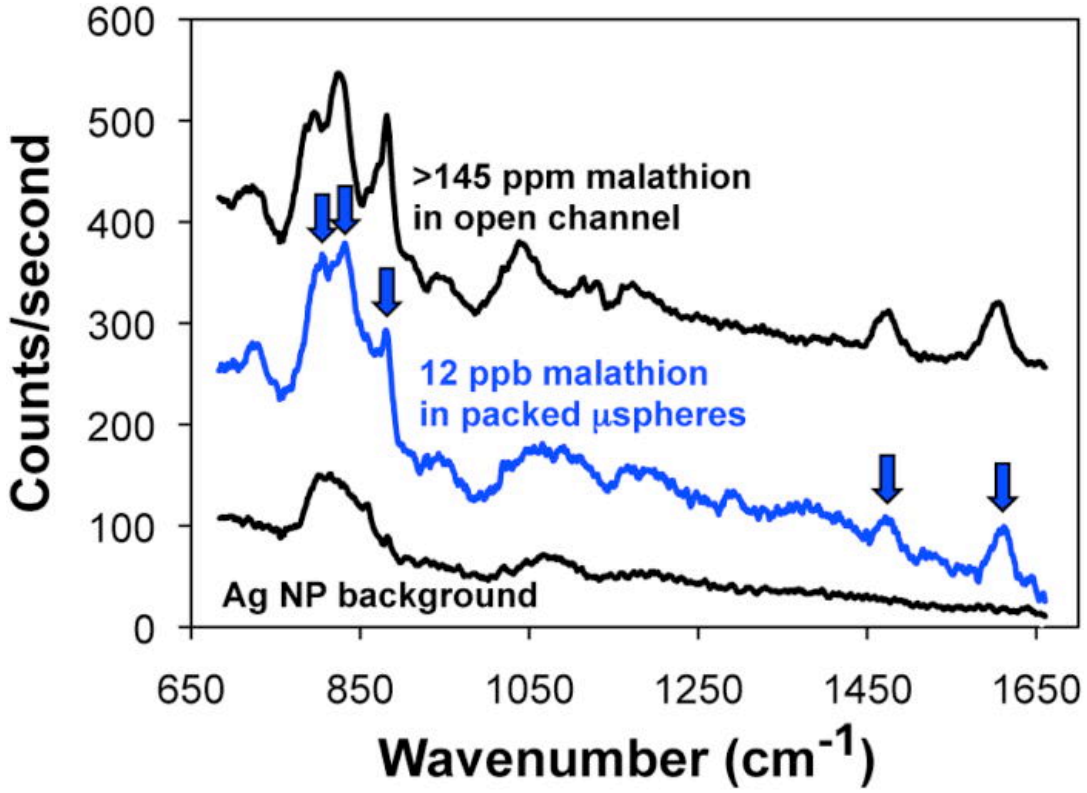

Figure 3.7 Recorded SERS spectra for greater than 145 ppm malathion in water (the solubility limit) in an open microfluidic channel and for 12 ppb malathion in water in the 3D porous matrix. Arrows indicate the Raman peaks for malathion. The background signal is also shown to enable the clear identification of the malathion Raman peaks.

However, our porous device recorded a SERS signal with only 12 ppb malathion in water after loading only 10 μl of sample. The SERS signal for 12 ppb malathion in the porous matrix is similar in intensity to the signal for greater than 145 ppm in the open microfluidic channel. This result demonstrates that the optofluidic SERS microsystem enables detection of the popular insecticide malathion, which is not detectable under practical conditions in a traditional microfluidic SERS device.

3.4 Conclusion

Collectively, the results presented here demonstrate that our easily fabricated optofluidic SERS device has a significantly improved performance as compared to conventional microfluidic SERS approaches. The porous matrix provides greater than two orders of magnitude signal enhancement due to sample concentration after only a few minutes of loading. This enables a detection limit of 100 pM R6G, even with only 4 µl of sample volume (i.e., 400 attomoles of analyte loaded into the microchannel). Furthermore, the device shows high linearity over a wide range of sample concentrations, and the measured results are highly repeatable from chip-to-chip. In addition, the three-dimensional porous matrix exhibits stable fluidic transport; it was observed that the silver colloid solution could be loaded through the matrix of silica microspheres for hours without clogging, which shows its capability to be used in assays requiring long reaction times. Finally, the use of a laser diode and alignment-free integrated fiber optic cables implies the potential for the device to be used in portable applications in the field. To illustrate one possible application for field-based SERS analysis in our microsystem, we detected the popular organophosphate insecticide malathion in water down to a concentration of 12 ppb.

In the next chapter, device's portability is improved even more by eliminating the need for a syringe pump for loading the sample. The sample is simply loaded utilizing a pipette by applying negative pressure. The device performance is examined by multiplexed detection of fungicides.

Chapter 4: Multiplexed Detection of Aquaculture Fungicides using a Pump-free Optofluidic SERS Microsystem[3]

4.1 Introduction

In this chapter, an optofluidic SERS device optimized for on-site analytics in the field is utilized for the multiplexed detection of three fungicides that are highly regulated in aquaculture. The optofluidic SERS microsystem does not require a bulky pump for sample loading, which significantly improves its portability; the sample is simply loaded into the device by applying negative pressure using a pipette. Moreover, integrated fiber optic cables automate sample excitation and signal collection without the need for alignment on a traditional Raman microscope. The detection zone of the device consists of a porous matrix of packed silica microspheres that accumulates silver nanoparticles and adsorbed analyte molecules. As presented in the previous chapter, this passive concentration matrix has been shown to boost the SERS signal by up to four orders of magnitude as compared to SERS in an open microfluidic channel. We were able to detect as low as 5 ppm methyl parathion, 0.1 ppb malachite green, and 5 ppb thiram simultaneously.

In chapter 3, we reported the development of a porous microchannel to passively concentrate AgNPs and analyte molecules. The increase in the number of analyte molecules and SERS active "hot spots" trapped in the detection volume leads to an increase in the SERS signal of up to four orders of magnitude as compared to

[3] **This chapter is adapted from: Soroush H. Yazdi and Ian M. White, Multiplexed detection of aquaculture fungicides using a pump-free optofluidic SERS microsystem, *Analyst*, 138, 100-103, 2013**

SERS in an open microfluidic channel. In addition, two fiber optic cables are inserted into the PDMS device via microchannels and aligned to the detection zone, which eliminates the need for a bulky microscope and for manual optical alignment before detection.

In this chapter, we report the multiplexed detection of three highly regulated aquaculture fungicides while greatly improving the portability and practicality of the system. We have eliminated the need for a syringe pump for sample loading by simply using a pipette and applying negative pressure from the outlet to load the sample droplet from the inlet. Fig. 4.1 presents the schematic of the device.

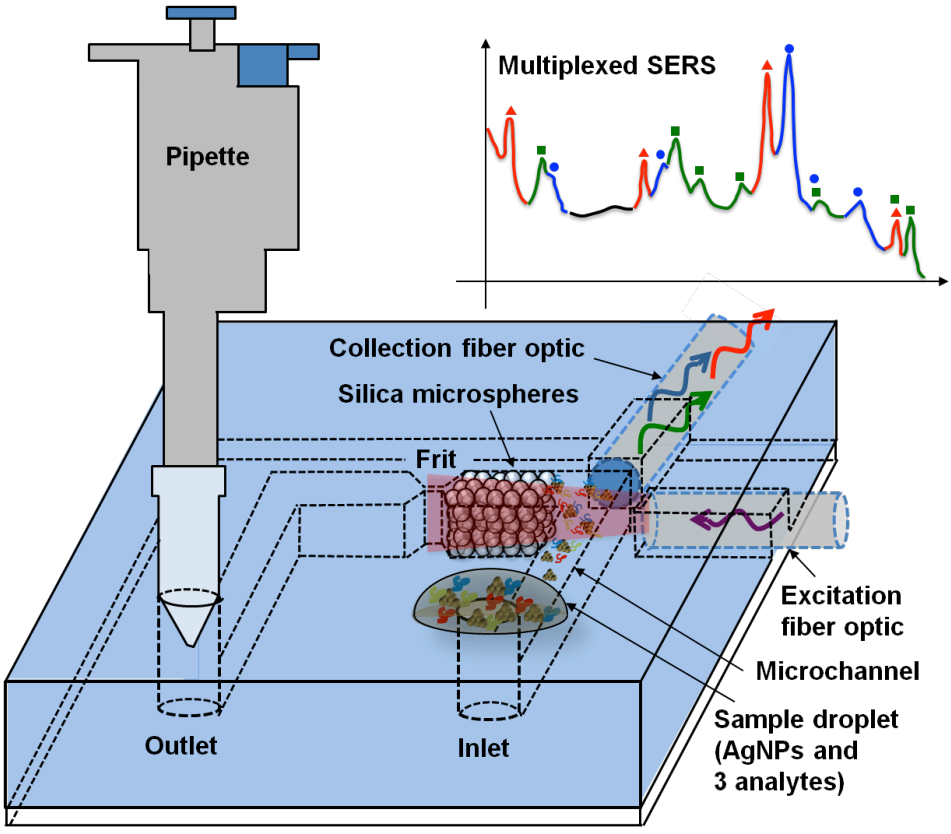

Figure 4.1 Concept of the pump-free optofluidic SERS device. Negative pressure from a pipette draws the sample into the channel. Packed silica microspheres trap and concentrate AgNPs and adsorbed analytes. Integrated fiber optic cables eliminate the need for a microscope.

The sample is drawn into the microsystem in a few seconds, which greatly improves the time for analysis as compared to using a syringe pump (2 minutes). As shown in the Figure 4.1, all that is necessary for on-site analysis with the optofluidic device is a pipette and a portable spectrometer system with a fiber optic interface.

To demonstrate a practical use of the optofluidic SERS microsystem for on-site analytics, we simultaneously detected methyl parathion, thiram, and malachite green. These fungicides have been used to control fungal infections in fish. However, their use is highly regulated due to potential toxicity to fish, as well as toxicity and carcinogenicity in humans.[137–139] As a result, there is a clear motivation to develop an on-site analytical tool that can simultaneously identify the presence of each of these fungicides in a single measurement. With our simple-to-operate SERS microsystem, we were able to detect simultaneously 0.1 ppb malachite green, 5 ppb thiram, and 5 ppm methyl parathion. While individual detection of these three fungicides using SERS has been reported in literature,[21,25,104,117,140,141] to our knowledge this is the first report of multiplexed detection of the fungicides with a SERS microsystem.

4.2 Experimental

4.2.1 Device Fabrication

The optofluidic microsystem was fabricated with polydimethylsiloxane (PDMS, Dow Corning) by standard photolithography techniques using silicon as the mold. The PDMS device was bonded to glass to seal the microchannels using a corona surface treatment. A frit is formed by narrowing the microchannel width from 125 μm to 20 μm in order to trap silica microspheres (15 μm, Kisker Biotech GmbH

& Co), which form a porous matrix to concentrate AgNPs and adsorbed analyte molecules. The surface of the silica microspheres was modified using 3-mercaptopropyltrimethoxysilane (3-MTS, Sigma) in order to improve AgNP capture within the detection zone. The 3-MTS modified silica microspheres were loaded into the device by placing a droplet of silica beads at the inlet and applying vacuum at the outlet. Two multimode fiber optic cables were inserted into PDMS through microchannels (125 μm in height) and aligned to the detection zone. We have shown previously that the use of multimode fiber optic cables aligned with the detection region reduces signal variability from device to device because there are a large number of silver nanoparticle aggregates within the detection region, making the device less vulnerable to the high variability of SERS "hot spots."

4.2.2 Silver Nanoparticle Synthesis

Silver nanoparticles were synthesized using the Lee–Meisel method. Sodium chloride (20 mM) was added to the AgNP colloid and mixed by vortexing the tube before the experiments to promote aggregation. Rhodamine 6G (Exciton), thiram (Sigma), malachite green oxalate (Sigma), and methyl parathion (Cerilliant) were used as the analytes.

4.2.3 SERS Measurements

For each experiment AgNPs were mixed with selected concentrations of analytes and introduced into the channel. Mixing was done by vortexing the solution in a microtube for a few seconds. As conceptually illustrated in Fig. 4.1, sample introduction was performed by placing a 4 μL droplet at the inlet and then applying a

vacuum at the outlet simply by using a 1000 µL pipette. Immediately after loading the sample, the Raman spectrum was acquired. For the SERS measurements, a 15 mW 785 nm laser diode was used for sample excitation and an iHR550 Horiba JY modular spectrometer was used to detect Raman scattered photons. An exposure time of five seconds was used in the measurements

4.3 Results

While it is visually evident that pipette-based sample injection pulls the sample through the device as effectively as the slow but systematic loading of a motorized syringe pump, the ultimate measure of comparability is in the detection performance and repeatability. In order to compare sample loading by a pipette versus a syringe pump, R6G was mixed with AgNPs and loaded into the device by either using a syringe pump or a pipette. For the syringe pump experiment, the sample was introduced into the channel at a flow rate of 2 µL min^{-1}; the SERS signal was recorded until it reached a maximum, which took 2 minutes (i.e., 4 µL sample passed through the silica bead matrix). In the pipette experiments, a 4 µL sample droplet was placed on the inlet and the sample was drawn into the device by applying negative pressure from the outlet using pipette. A 1000 µL pipette was used to ensure enough pressure for loading. The experiments were repeated three times, each on a different device.

Average SERS spectra for each sample loading procedure are shown in Fig. 4.2. The intensity of the measured SERS signal is quite similar for each case. Furthermore, we investigated the repeatability of the detection performance using the pipette. The error bars on three prominent R6G Raman peaks show the standard

deviation of the peak intensity. Across three trials, the relative standard deviation of the height of the three Raman peaks was only 7.4% (1310 cm^{-1}), 7.5% (1360 cm^{-1}), and 7.7% (1508 cm^{-1}). This indicates that pipette-based loading of the optofluidic SERS device results in a repeatable SERS signal. Finally, in addition to being highly repeatable and as effective as the syringe pump, the analysis time was reduced from 2 minutes (using the syringe pump) to approximately 5 seconds (using the pipette).

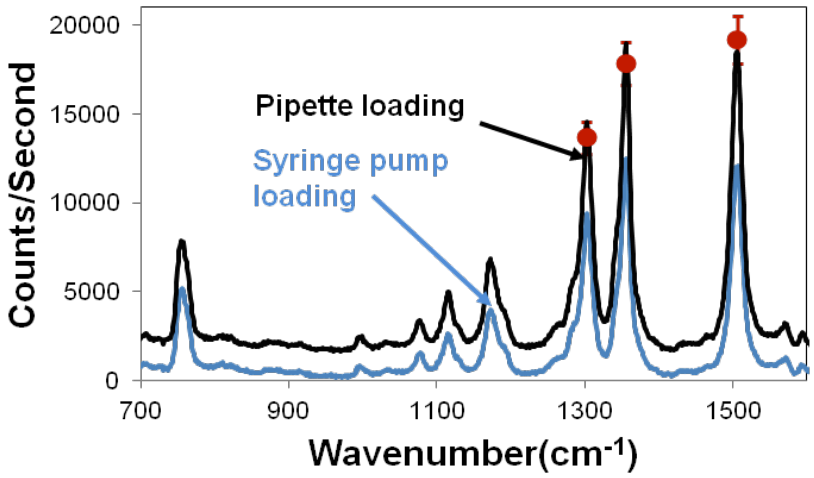

Figure 4.2 Representative SERS spectra acquired when loading R6G samples either by pipette or syringe pump. Error bars represent the standard deviation of the intensity of the peaks. Spectra are shifted vertically for clarity.

To demonstrate the simple-to-operate optofluidic SERS device for practical on-site analytical applications, we assessed the device's performance for detecting three highly regulated aquaculture fungicides. Before performing multiplexed detection of the fungicides, each fungicide was detected separately to investigate its SERS spectra. Methyl parathion, malachite green oxalate, or thiram was mixed with AgNP colloid and a 4 µL droplet was placed at the inlet and drawn into the microchannel using a pipette.

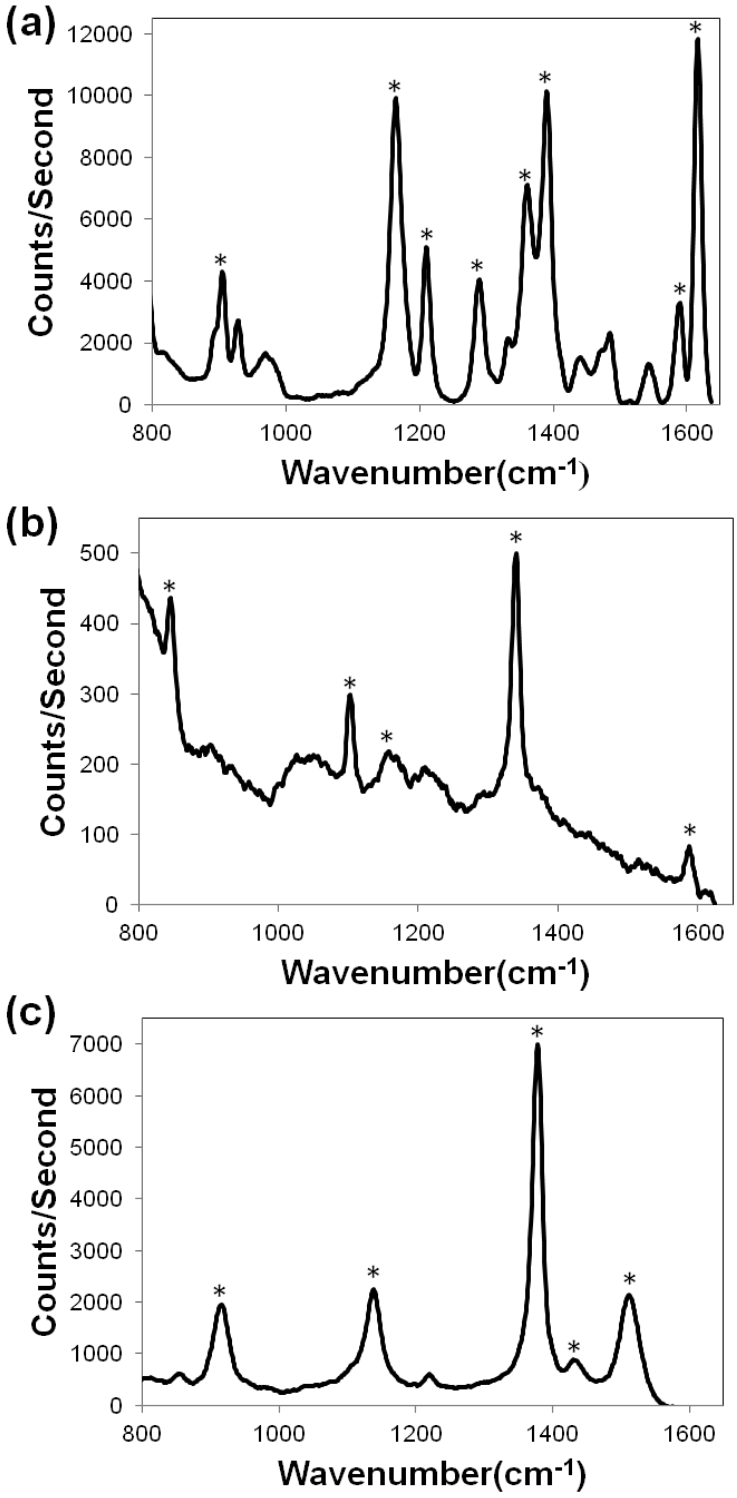

Figure 4.3 SERS spectra of (a) 50 ppb malachite green, (b) 10 ppm methyl parathion, (c) 50 ppb thiram.

Fig. 4.3 shows the SERS spectra of each fungicide. The major peaks of each fungicide are denoted in the spectrum. The major SERS peaks for malachite green oxalate are 902, 1162, 1208, 1286, 1359, 1387, 1585, and 1614 cm^{-1}. Methyl parathion is identified with peaks at 844, 1100, 1153, 1337, and 1583 cm^{-1}. The thiram peaks are located at 911, 1133, 1375, 1430, and 1508 cm^{-1}. Using our optofluidic SERS device, we are able to detect malachite green oxalate, methyl parathion, and thiram down to concentrations as low as 0.1 ppb, 5 ppm, and 1 ppb respectively.

Finally, the respective concentrations of the three fungicides were mixed together, added to the aggregated silver colloid, and pipetted into the device. The SERS spectrum for 0.1 ppb malachite green oxalate, 5 ppm methyl parathion, and 5 ppb thiram is shown in Fig. 4.4. Although the spectral peaks for thiram were visible at 1 ppb when detected alone, its presence at 1 ppb could not be confirmed in the multiplexing experiment because its most prominent peak, 1375 cm^{-1}, is masked by the malachite green spectral peaks at 1359 and 1387 cm^{-1}. However, at a concentration of 5 ppb, the thiram peaks at 1375 and 1508 cm^{-1} become apparent, thus enabling detection of all three fungicides simultaneously. This detection performance for each analyte is comparable to or better than current reports in the literature for the SERS-based detection of each fungicide individually[21,24,25,104,117,140,141], with the exception of the report by Lee, et al., in which methyl parathion was detected down to 100 ppb[21] (a superior optical system and larger integration times were used in that work).

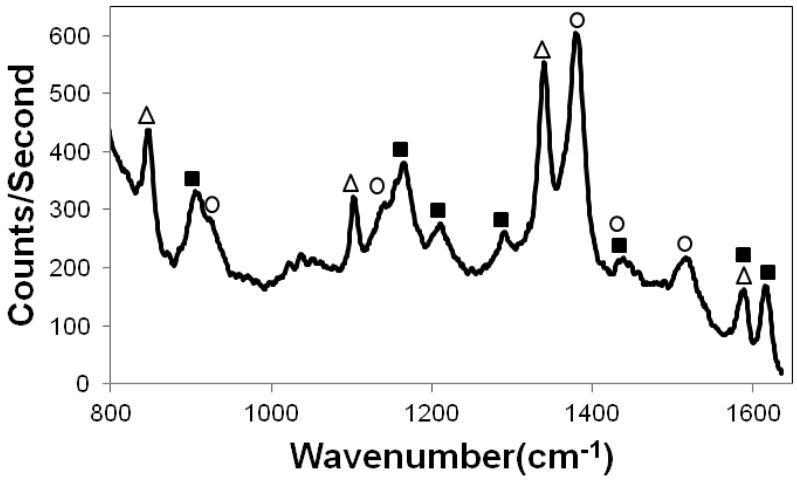

Figure 4.4 Multiplexed SERS spectrum of 0.1 ppb malachite green oxalate (■), 5 ppm methyl parathion (△), and 5 ppb thiram

4.4 Conclusion

To our knowledge, this represents the first report of multiplexed detection of these three fungicides using SERS. Moreover, our detection system is optimized for the on-site analysis of water samples to detect these and other fungicides at aquafarms. The user simply needs the microfluidic chip, a pipette, a sample vial, and a portable spectrometer system with a fiber optic interface. A microscope and a syringe pump, which are typically utilized in other microfluidic SERS reports, are not necessary.

In the future, the optofluidic SERS microsystem can be extended to many other applications that can benefit from on-site analysis, including pesticide detection in water sources, antibiotics detection in food and drinking products, and chemical analysis for forensics. In moving towards these and other applications, a number of practical considerations can be explored. First, although we are able to demonstrate simultaneous detection of three analytes by the identification of Raman peaks unique

to each analyte, the use of principal component analysis can enable us to increase the number of targeted analytes while also improving the detection limit. In addition, as the number of analytes increases, or as the sample matrix complexity increases, additional filtering and separation may need to be performed. For example, a membrane filter can be inserted at the inlet to remove particulates or microorganisms.

Furthermore, the microfluidic channel could be designed to provide chromatographic separation as well. One can envision an extension of the device reported here such that packed silica beads in the microfluidic channel are not only used to concentrate nanoparticles, but are employed as a chromatographic separation column to provide at least coarse separation of the molecular components of the sample.

Ultimately, we expect that the development of powerful yet portable and simple-to-operate devices are the key to differentiating SERS from traditional chemical analysis techniques used in central lab facilities. Optofluidic SERS devices, such as the one reported here, can enable low-cost measurements in the field, thus opening many new analytical applications. As a result, SERS may finally realize its potential as a highly sensitive and specific analytical technique for trace chemical and biomolecule detection.

The simple fabrication and the reliable, clog-free performance of the porous matrix implies that it can be integrated with other microfluidic functions such as on-chip mixing which will be presented in the next chapter. Integration of additional microfluidic functions allows higher automation as well as performing more complicated detection assays.

Chapter 5: An Optofluidic Surface Enhanced Raman Spectroscopy Microsystem integrated with an on-chip micromixer[4]

5.1 Introduction

In this chapter, we demonstrate highly sensitive detection of real-world food and water contaminants. using a portable and automated optofluidic surface enhanced Raman spectroscopy (SERS) microsystem. A passive micromixer that mixes silver nanoparticles into the sample solution is integrated into the device for improved automation.

Using the optofluidic SERS device, the food contaminant melamine was detected in low concentrations, with an estimated limit of detection (LOD) of 63 ppb, while the fungicide thiram was detected down to an estimated LOD of 50 ppt. In both cases, the reported results meet the U.S. federal requirements.

Additionally, it is shown that the device continues to exhibit excellent performance even when mated to a commercially available portable spectrometer for the trace detection of thiram. This combination of the optofluidic SERS microsystem with a portable spectrometer will lead to highly sensitive and automated sensing systems for on-site detection of food and water contaminants in the field.

As stated previously, active concentration techniques to enhance the SERS signal may require additional fabrication steps (e.g., metal electrodes) and active

---

[4] This chapter is adapted from: Soroush H. Yazdi and Ian M. White, An Optofluidic SERS Microsystem for Sensitive and Repeatable On-Site Detection of Chemical Contaminants, *Analytical Chemistry*, 84, 7992-7998, 2012.

components (e.g., power supplies), resulting in more cost and complexity and less portability of the final device. On the other hand, utilizing a single nanochannel that passively concentrates analytes/nanoparticles risks clogging and may require long sample loading times. Moreover, nanofabrication can be complicated and less repeatable as compared to well-established microfabrication techniques.

In the previous chapters, we have demonstrated an optofluidic SERS microsystem that utilizes packed silica microspheres in a microfluidic channel to passively concentrate silver nanoparticles and adsorbed analyte molecules prior to detection. Numerous micro/nanofluidic channels that trap silver nanoparticles are formed within the flow path without the need for nanofabrication. This approach is less prone to clogging as compared to single nanochannel designs, and it results in high repeatability.

In this chapter, we build upon our passive concentration technique by implementing a highly automated and sensitive chemical detection microsystem consisting of a porous microfluidic concentration and detection zone integrated with an on-chip micromixer. The schematic of the device is shown in Figure 5.1.

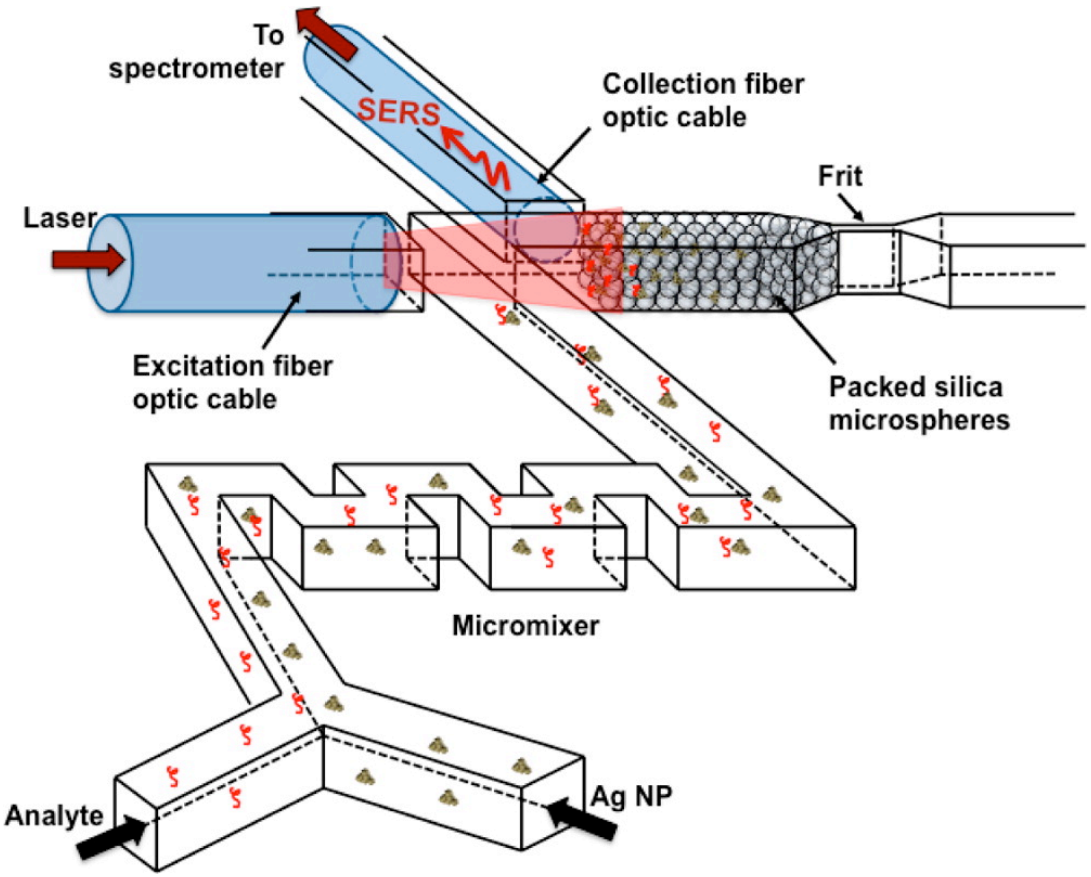

Figure 5.1 Optofluidic SERS microsystem with packed microspheres for passive concentration, an integrated micromixer to promote adsorption of the target analyte, and integrated fiber optic cables for optical excitation and collection.

The microsystem features a passive mixer to combine the silver colloid solution and sample solution and to promote adsorption of analyte molecules onto the silver nanoclusters. To utilize the device in the field, the sample is loaded into one inlet while a silver colloid is simultaneously loaded at the other; the sample does not need to be added to the colloid and manually mixed before loading. As nanoparticle–analyte aggregates flow out of the on-chip mixer, they become trapped in the packed column of silica microspheres. Integrated fiber optic cables are aligned to this trap

and are used to acquire the SERS signal from the concentrated nanoparticle–analyte aggregates.

On-chip mixing has been utilized in previous reports to promote the interaction between multiple independent streams of analytes inside a microfluidic device. Active mixers typically utilize electric fields,[142,143] thermally induced bubbles,[144] magnetic silica beads,[145] or ultrasound[146,147] to improve mixing in the microchannels. While these active mixing methods are effective, passive mixers do not require the incorporation of additional materials into the microdevice, additional fabrication steps to incorporate these materials, or the use of external equipment to supply the necessary energy. Passive microfluidic mixers have also been reported for on-chip mixing of multiple streams in microsystems.[148–150] Moreover, passive mixers have been used for improved interaction of AgNPs and analytes for SERS detection.[104–106] In these reports, angled step structures are fabricated into the top and bottom of the channel, which requires the careful alignment during assembly of the device; these fabrication steps can complicate the fabrication and increase the cost of the device. Herein, we utilized a simple-to-fabricate micromixer to promote interaction between silver nanoparticles (AgNPs) and analyte molecules. As shown in Figure 5.1, the mixer consists of blocks protruding from the channel sidewalls to promote mixing; no alignment is necessary between the top and bottom of the device. Importantly, the simplicity and low cost of fabrication enable the device to be disposable, which is important for a technique such as SERS that is highly sensitive to contaminating molecules.

After passive mixing of silver nanoparticles and analyte molecules, they are trapped in the silica microsphere matrix, which is formed against a frit in the microfluidic channel. We leverage a number of advantages of the use of packed silica microspheres as a concentration matrix. First, we applied simple surface chemistry modification techniques to generate thiol groups on the surface of the silica microspheres, which promote the capture of silver nanoparticles in the silica microsphere matrix. Second, while other materials, including polymers, can be used to form porous microfluidic channels, silica has very little optical absorption, which is important in SERS detection. Finally, in contrast to single nanofluidic channels, packed microspheres form numerous channels, which improves the device throughput.

Upon capturing and concentrating silver nanoparticles and adsorbed analyte molecules in the silica microsphere matrix, the SERS signal can be acquired. Typically, when applying the SERS technique to microfluidic devices, a confocal Raman system is used. The microfluidic device is placed under a microscope objective, which must be aligned and focused. However, this may not be an appropriate technique for on-site detection in the field. In our design, two fiber optic cables are prealigned to the detection zone for excitation of the sample and collection of the scattered photons (Figure 5.1). Thus, instead of alignment and focusing, the user simply connects the fiber optic cables from the device to a portable spectrometer and laser diode; this improves the ease-of-use and the chip-to-chip repeatability.

We demonstrate the performance of our device by detecting two potential food/water contaminants. Melamine, a nitrogen-based compound, is illegally added to

food products to bolster the apparent protein content. It can cause kidney stones and renal failure. The safety/risk assessment performed by the U.S. Food and Drug Administration (FDA) set the maximum limit of 2.5 ppm for levels of melamine in foods.[151] Melamine detection using SERS has been reported previously, with detection capabilities as low as 50 nM (6.3 ppb).[22,152–154]

We also detected thiram, a fungicide that is used to prevent crop damage in the field and to protect harvested crops from deterioration in storage or transport. It is also used as a seed protectant and to guard turf from fungal diseases. Thiram is a neurotoxin and can cause lethargy and reduced motor activity. The U.S. Environmental Protection Agency (EPA) has set a maximum limit of 1 ng/mL (1 ppb) for contaminants (e.g., pesticides, fungicides, etc.) in water. Thiram detection with SERS has been also been reported in the literature, including detection down to 2 ppb.[25,155–157]

Using our optofluidic SERS device, we demonstrate trace detection of melamine and thiram at levels below the U.S. federal requirements. On the basis of the results presented here, the calculated detection limit is 63 ppb for melamine and 50 ppt for thiram. While these detection limits are on the same order as many of the previous reports in the literature, the detection system reported here is optimized for on-site detection of trace concentrations of contaminants in the field. Fiber optic connectivity, the capability to integrate sample processing functions, and microfluidic sample handling with nanofluidic sample concentration provide the necessary detection performance, repeatability, and ease of use for sample analysis in the field.

5.2 Experimental Section

5.2.1 Preparation of Silver Nanoparticles

Silver nanoparticles (Ag NPs) were synthesized by the Lee and Meisel method. Briefly, 90 mg of silver nitrate (Sigma) was dissolved in 500 mL of deionized water. The solution was brought to the boiling point in a flask while stirring. Then, 100 mg of sodium citrate (Sigma) was added, and the solution was boiled for 10 min, after which the solution color had turned greenish brown. Sodium chloride (10 mM, Sigma) was added to the silver nanoparticle solution to promote aggregation before running each experiment. According to scanning electron microscopy (SEM) images, Ag NPs are approximately 70 nm in diameter and form clusters of tens of nanoparticles.

5.2.2 Micromixer Design and Simulation

Using COMSOL 4.1, we simulated the nanoparticle mixing in the micromixer by modeling convection and diffusion under laminar flow and solving the Navier–Stokes equations. The diffusion coefficient of silver nanoparticles is estimated using the following equation[158] in which D is the diffusion coefficient and W is mass of the particle in Daltons:

$$D = 1.013 \times 10^{-4} \times (W)^{-0.46} \quad (2)$$

In the simulations, we considered only low flow rates (1–10 μL/min) in our design because higher flow rates would cause high-pressure build-up due to the packed silica microspheres. The channel width and height throughout the mixing zone is 50 μm × 125 μm.

5.2.3 Thiol-Modification of Silica Microspheres

The surface of the silica microspheres (Kisker Biotech GmbH & Co) was functionalized with thiol groups, which have a high affinity to silver, to improve the adsorption of silver nanoparticles to the silica bead matrix. Surface modification was performed by first adding 100 μL of silica microspheres in water to 500 μL of methanol. Then, 50 μL of (3-mercaptopropyl)trimethoxysilane (3MTS) (Sigma) was added to the solution. The solution was rocked for 24 h to ensure a high density of thiol groups on the surface of the silica microspheres. After mixing, the silica beads were spun down by centrifugation and the supernatant was replaced with methanol for rinsing. Rinsing was repeated three times. The thiol-modified silica microspheres were suspended in water (5 mg/mL) before being loaded into the optofluidic device.

5.2.4 Fabrication of the Optofluidic Device

The PDMS microfluidic device was fabricated with typical soft lithography methods. Briefly, AZ 4620 (AZ Electronics Materials) was spun and patterned on a silicon wafer (University Wafer) using standard photolithography. Then, the silicon mold was etched by deep reactive ion etching (DRIE) to a depth of 125 μm. The height of 125 μm was selected to fit the standard size of the integrated fiber optic cables. Vapor-phase silanization of the silicon mold with fluoro-silane (Pflatz and Bauer) was performed to enable removal of the PDMS (Dow Corning). Then, PDMS was poured onto the silicon wafer, and air bubbles were removed by applying a vacuum. The PDMS was cured at 60 °C for 4 h. Finally, the PDMS channels were sealed onto a piranha-cleaned glass substrate through corona treatment and stored at

60 °C overnight (piranha solution is exothermic and strongly reacts with organic compounds; it should be used with extreme caution).

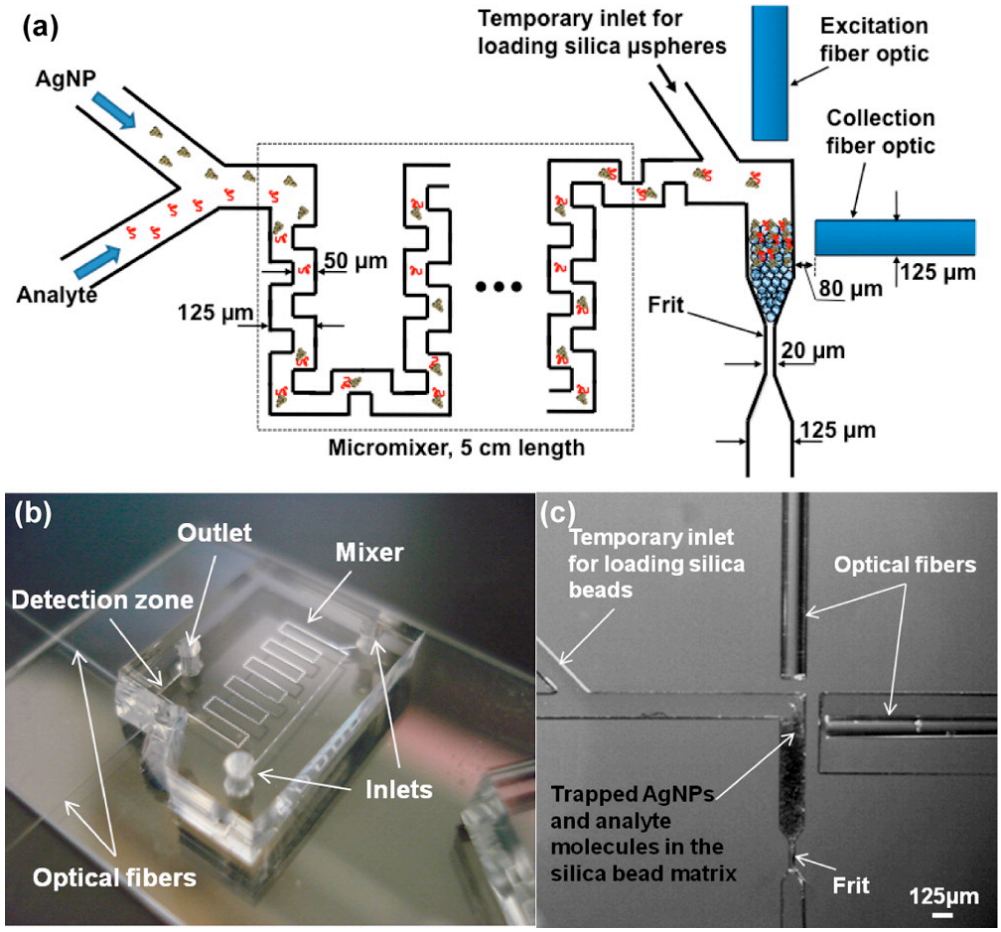

Figure 5.2 (a) Schematic of optofluidic SERS microsystem. (b) Photo of optofluidic SERS microsystem. (c) Micrograph of packed microspheres and integrated fiber optic cables.

A schematic of the final device is presented in Figure 5.2a. Silica microspheres were trapped against a frit structure inside the microchannel. The 125 μm channel narrows to a width of 20 μm at the frit. An additional temporary inlet was included near the frit to enable the loading of silica microspheres (microspheres may become trapped in the tortuous micromixer, and thus, it is necessary to load the microspheres immediately at the inlet to the frit). The temporary inlet was sealed with

silicone rubber (Dow Corning) after loading the microspheres. A 1 μL droplet of silica microspheres was placed at the temporary inlet and packed inside the channel by applying vacuum from the outlet. Devices were used within one day of loading microspheres.

Channels (125 μm × 125 μm) were formed within the PDMS near the detection region to enable the integration of fiber optic cables. The distance from the fiber optic tips to the detection zone in the microfluidic channel was designed to be 80 μm; this was experimentally determined to be the minimum distance that can prevent sample leakage from the microfluidic channel into the fiber optic channels. An image of the final optofluidic SERS device is illustrated in Figure 5.2b. The device is 1.7 cm × 1.2 cm. The packed silica microspheres are also shown in Figure 5.2c.

5.2.5 SERS Measurements

A 785 nm diode laser (10 mW, Ocean Optics) excites the sample via the excitation fiber optic cable. The second fiber optic cable collects the scattered photons and guides them to the Raman spectrometer (iHR550 Horiba JY or Ocean Optics QE65000). A band-pass filter and a high pass filter (Omega Optical) used to reduce the optical background are located at the excitation and collection, respectively. For each experiment, the aggregated silver nanoparticles were introduced to one inlet while selected concentrations of melamine or thiram were introduced to the other inlet at a flow rate of 2 μL/min for 1 min using a digital syringe pump (Fisher Scientific). Melamine concentrations of 125 ppb, 1.25 ppm, 12.5 ppm, and 125 ppm were each tested on three devices. For thiram, concentrations

of 1 ppb, 10 ppb, 100 ppb, and 1 ppm were tested in the same way. A one-second exposure time was used for all the concentrations when utilizing the iHR550 Horiba JY spectrometer. A five-second exposure time was used for the Ocean Optics QE65000 spectrometer.

Estimated detection limits are calculated through the following steps. First, the standard deviation of the background noise is measured. The minimum signal level required for detection is taken as three times the standard deviation (3σ). The detection limit is then calculated by interpolating from the concentration dilution curves the minimum concentration that results in a signal larger than the 3σ level.

5.3 Results

The integrated micromixer improves the device automation by mixing the analyte and silver nanoparticles inside the chip before SERS measurements, thus reducing the number of manual preparation steps for sample detection. Additionally, integration of the micromixer and other laboratory functions into the optofluidic device leads to more complicated assays such as DNA sequence and protein detection with high automation. To verify that our simple-to-fabricate microfluidic mixer is sufficient to mix the silver colloid with the sample, we simulated the concentration of nanoparticles throughout the mixer under flow conditions. The result of the simulation for the micromixer and the comparison with a straight channel are shown in Figure 5.3. The approximate diffusion coefficient of silver nanoparticles (~70 nm) was calculated to be 6.8×10^{-9} cm^2/s using eq 2. On the basis of these results, for the flow rate of 2 μL/min, silver nanoparticles are completely mixed after the sample

travels 8 mm along the mixer. To enable the analyte molecules to adsorb onto the nanoparticles after mixing, the mixer is designed to be 5 cm in length.

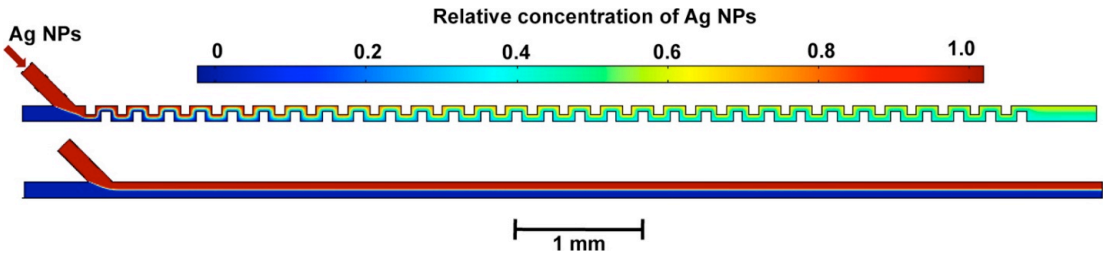

Figure 5.3 COMSOL simulation results, demonstrating that AgNPs are completely mixed throughout the microfluidic mixer within 8 mm, while for a straight channel mixing of the AgNPs does not occur.

We verified the simulation results of the on-chip micromixer by imaging the mixing process on the optofluidic SERS chip. Figure 5.4 shows the progress of the mixing of the silver nanoparticles and sample solution. The nanoparticles and R6G dye appear to be completely mixed after 8 mm, in accordance with the COMSOL simulation. We then compared the performance of on-chip mixing with off-chip mixing by measuring the SERS detection performance for each case. First, 100 nM R6G was mixed with silver nanoparticles on-chip utilizing the on-chip micromixer, and the SERS signal from the accumulating nanoparticles/analyte in the silica microsphere matrix was recorded. Then, 100 nM R6G was premixed with silver nanoparticles in a 1.5 mL centrifuge tube by vortexing the tube; this solution was then introduced into the packed silica matrix on a chip with no on-chip mixer, and the SERS signal was recorded. Figure 5.5 compares the R6G SERS signal using on-chip and off-chip mixing. The average peak height of the on-chip mixing SERS signal is 88% of the off-chip mixing signal (three trials), demonstrating that the on-chip

micromixer promotes adsorption of the analyte molecules onto silver nanoparticles nearly as well as manual sample mixing in a vial.

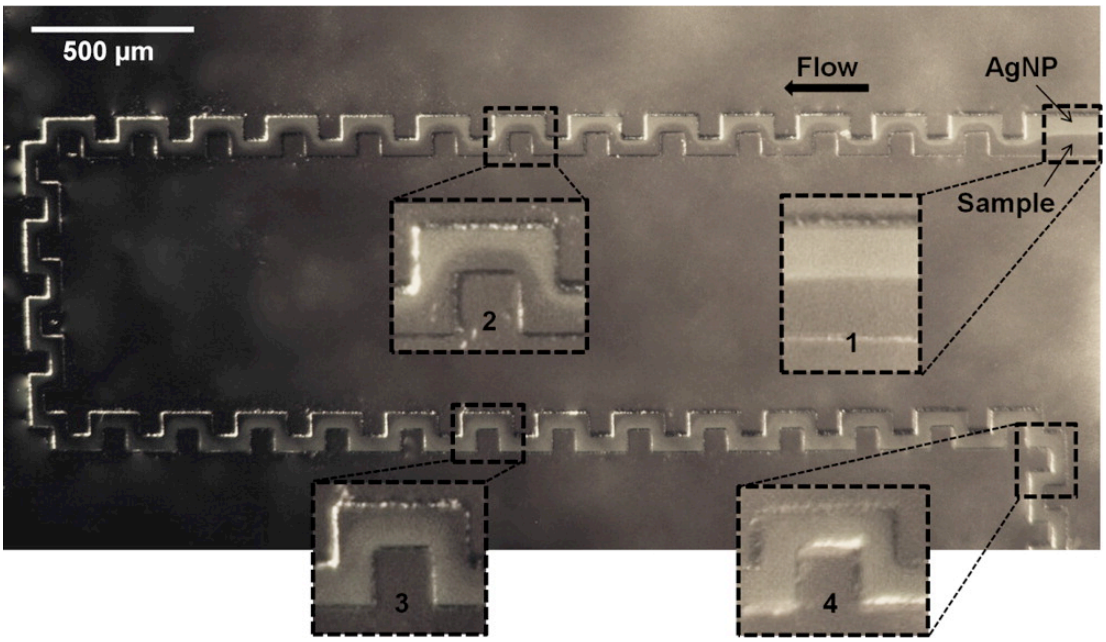

Figure 5.4 Micrograph verifying the mixing of AgNPs with the sample. At the inlet (1), the discrete separation of the two flows is evident, while at (4), after 8 mm in the channel, the AgNPs are mixed throughout the channel.

In order to investigate the SERS performance of the device in practical applications, melamine solutions (0.125–125 ppm) were prepared and introduced into one inlet. Aggregated silver nanoparticles were also pumped into the other inlet. Solutions were pumped for 1 min; after that time, the measured SERS signal intensity had reached its maximum. Figure 5.6a,b presents the melamine SERS signal for the four tested concentrations. The Raman peak due to melamine is evident at 690 cm^{-1} even for as low as 125 ppb melamine, which is 20 times better than the FDA requirement.

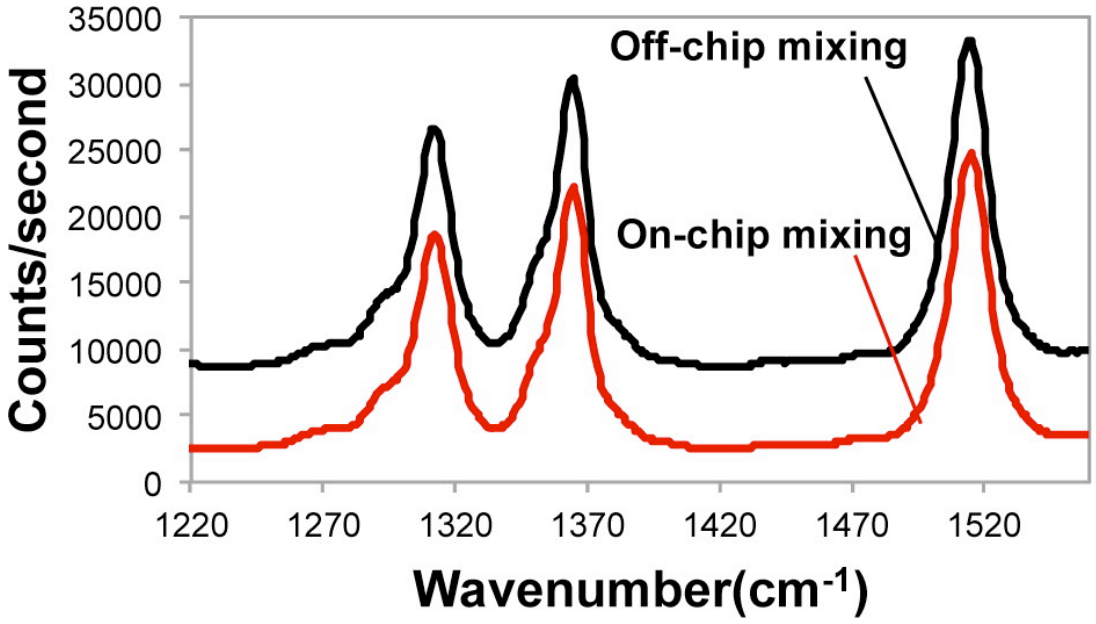

Figure 5.5 Comparison of the SERS signal acquired for R6G when off-chip mixing and on-chip mixing are used.

Figure 5.6c shows the dynamic range and chip-to-chip repeatability of the device. The data exhibits a Langmuir relation ($R^2 = 0.999$) between the height of the 690 cm^{-1} Raman peak and the melamine concentration, implying that detection of melamine can be quantitative. The low variation of the measured peak heights demonstrates the high chip-to-chip repeatability. The calculated detection limit for the device is 63 ppb on the basis of three standard deviations of the background signal.

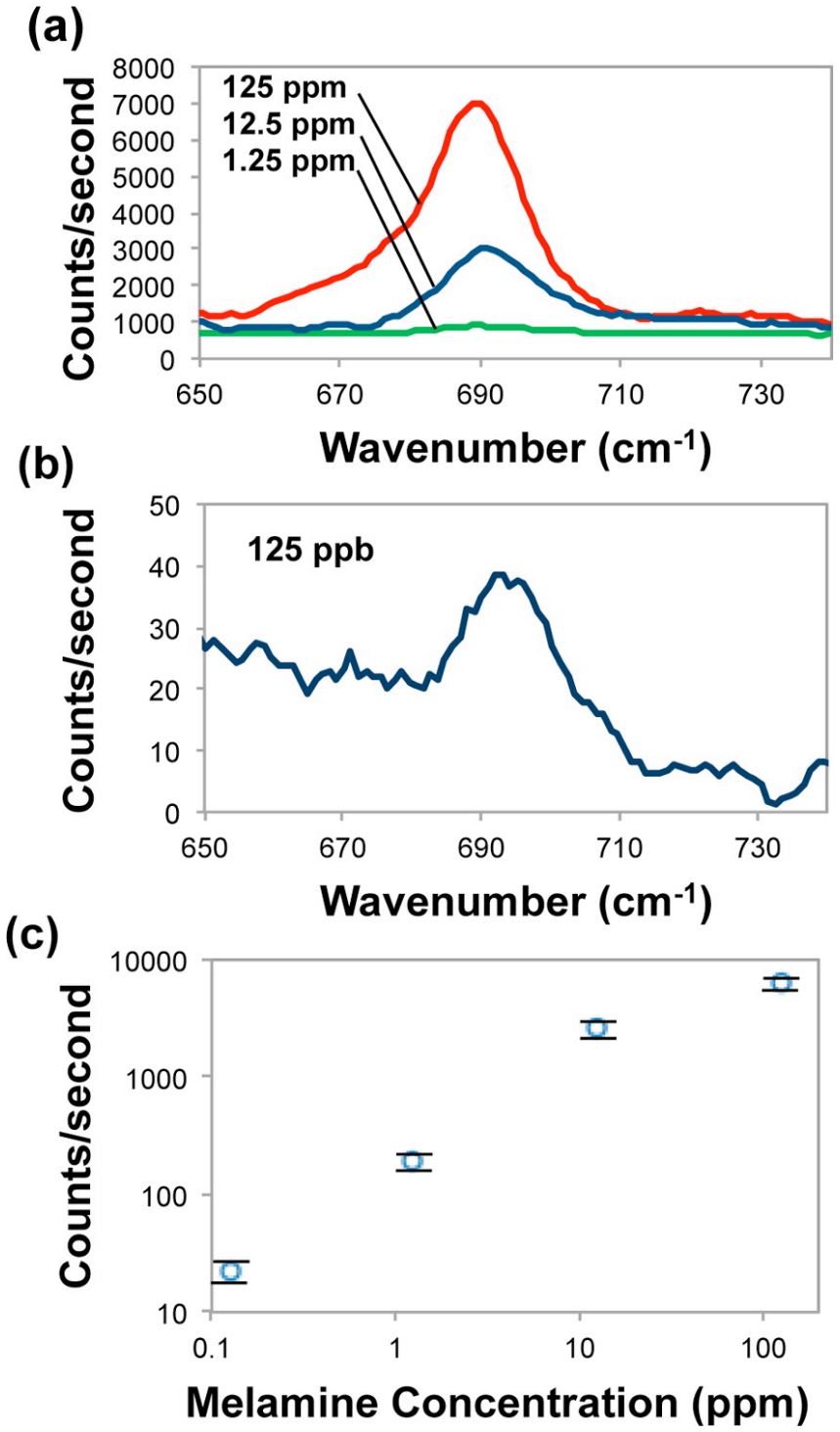

Figure 5.6 Detection of melamine in the optofluidic SERS microsystem. (a) Acquired SERS spectra for 125, 12.5, and 1.25 ppm melamine. (b) Acquired spectra for 125 ppb melamine. (c) Height of the 690 cm^{-1} Raman peak vs melamine concentration. Data points represent the average of three trials while the error bars represent the standard deviation.

In order to estimate the detection improvement due to sample concentration as compared to a conventional open microfluidic SERS device, in which there is no sample accumulation, we premixed melamine and silver nanoparticles and introduced them into an open microfluidic channel (no concentration matrix). Again, two optical fibers were aligned to the detection zone to excite and collect the sample. As is shown in Figure 5.7, our device improves the detection limit for melamine by a factor of approximately 100. This experiment was repeated three times with similar results.

To further illustrate the practical uses of our optofluidic SERS device, we detected the fungicide thiram in water. Four concentrations of thiram (1–1000 ppb) were prepared and tested using the optofluidic SERS device. The thiram sample was pumped into one inlet while AgNPs were pumped through the other inlet.

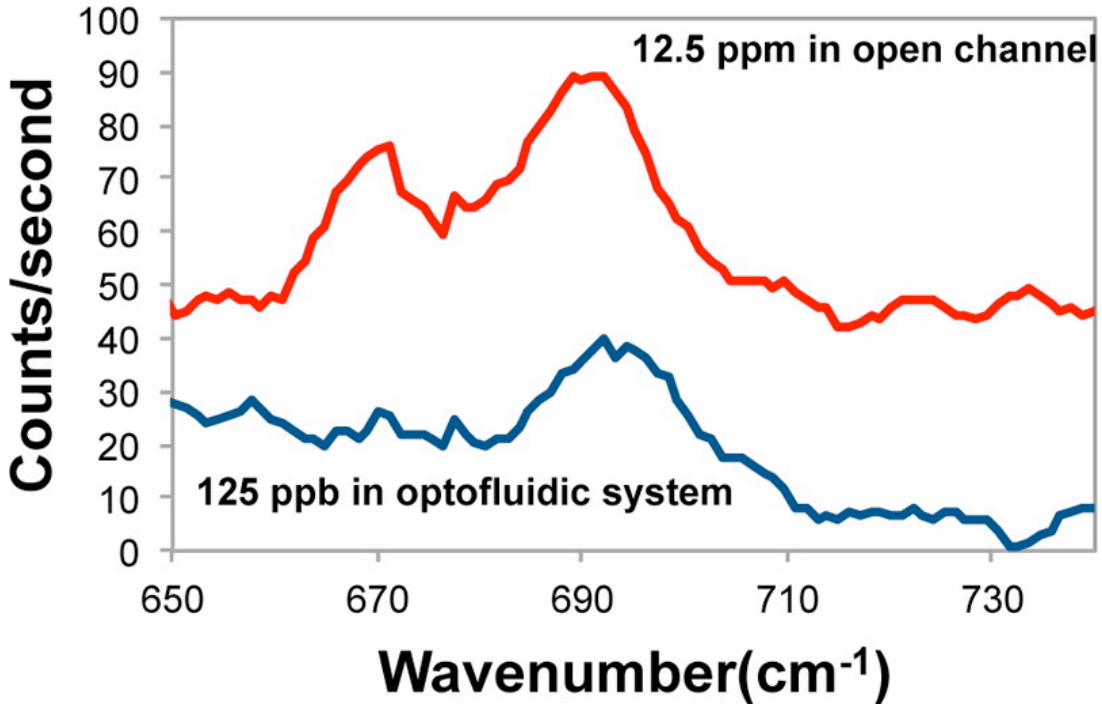

Figure 5.7 Comparison of melamine detection in an open channel (12.5 ppm) and in the packed silica microsphere (125 ppb) detection region. The passive concentration improves the detection limit by 2 orders of magnitude.

Measurements for each of the four tested concentrations were repeated 3 times. The results presented in Figure 5.8a,b show that the highest thiram SERS peak (1380 cm^{-1}) is easily visible in the signal, even with a concentration as low as 1 ppb. The calculated detection limit for thiram is calculated to be 0.05 ppb based on three standard deviations of the background. Figure 5.8c shows the repeatability and quantitative analysis of thiram detection. The thiram SERS intensity shows a good fit with the Langmuir equation ($R^2 = 0.993$), thus demonstrating the capability for quantitative analysis of the sample concentration. Additionally, the low standard deviation of the data points illustrates the high chip-to-chip repeatability.

The results presented illustrate that the optofluidic SERS device is well-suited for field use. The fiber optic interface eliminates the need for a microscope, and the microsystem design enables functions, such as mixing, to be integrated on-chip in order to save preparation steps in the field. To verify that the performance of the device is sufficient for field use, we detected thiram using the optofluidic SERS chip and a portable Raman spectrometer. The spectrometer, a QE65000 from Ocean Optics, features a small footprint and a fiber optic interface and can be carried in one hand. Along with the 785 nm laser diode, the entire system can easily fit in a portable unit.

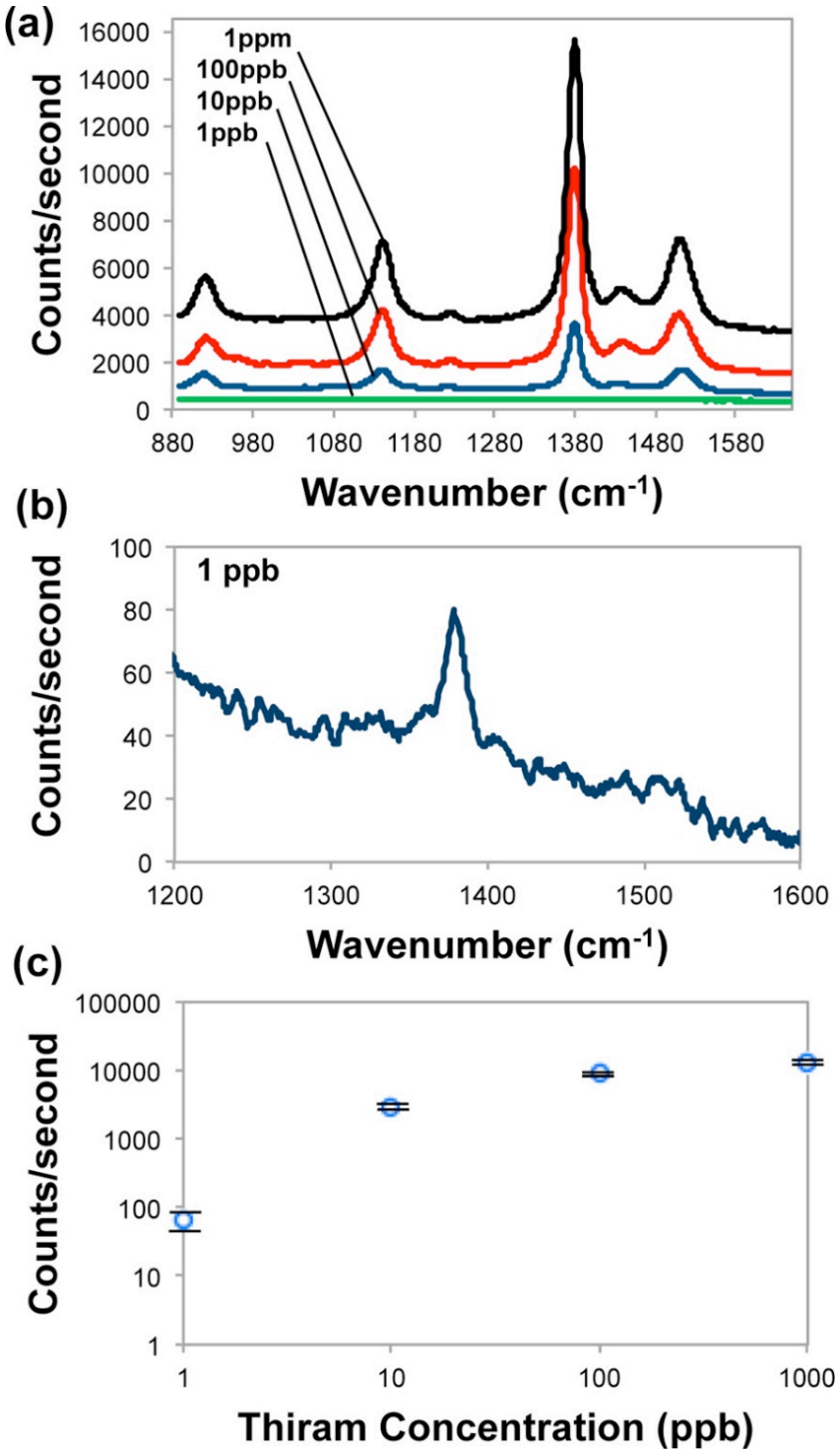

Figure 5.8 Detection of thiram in the optofluidic SERS microsystem. (a) Acquired SERS spectra for 1 ppm, 100 ppb, 10 ppb, and 1 ppb thiram. (b) Acquired spectra for 1 ppb thiram. (c) Height of the 1380 cm^{-1} Raman peak vs thiram concentration. Data points represent the average of three trials while the error bars represent the standard deviation.

Figure 5.9 shows the SERS spectrum for 8 ppb thiram when the portable spectrometer is used to collect the signal. Comparing this signal to the spectrum collected using the larger spectrometer and considering the signal-to-noise ratio, it is clear that the detection limit is worse by less than only 1 order of magnitude when the portable spectrometer is used. As a result, the combination of the optofluidic SERS device and a portable system that is appropriate for field use is capable of detecting contaminants below the U.S. federal requirements.

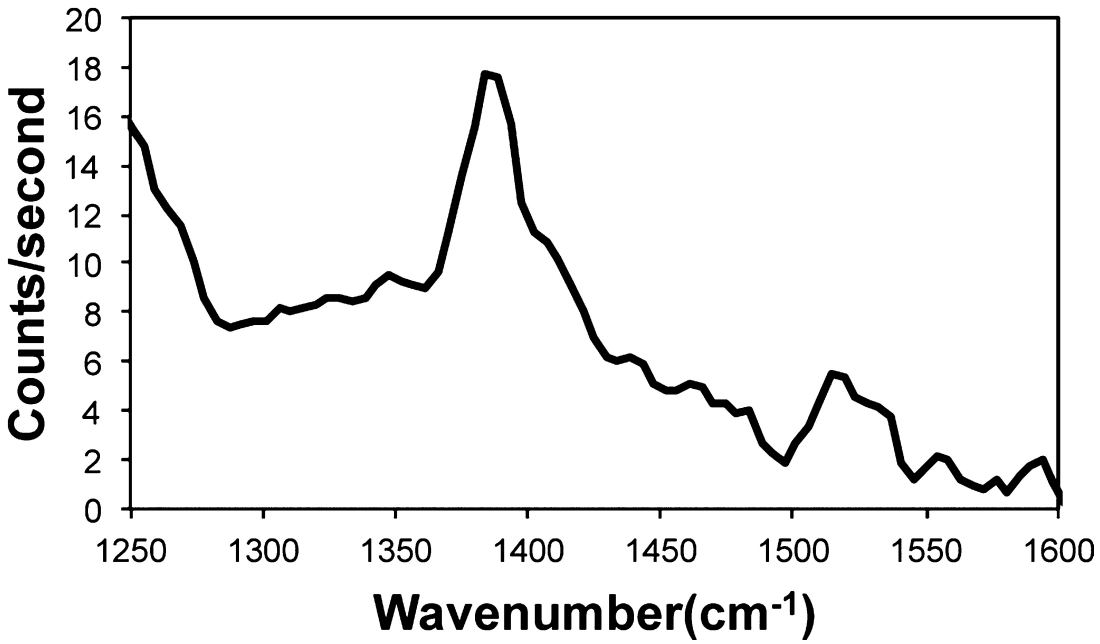

Figure 5.9 SERS spectrum of 8 ppb thiram recorded with a portable spectrometer.

5.4 Conclusion

Collectively, the results presented here demonstrate the advantages of our optofluidic SERS microsystem for the on-site detection of chemical species. The packed silica microspheres in the detection zone concentrate silver nanoparticles and adsorbed analytes, thus significantly boosting the signal as compared to conventional microfluidic SERS. The on-chip mixer eliminates manual sample preparation steps

without the need for complicated or costly fabrication, thus enabling the device to be low in cost and disposable. Furthermore, the integration of fiber optic cables eliminates the need for optical alignment and focusing, which can be burdensome in on-site detection.

In this chapter, we have illustrated the use of the optofluidic SERS device for the detection of chemical contaminants for which on-site analysis is important. We detected melamine, a food contaminant, with a calculated detection limit of 63 ppb. In addition, we detected thiram, a fungicide, with a calculated detection limit of 50 ppt. Both limits of detection exceed requirements established by the U.S. government. In addition, we utilized a commercially available portable spectrometer with a fiber optic interface for the detection of thiram to demonstrate the potential for our microsystem to be utilized for the on-site detection of contaminants. Taken together, the results presented here illustrate that highly sensitive and easy-to-use SERS devices, such as the microsystem demonstrated here, will make it feasible to perform chemical identification on site, without the cost and delays associated with sending samples to highly sophisticated central lab facilities.

Chapter 6: Multiplexed detection of DNA sequences using a competitive displacement assay in an optofluidic SERRS-based microsystem[5]

6.1 Introduction

In this chapter, we demonstrate sensitive and multiplexed detection of DNA sequences through a surface enhanced resonance Raman spectroscopy (SERRS)-based competitive displacement assay in an integrated microsystem. The use of the competitive displacement scheme, in which the target DNA sequence displaces a Raman-labeled reporter sequence that has lower affinity for the immobilized probe, enables detection of unlabeled target DNA sequences with a simple single-step procedure. In our implementation, the displacement reaction occurs in a microporous packed column of silica beads pre-functionalized with probe-reporter pairs. The use of a functionalized packed-bead column in a microfluidic channel provides two major advantages: (i) immobilization surface chemistry can be performed as a batch process instead of on a chip-by-chip basis, and (ii) the microporous network eliminates the diffusion limitations of a typical biological assay, which increases the sensitivity. Packed silica beads are also leveraged to improve the SERRS detection of the Raman-labeled reporter.

Following displacement, the reporter adsorbs onto aggregated silver nanoparticles in a microfluidic mixer; the nanoparticle-reporter conjugates are then

---

[5] **This chapter is adapted from: Soroush H. Yazdi, Kristen Giles, and Ian M. White, Multiplexed detection of DNA sequences using a competitive displacement assay in an optofluidic SERRS-based microsystem (under review)**

trapped and concentrated in the silica bead matrix, which leads to a significant increase in plasmonic nanoparticles and adsorbed Raman reporters within the detection volume as compared to an open microfluidic channel. We report the detection of down to 100 pM target DNA sequence, and we demonstrate that detection is specific, repeatable, and quantitative. Furthermore, we illustrate the advantage of using SERRS by demonstrating multiplexed detection. The sensitivity of the assay, combined with the advantages of multiplexed detection and single-step operation with unlabeled target sequences makes this method attractive for practical applications. Importantly, while we illustrate DNA sequence detection, the SERRS-based displacement assay is applicable to detection of a variety of biological macromolecules, including proteins and proteolytic enzymes.

For the sensitive and specific detection of biomacromolecules, such as proteins and DNA sequences, it is more common to employ SERS in a *labeled* immunoassay or DNA hybridization format. The labels, which are often fluorophores or other strong Raman scatterers, are referred to as Raman labels. As opposed to fluorescence-based transduction, however, the Raman labels each generate a unique and narrowband Raman spectral fingerprint upon laser excitation, which enables an increase in multiplexing density as compared to fluorescence while utilizing only a single laser and a single filter set.[37,103] A further optimization of the fluorophore-labeled SERS detection strategy is to utilize an excitation wavelength that is matched with the optical absorption of the Raman labels.[54,55] This technique, referred to as surface enhanced resonance Raman spectroscopy (SERRS), leads to an improved

detection limit for biomacromolecules due to the sensitivity enhancement of the Raman label.

Vo-Dinh's group was the first to demonstrate SERS detection of DNA sequences using a hybridization assay. In that pioneering work, the target was labeled with a Raman reporter through PCR amplification.[39] In recent years, other groups have also reported SERS detection using labeled DNA targets.[58,159,160] For broader applications, Mirkin's group illustrated the use of SERS for multiplexed DNA sequence detection in a hybridization sandwich assay with an unlabeled target.[37] In this assay, one probe sequence was immobilized to a substrate while a second probe sequence was linked to a gold nanoparticle with a fluorophore label; the fluorophore Raman label serves as a barcoding molecule for the respective sequence in a multiplexed format. When the unlabeled target DNA sequence is present in solution, the second probe can be attached to the substrate through the hybridization sandwich, and thus the barcoding molecule's SERS spectrum is measured. Other reports utilizing SERS-based sandwich hybridization implementations have followed over the last decade.[102,161,162]

As with all sandwich assays, the DNA hybridization sandwich requires multiple steps and rinses, which extends the time and cost of the assay while introducing the possibility of false positives due to insufficient rinsing and false negatives due to overly harsh rinses. An alternative to detect unlabeled targets that can be performed in a single step is the SERS beacon.[53,56] In this assay design, a nucleic acid probe is designed to form a hairpin, forcing the Raman reporter on one end of the oligo to locate near a metal nanoparticle (or metal nanostructured surface)

at the other end of the oligo; the SERS signal is present in this condition. When the target DNA sequence is added, it binds to the probe, causing it to unfold, which leads to a decrease in the SERS signal. Thus, the SERS signal is inversely proportional to the target concentration. While this clever single step method generates a distinguishable SERS signal for high target concentrations, at low concentrations it may be difficult to separate the signal change due to target sequence hybridization from the typical large signal variations for which SERS is infamous.

Herein we report the demonstration of an alternative single-step technique for the detection of DNA sequences using labeled reporters that positively correlates the SERS signal intensity with the concentration of the target DNA sequence. Our design is based on the concept of competitive displacement, which is presented in Fig. 6.1. In the assay, the Raman-labeled DNA reporter is pre-hybridized to the immobilized DNA probe. The reporter is designed to hybridize to the probe, but with a lower affinity than the target sequence. Once the DNA target sequence is introduced, it hybridizes to the DNA probe due to its higher affinity (i.e., greater number of matching base pairs) as compared to the reporter. The displaced reporter then flows downstream in the microfluidic channel to a SER(R)S detection region. Competitive displacement with DNA hybridization has been previously reported in a microfluidic channel.[163] To our knowledge, the present work represents the first application of competitive displacement for single-step SERS detection.

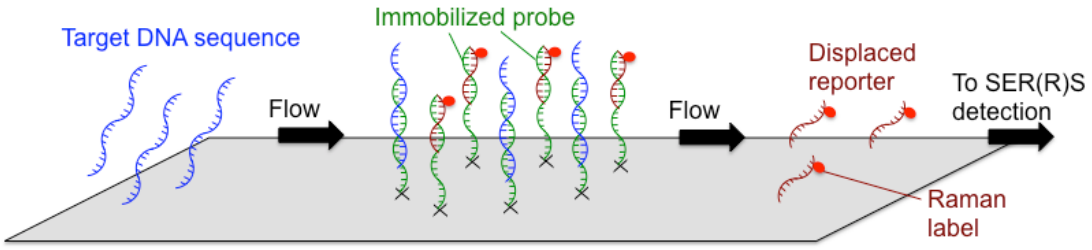

Figure 6.1 Competitive displacement assay concept. Probes hybridized to reporter molecules (with an attached Raman label) are immobilized onto the substrate. The reporter is designed to hybridize to the probe, but with lower affinity than the target, thus enabling the target to displace the reporter. The displaced reporter sequence then flows to the SER(R)S detection region

The competitive displacement assay reported here utilizes multiplexed DNA sequence detection as a proof of concept. However, the displacement assay concept also has the potential to be used to detect other biomacromolecules, including a specific protein or a specific enzyme's activity. The key consideration for different applications is to design the assay in such a way that the labeled reporter is displaced due to the target molecule. For protein detection, the displaced reporter could also be a nucleic acid sequence that was hybridized with an aptamer, but with lower affinity than the protein target. For proteolytic activity detection (e.g., neurotoxins), the displaced reporter could be the free end of a cleaved peptide, which would flow to the SER(R)S detection region upon proteolytic activity.

In our implementation, the SERS detection region is integrated into the same microfluidic channel as the bio-reaction region where the competitive displacement occurs, as shown in the microsystem design presented in Fig. 6.2. The bio-reaction region consists of DNA-conjugated silica beads packed against a frit inside the microchannel. There are two major advantages to using packed silica beads as the

reaction region instead of immobilizing the DNA probes onto the surface of the channel sidewalls. First, when using beads as the immobilization substrate, the immobilization surface chemistry can be performed as a batch process, and then a selected aliquot of beads can be packed into the microfluidic channel.

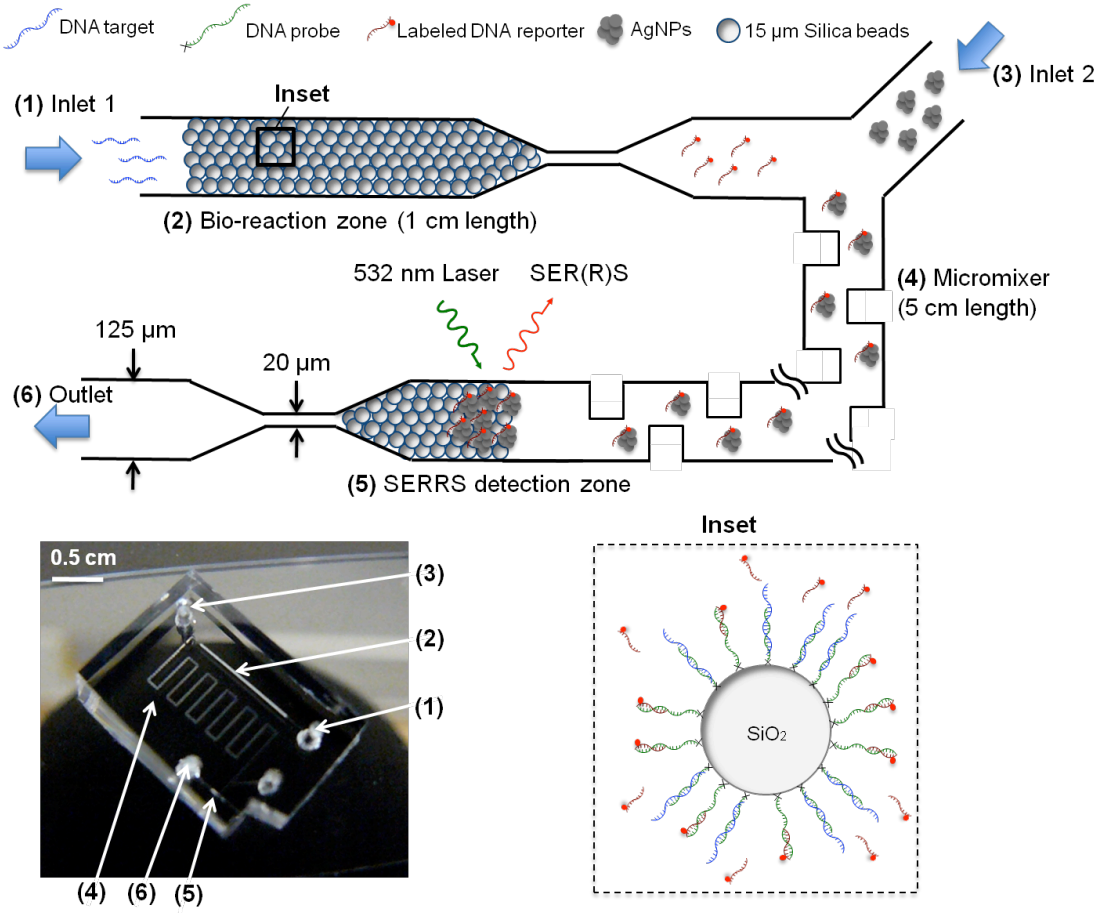

Figure 6.2 Optofluidic SERRS microsystem with integrated competitive displacement for DNA sequence detection. Silica microspheres functionalized with DNA probe-reporter pairs (inset) are packed against a frit. When the target sequence is introduced at the inlet, Raman-labeled reporter oligos are displaced. As they flow along the channel, they are mixed with metal nanoclusters and trapped in the optofluidic SERRS detection region

This is simpler than conventional microfluidic biosensors in which the multi-step immobilization chemistry must be performed on a chip-by-chip basis. Secondly,

the functionalized packed beads create a microporous channel that eliminates the diffusion limitations that exist in well-plate assays and open-channel microfluidic assays, resulting in faster and more sensitive detection.[164–167]

As shown in Fig. 6.2, the SERRS detection region also leverages packed beads. Here the packed beads serve to trap aggregated metal nanoparticles and adsorbed molecules, which greatly improves the SER(R)S detection performance as compared to an open microfluidic channel. Previously, we have shown sensitive and automated detection of pesticides and food contaminants using this optofluidic SERS concept. In that chapter, the microsystem consisted of a SERS detection zone integrated with an on-chip micromixer. In the present work, we have added the microporous bio-reaction zone to the system, which enables us to perform multiplexed and sensitive detection of specific DNA sequences using competitive displacement.

Using this optofluidic SERRS microsystem, we demonstrate detection of a targeted DNA sequence at a concentration as low as 100 pM. We show that the signal is only present in the case of a sequence match between the DNA probe and the target sequence, thus enabling specific and sensitive detection. We also show multiplexed detection by utilizing two different Raman labels for respective probe-reporter-target sequence systems. Ultimately, it is apparent that the combination of the competitive displacement assay and optofluidic SERRS detection can be used to detect a variety of biological macromolecule targets in a single-step assay without the need for labeling the target, which makes this method highly practical for real-world applications.

6.2 Experimental Section

6.2.1 Preparation of Silver Colloid

Silver nanoparticles (AgNPs) were synthesized through a simple reduction technique. 90 mg of silver nitrate (Sigma) was dissolved in 500 mL of deionized (DI) water. The solution was brought to a boil in the flask while stirring. 100 mg sodium citrate (Sigma) was added, and the solution was boiled for 10 min until its color turned greenish brown. Sodium chloride (Sigma) was added to the silver nanoparticle solution to generate a 10 mM concentration to promote aggregation before running each experiment. AgNP aggregation is required for the formation of "hot spots" between nanoparticle junctions, resulting in a high electromagnetic field generation, which consequently enhances the Raman signal.

6.2.2 Preparation of DNA-functionalized Chitosan-silica Beads

The bio-reaction zone in the optofluidic chip (Fig. 6.2) is formed by packed silica beads functionalized with probe and reporter oligonucleotides. As the first step, silica beads (15 µm, Corpuscular Inc.) were washed using piranha solution. 300 µL sulfuric acid (Sigma) and 100 µL hydrogen peroxide (Fisher Scientific) were added to 300 µL silica bead solution. The solution was left on the hot plate (60º C) for 20 minutes and the beads were subsequently rinsed with DI water three times. All rinsing steps were performed by vortexing the beads in DI water or phosphate-buffered saline (PBS) (Sigma), spinning the beads down by centrifugation and replacing the supernatant with DI water or PBS. The cleaned silica beads were suspended in 500 µL DI water with 10% (3-Glycidyloxypropyl)trimethoxysilane (GOPS) (Gelest

Inc.) and 5% acetic acid (Fisher Scientific). The solution was rocked for two hours to modify the surface of the beads with epoxy functional groups. Surface modified silica beads were washed three times with DI water.

The beads were then amine-functionalized using chitosan, an amino-polysaccharide derived from naturally occurring chitin. Chitosan is abundant, biocompatible and biodegradable, and importantly, contains free primary amine groups at each link in the polysaccharide chain. The chitosan solution was prepared by adding 20 mg chitosan oligosaccharide lactate (Sigma) to 500 µL DI water with 5% acetic acid. Chitosan was dissolved in the solution for two hours. After this, GOPS-modified silica beads were suspended in the chitosan solution. The solution was rocked overnight in order to coat the silica beads with chitosan. Afterward, chitosan (CS)-silica beads were rinsed three times with PBS (pH 7.2) and resuspended in 500 µL PBS with 10% glutaraldehyde (GA). The GA (Sigma) treatment was performed for two hours. Then, GA-CS-silica beads were rinsed with PBS three times and the supernatant was removed. The glutaraldehyde molecule has aldehydes on both sides that covalently bind to amines, resulting in a link between the chitosan and the amine-modified DNA probe.

The presence of chitosan at the bead surface was verified using a low-pH gold nanoparticle (AuNP) colloid (pH 3.5). At a pH below 6, negatively charged AuNPs stick to the CS-silica beads due to the presence of protonated amine groups. Attraction of AuNPs to the beads' surface results in a color change of the solution from red to black (Figure 6.3b). However, when the colloid pH was adjusted to 9 using sodium hydroxide, no color change was observed in the colloid solution after

CS-silica beads were added (Fig. 6.3c). No color change was observed after plain silica beads (the control experiment) were added to the AuNP solution.

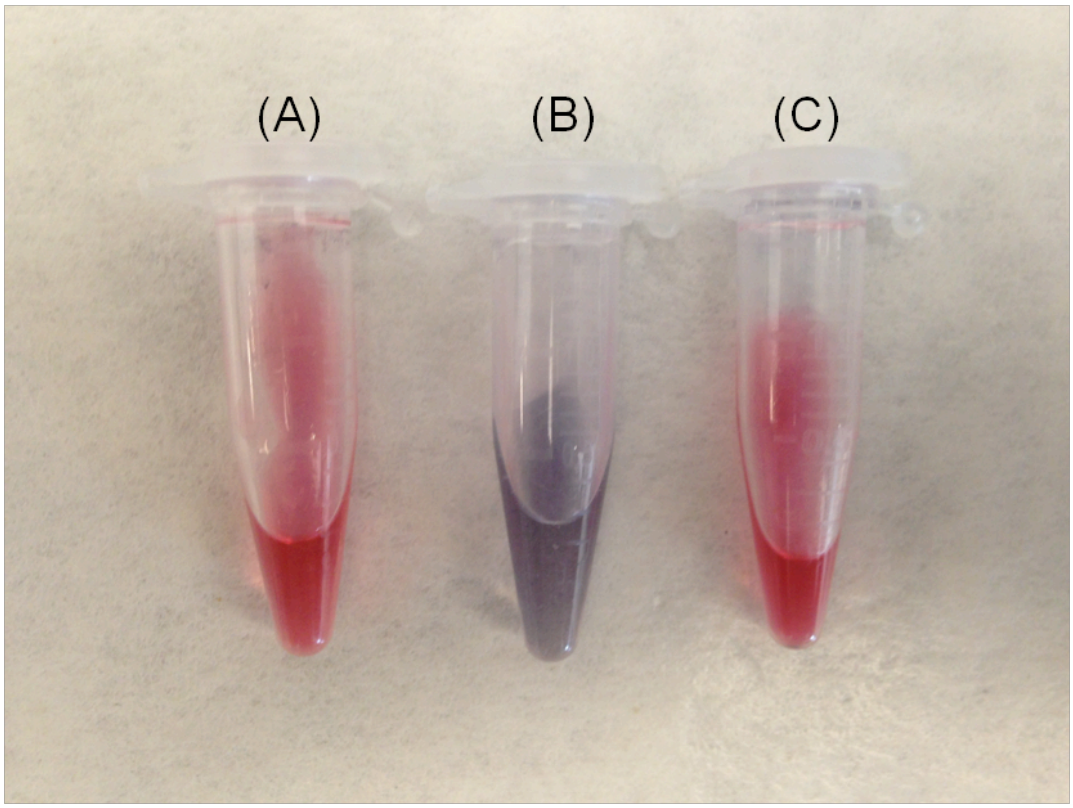

Figure 6.3 (A) Au colloid (pH=3.5) (B) Au colloid after adding CS-silica beads (pH=3.5) (C) Au colloid after adjusting pH to 9 and then adding CS-silica beads

After chitosan and glutaraldehyde functionalization, 15 µL of 100 µM amine-modified DNA probe (IDT) was added to the GA-CS-silica beads (experimental evaluation of the protocol demonstrated that 100 µM DNA probe provided the largest amount of reporter immobilization as compared to lower DNA probe concentrations (Fig. 6.4)). The solution was left to react overnight and the beads were rinsed with PBS (three times) the next day. After the probe conjugation, the samples were treated with sodium borohydride ($NaBH_4$) to convert Schiff bases to more stable secondary amine bonds. To perform the $NaBH_4$ (Fisher Scientific) treatment, probe-conjugated

beads were suspended in a $NaBH_4$ solution (5 mg $NaBH_4$, 750 µL PBS, 250 µL ethanol) for 5 minutes. This step was followed by three rinses with PBS. At this point, the beads were ready for hybridization and competitive displacement experiments.

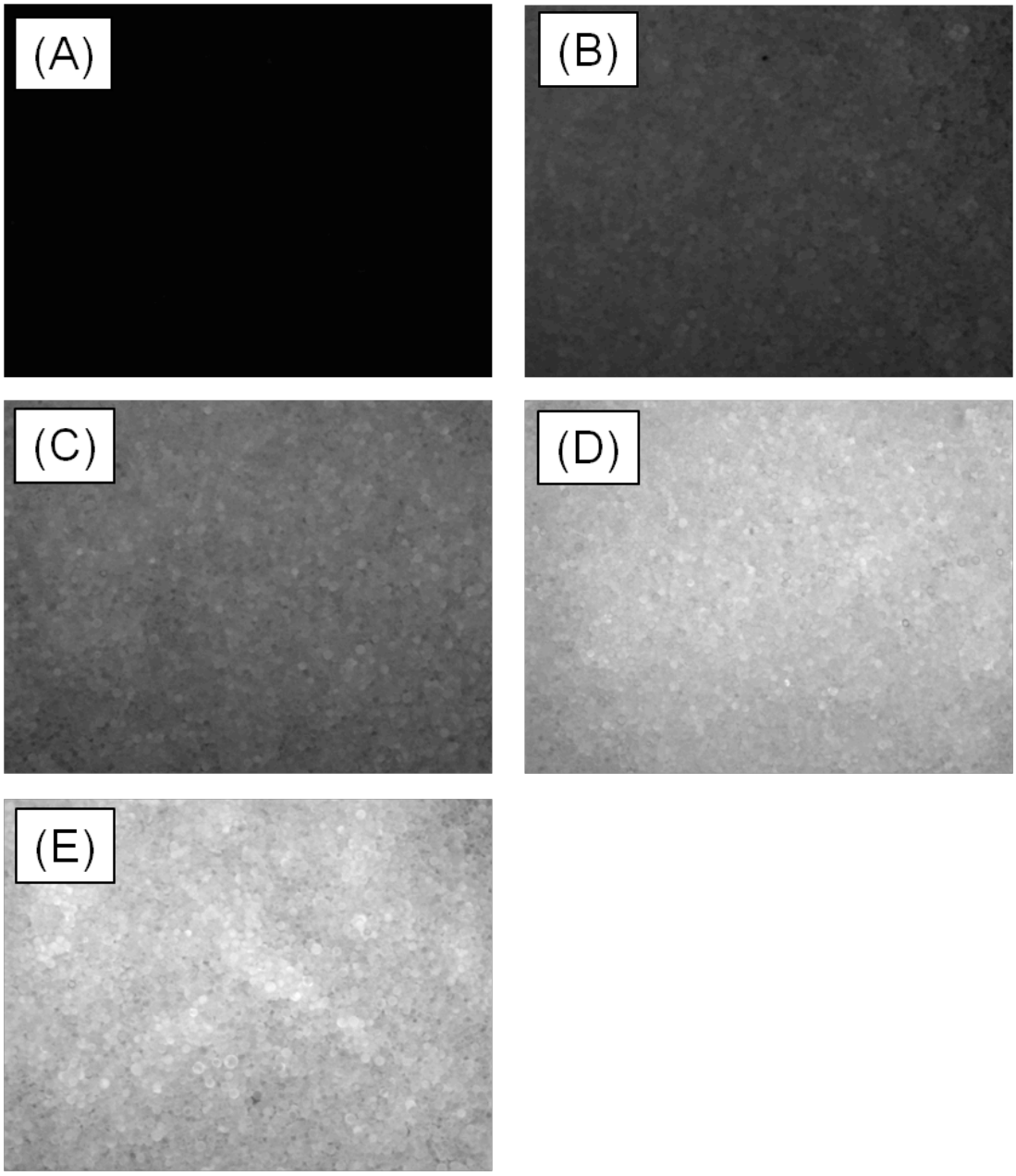

Figure 6.4 Effect of DNA probe concentration on DNA reporter hybridization (DNA reporter concentration = 10 µM). DNA probe concentration; (A) 0 µM (B) 1 µM (C) 10 µM (D) 50 µM (E) 100 µM.

6.2.3 Verification of DNA Hybridization and Competitive Displacement

Before demonstrating the competitive displacement assay in the SERRS optofluidic device, the displacement was assessed using fluorescence microscopy. 10 μL of 10 μM TAMRA-labeled DNA reporter was added to the probe-conjugated beads in a microtube and allowed to hybridize for 1 hour. Then, the beads were rinsed three times with PBS to remove non-specifically attached TAMRA-labeled DNA. Also, 10 μL of 10 μM TAMRA-labeled DNA was added to GA-CS-silica beads with no DNA probe at the surface as a negative control. After measuring the fluorescence of the beads, 10 μL of 10 μM DNA target was added to the beads to hybridize to the DNA probe and to displace the reporter. After the 1 hour competitive displacement reaction, the beads were washed three times with PBS. The fluorescence of the beads was then measured. Fluorescence levels were measured using an Olympus IX-51 fluorescence microscope and were quantified using ImageJ (National Institutes of Health).

6.2.4 Optimizing the Number of Matching Bases Between DNA Probe and DNA Reporter

The number of matching bases between DNA probe and DNA reporter should be optimized to provide the largest possible assay sensitivity. An important consideration for probe and reporter design is to have enough matching bases to assure an effective and stable hybridization between the two. However, too many matching bases results in an overly strong hybridization, which does not allow the DNA target to displace the reporter at room temperature. In order to optimize the

number of matching bases for our detection assay, we attempted three probe-reporter pairs with different numbers of complementary base pairs (8, 12, and 16 matching bases). Three batches of GA-CS-silica beads were prepared separately using three different probe sequences designed to provide different numbers of base-pair matches with a single reporter sequence. The reporter, probe and target sequences are as follows:

Reporter: 5'-GAA GTC CAT CGA TTG TAT CAC TA-TAMRA-3'

Target 1: 5'-GAA GTC CAT CGA TTG TG-3'

Probe 1: 5'-C6-amine-GAC TGA GCT CTG CAC AAT CGA TGG ACT TC-3' (16-base-match with reporter, 17-base match with Target 1)

Target 2: 5'-GAA GTC CAT CGA AGT GT-3'

Probe 2: 5'-C6-amine-TCG TAC AGT CTG ACA CTT CGA TGG ACT TC-3' (12-base-match with reporter, 17-base match with Target 2)

Target 3: 5'-GAA GTC CAC ATT CGT CG-3'

Probe 3: 5'-C6-amine-GTA GAG ACA GCT CGA CGA ATG TGG ACT TC-3' (8-base-match with reporter, 17-base match with Target 3)

All oligonucleotides were purchased from IDT.

6.2.5 Fabrication of the Optofluidic Device

The polydimethylsiloxane (PDMS) microfluidic device was fabricated using typical soft lithography methods. AZ 4620 (AZ Electronic Materials) was spun and then patterned on a silicon wafer using standard photolithography. Next, the silicon mold was etched by deep reactive ion etching (DRIE) to a depth of 125 μm. Vapor-phase silanization of the silicon mold with Tridecafluoro-1,1,2,2-tetrahydrooctyl-1-

trichlorosilane (Pflatz and Bauer) was performed to enable removal of the PDMS (Dow Corning). Then, PDMS was poured onto the silicon wafer and air bubbles were removed by applying a vacuum. The PDMS was cured at 60º C for 4 hours. Finally, the PDMS channels were sealed onto a piranha-cleaned glass substrate through corona treatment and stored at 60º C overnight.

The device design is presented in Fig. 6.2. For both the bioreaction and detection zones, silica beads were loaded and trapped against a frit structure inside the microchannel. The 125 µm channel narrows to a width of 20 µm at the frit. An additional temporary inlet was included near the second frit at the outlet to enable the loading of silica beads into the detection zone. The temporary inlet was sealed with silicone rubber (Dow Corning) after the beads were loaded. A droplet of silica beads was placed at both inlet 1 and the temporary inlet and packed inside the channel by applying vacuum from inlet 2 and the outlet, respectively.

6.2.6 Thiol-Modification of Silica Beads

The surface of the silica beads utilized in the SERRS detection region was functionalized with thiol groups, which have a high affinity for Ag, to improve the adsorption of silver nanoparticles to the silica bead matrix. Surface modification was performed by first adding 100 µL of silica beads in water to 500 µL methanol. Then, 50 µL (3-Mercaptopropyl)trimethoxysilane (3MTS, Sigma) was added to the solution. The solution was rocked for 24 hours to ensure a high density of thiol groups on the surface of the silica beads. After mixing, the silica beads were rinsed three times in methanol and resuspended in DI water before being loaded into the optofluidic device.

6.2.7 SERRS Measurements

A Horiba Jobin Yvon LabRam ARAMIS Raman microscope was used to excite the sample and collect Raman scattered photons. For all measurements, a 10X objective was used. A 532 nm laser (6 mW) was used for excitation; TAMRA and R6G, the Raman labels, absorb photons at 532 nm, which enables SERRS. For each experiment, the aggregated silver nanoparticles were introduced at inlet 2 while selected concentrations of the DNA target (0.1-10000 nM) were introduced at inlet 1. The samples were loaded at a flow rate of 10 μL/hour. Target DNA and AgNP colloid were introduced into the channel for 30 minutes. Then, the SERRS signal was collected from the detection zone. A 2-second exposure time was used for each experiment.

6.2.8 Multiplexed Detection using SERRS and Competitive Displacement

For on-chip multiplexed DNA sequence detection using SERRS, two batches of GA-CS-silica beads were pre-functionalized with two different probe-reporter pairs separately. One batch was modified with the selected pair from the single-plex experiment described above (TAMRA-labeled reporter), while the other batch was modified with the following probe-reporter sequence pairs.

R6G-labeled reporter: 5'-cR6G-TGG TAT CTG CGC TCT GCT GAA GCC AGT-3'

Probe: 5'-C6-amine-ATT TAA TGT GCC TGC ATG CGC AGA TAC CA-3'

Target: 5'-TGG TAT CTG CGC ATG CA-3'

Then, the modified beads were mixed with the same ratio and introduced into the device as stated previously. Two DNA target sequences corresponding to each

pair were mixed (final concentration of 100 nM) and introduced into the device while AgNPs were loaded from the other inlet. The sample was loaded for 30 minutes and the SERRS signal was subsequently recorded.

6.3 Results

6.3.1 Analysis of DNA Competitive Displacement

To optimize the molecular design of the competitive displacement assay, the assay design was quantitatively assessed with fluorescence microscopy. After TAMRA-labeled reporter hybridization, the fluorescence intensity of the three types of probe-modified beads (probe 1, 2, or 3) was measured; high fluorescence is indicative of successful hybridization of the reporter with the immobilized probe. The fluorescence signal was then evaluated after 10 μM target DNA was added. Figure 6.5 shows the fluorescent images of the beads (before and after the addition of target DNA) dried onto a glass slide. The fluorescence intensity (computed with ImageJ and normalized to the intensity of Probe-1:reporter beads) for each probe and target sequence before and after target DNA was added is presented in Fig. 6.6.

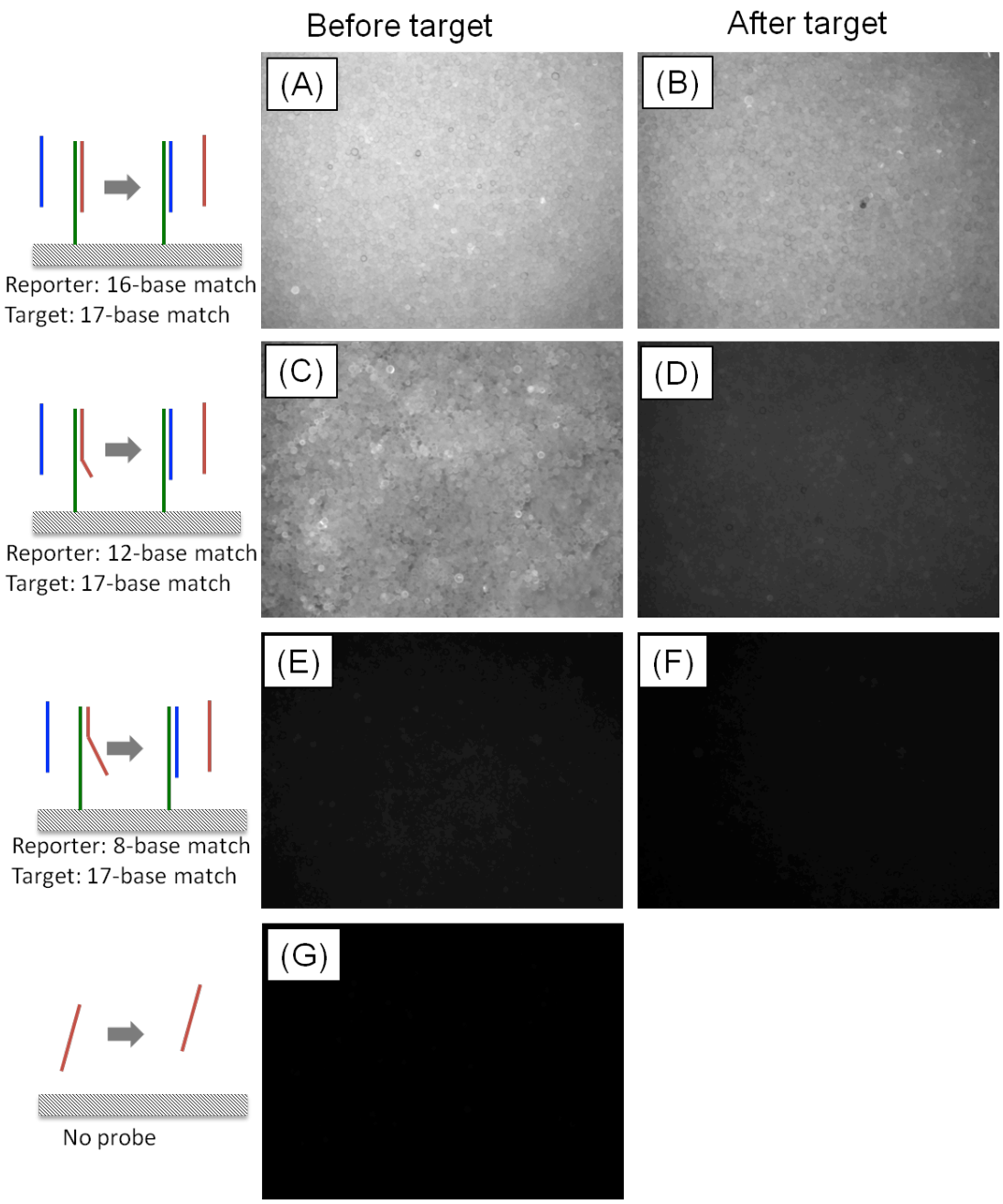

Figure 6.5 Fluorescence microscopy images of probe-functionalized microspheres to analyze the competitive displacement for varying probe-reporter affinities. Higher fluorescence in the left column indicates increased hybridization between probe and reporter; lower fluorescence in the right column indicates higher displacement of reporter by the target sequence

The ideal number of matching bases between the probe and reporter results in a high fluorescence signal before the target is added as well as a high contrast after the DNA target is added. It can be seen in Fig. 6.6 that both Probe 1 (16-base match with reporter) and Probe 2 (12-base match with reporter) have strong hybridization with the TAMRA-labeled reporter sequence. However, Probe 2 shows a significantly higher signal contrast between the image taken before and the image taken after the addition of the target DNA sequence. This implies that the most TAMRA-labeled reporter displacement occurs in the case of Probe 2. Because of this, we selected Probe 2 for all further SERRS experiments.

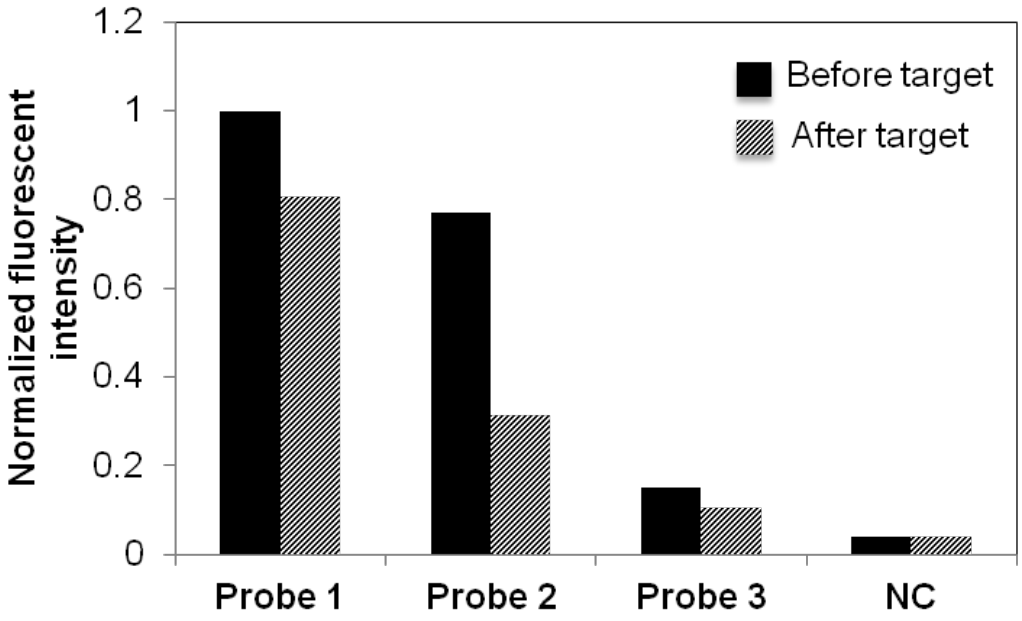

Figure 6.6 Quantified fluorescence from microspheres for the three probe-reporter-target systems. The use of Probe 2, which has a 12-base match with the reporter and a 17-base match with the target, generates the highest contrast due to displacement while also exhibiting strong probe-reporter hybridization. Thus, Probe 2 is selected for the SERRS measurements.

6.3.2 Optofluidic SERRS Detection with Competitive Displacement

To generate a SER(R)S signal, it is critical for the Raman label to interact with the surface of the metal nanoparticles. We have observed that TAMRA and TAMRA-labeled DNA do not exhibit a large SERRS signal when added to our silver colloid. Thus, we investigated the use of nitric acid to promote interaction between the TAMRA-labeled DNA and the AgNPs. 1 µL of 10 µM TAMRA-labeled DNA was added to 500 µL of AgNP solution (the final TAMRA-labeled DNA concentration was 20 nM). After vortexing to promote mixing, a 1 µL droplet of the solution was placed under the Raman microscope. However, no TAMRA Raman peaks were observed. This is likely due to a lack of interaction between TAMRA molecules and AgNPs. However, the addition of 0.01% nitric acid to the silver colloid results in the appearance of strong TAMRA SERRS peaks, as shown in Fig. 6.7. Thus, we can conclude that the inclusion of nitric acid promotes interaction between the TAMRA Raman label and the AgNPs.

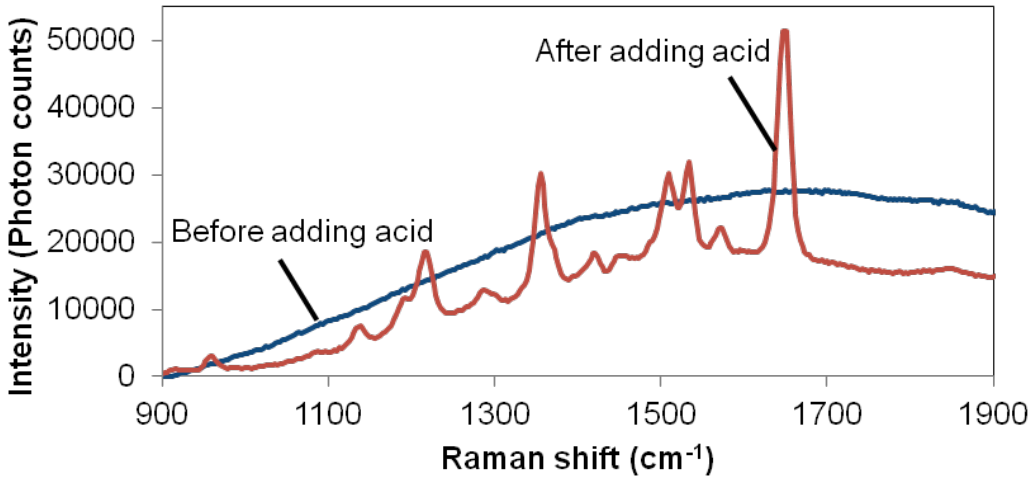

Figure 6.7 Addition of nitric acid promotes interaction between the TAMRA-labeled reporter and the metal nanostructures, enabling the SERS spectrum of TAMRA to be observed

Based on these results, we added 0.01% nitric acid to the silver colloid solution for on-chip experiments. Figure 6.8 shows the measured SERRS signal intensity (the net peak height at 1650 cm^{-1}) for different target DNA concentrations loaded into the optofluidic chip.

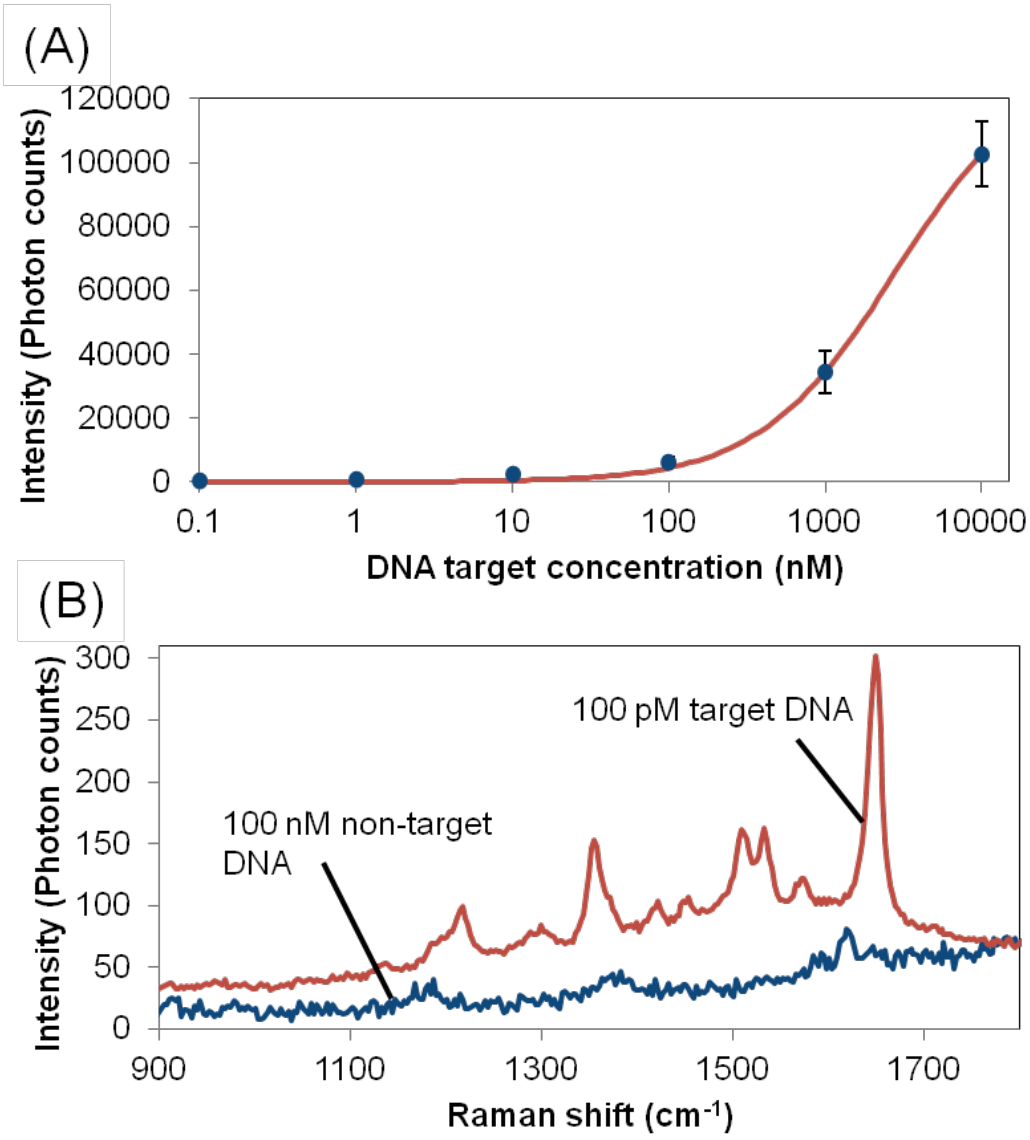

Figure 6.8 (A) Net intensity of the 1650 cm^{-1} SERRS peak for various DNA target sequence concentrations. Error bars represent the standard deviation of three trials. The data is fit to a Langmuir isotherm. (B) The TAMRA SERRS signal is easily observed, even with only 100 pM target DNA. When adding 100 nM non-matching DNA, no signal is observed.

Each concentration was tested three times to evaluate chip-to-chip repeatability (the error bars in Fig. 6.8 represent the standard deviation). The data is fit with a Langmuir isotherm (R2 = 0.99), which indicates the capability for quantitative analysis. We were able to detect a target DNA concentration as low as 100 pM (Fig. 6.8B). Even at this low concentration of target DNA, SERRS peaks of the TAMRA-labeled DNA reporter can be easily observed at 1360, 1511, 1530, and 1650 cm^{-1}. To validate the specificity of this competitive displacement assay, non-target DNA (Target 3, 8 bases match with Probe 2) was loaded into the device as a negative control. As shown in Fig. 6.8B, while the addition of 100 pM of target DNA generates an obvious SERRS spectrum for TAMRA, no signal is apparent after the addition of 100 nM of non-target DNA.

6.3.3 Multiplexed Detection with the Competitive Displacement SERRS Assay

As described previously, one of the advantages of Raman spectroscopy is the narrowband spectrum of the Raman-scattered photons, which leads to the capability for multiplexed detection of analytes using a simple optical setup. It is this advantage of Raman spectroscopy that motivates our use of SERRS for DNA sequence detection. In order to demonstrate this multiplexing capability using our assay, two target sequences were detected simultaneously; one target sequence displaces a TAMRA-labeled reporter as above, while the other target displaces an R6G-labeled reporter. The result of on-chip multiplexed detection of the two target sequences (100 nM each) is shown in Fig. 6.9. The SERRS peaks due to each reporter are indicated in the figure. The unique R6G peaks are at 773, 1090, 1180, 1310, and 1570 cm^{-1}. Although TAMRA and R6G have overlapping peaks at 1360, 1511, and 1650 cm^{-1},

TAMRA's signature can still be identified in the spectrum based on the 1530 cm^{-1} peak, which is unique to TAMRA.

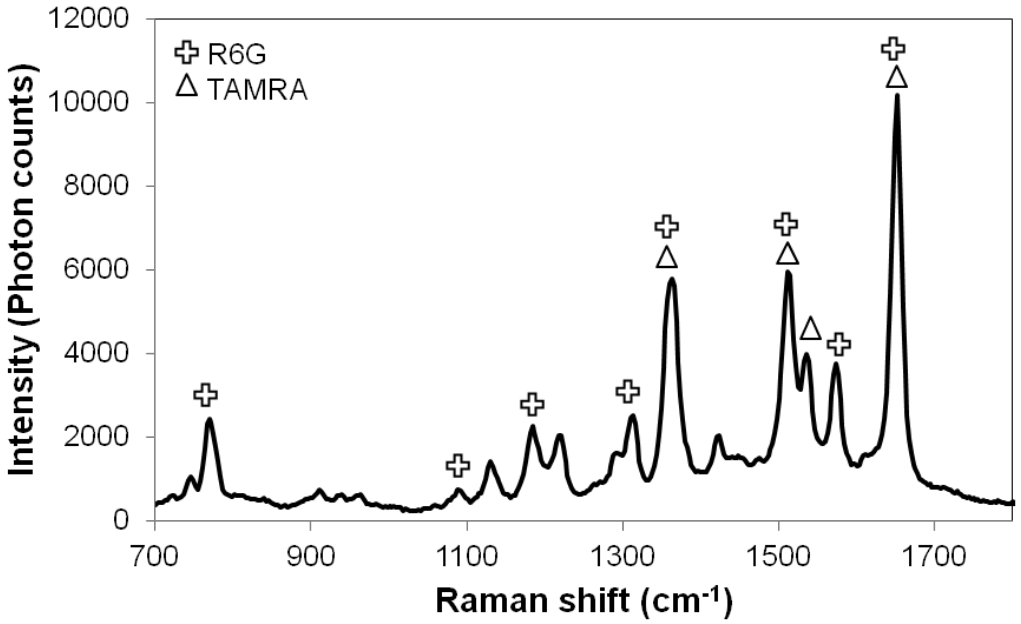

Figure 6.9 Multiplexed detection of target DNA sequences using competitive displacement in the optofluidic SERRS microsystem when 100 nM of each target sequence is added. Triangle = TAMRA; Plus = R6G.

In future work, we anticipate increasing the multiplexing density. Mirkin, et al., demonstrated that the level of multiplexing can be increased up to six reporters.[37] Further multiplexing might be enabled by multivariate analysis, such as principal component analysis (PCA), independent component analysis (ICA), and hierarchical cluster analysis (HCA), which have been used to resolve spectra into multiple components in order to detect the presence of multiple targeted chemical species.[38,51,168–170]

6.4 Conclusion

We have introduced a new optofluidic SERRS assay that utilizes the concept of competitive displacement for the multiplexed detection of DNA sequences. Competitive displacement is advantageous as compared to previous SERS assays for DNA sequence detection because it requires only a single step, saving the user multiple steps as compared to the typical DNA hybridization sandwich assay. To further improve the competitive displacement concept, we immobilized the probe-reporter pair onto silica beads, which provides two advantages: (i) immobilization surface chemistry can be performed as a batch process instead of on a chip-by-chip basis, and (ii) the packed beads form a microporous channel, which eliminates the limitations of diffusion that exist in well-plate and open-channel microfluidic assays, thus increasing the sensitivity of the assay. Using competitive displacement in our optofluidic SERS device, we were able to detect down to 100 pM of the target DNA sequence. Detection was quantitative (the measured data is an excellent fit with the Langmuir isotherm), and specific (no SERRS signal was observed with 100 nM of a mismatched sequence).

Although the competitive displacement concept was illustrated for DNA sequence detection here, we expect that it can be adopted for specific detection of proteins as well through the use of aptamer probes and labeled reporter oligonucleotides. Similarly, the assay reported here is also suggestive of an enzymatic activity assay in which the reporter is the cleaved portion of an immobilized peptide that is specific to a targeted enzyme. Thus, this sensitive and simple-to-perform optofluidic SERRS assay may become a useful diagnostic tool that

can quantitatively detect a multiplexed panel of biomarkers through a simple single-step operation.

Chapter 7: Conclusion

7.1 Summary

In this work, we have demonstrated the feasibility of utilizing silica beads to form a porous matrix inside a microfluidic channel to passively concentrate the analyte and metal nanoparticles to enhance the SERS signal. More than two orders of magnitude signal enhancement was achieved as compared to traditional open microfluidic SERS microsystems, which rely on slow diffusion of analytes and metal nanoparticles. The device is extremely easy to fabricate since it does not require nanofabrication. Silica beads are simply loaded inside the microchannel by applying negative pressure while a droplet is placed at the inlet. A variety of real world applications including pesticides, fungicides, food contaminant, and DNA sequence detection were demonstrated.

In chapter 3, the performance of the device was evaluated by testing two different analytes. The device exhibited two orders of magnitude enhancement in SERS signal while it showed improved portability and automation due to the integration of fiber optics for sample excitation and SERS collection. The use of silica beads to form the porous matrix simplifies the fabrication as compared to nanochannels. Moreover, utilizing a passive concentration approach eliminates the need for active components/devices as opposed to active concentrating techniques which results in improved portability and reduced costs. The device demonstrated highly repeatable and quantifiable detection for analytes in a wide range of sample concentrations.

In chapter 4, multiplexed detection of three highly regulated fungicides for aquaculture was presented. The portability of the device was improved by replacing the syringe pump with a pipette for sample loading. It was shown that introducing the sample by simply applying negative pressure at the outlet using a pipette results in comparable SERS signal as if the sample is loaded using a syringe pump. This eliminated the need for bulky syringe pump and highly improves the portability, which makes the device more suitable for on-site sample detection of a variety of analytes. Moreover, sample loading can be performed much faster (in a few seconds rather than a couple of minutes).

In chapter 5, the device automation was improved by adding an on-chip micromixer to the device. For this purpose, a passive micromixer was designed, simulated, and fabricated. Addition of the on-chip micromixer improves automation by reducing the number of manual preparation steps. The analyte solution and metal nanoparticle colloid are introduced through two inlets and are mixed inside the device before SERS detection is performed. Additionally, integration of an on-chip micromixer provides the potential for performing more complicated assays, e.g. biomolecule detection, with the optofluidic SERS microsystems. Food contaminants and pesticides were tested using the new device. The detection performance using the optofluidic microsystem showed high sensitivity and repeatability.

In chapter 6, the device was tested for biological samples detection. To perform biomolecular reactions, a bio-reaction zone was created inside the device by packing surface-modified silica beads inside the microchannel. Utilizing packed silica beads for bio-reaction zone results in faster and more sensitive assay as compared to

planar assays. A competitive displacement assay was utilized for detection of multiple DNA sequences as the proof of concept. In the competitive displacement assay, a reporter molecule is pre-reacted with the immobilized probe and then the reporter is displaced by the target due to the target's higher affinity to the probe. This technique is highly practical for biological sample detection since it does not require target labeling.

In the competitive DNA detection assay, the pre-hybridized DNA reporter was displaced by the target DNA. As it flows inside the on-chip micromixer, the displaced reporter gets mixed with metal nanoparticles and concentrated at the detection zone for SERRS signal collection. Sensitive, repeatable, and multiplex detection of DNA sequences was demonstrated utilizing our device.

7.2 Contributions to the Field

For the last thirty years, after discovery of SERS effect, there have been extensive efforts to make this technique practical for real world applications. In spite of its tremendous power in highly sensitive, multiplexed, and quantitative detection of analytes, it has been mostly limited to the research labs due to the need of bulky and high cost SERS-active substrates and instruments. SERS has the potential to become applicable to many practical applications through the integration of microfluidic functions in optofluidic SERS systems. This combination enables high sensitivity SERS performance while miniaturizing all the required laboratory functions on a small chip. Moreover, integration of such a small optofluidic device with available state-of-the art hand-held spectrometers could result in developing a portable, automated, and sensitive sensing platform for a variety of applications. With this

vision, SERS has the potential to become suitable for real world applications with its benefits over traditional sensing techniques such as mass spectrometry and fluorescent-based detection techniques.

The developed optofluidic SERS microsystem in this work has aimed to achieve this goal. The device can be fabricated easily with standard microfabrication techniques. Utilizing silica beads to form a concentrating matrix for SERS detection was demonstrated for the first time. Nanoparticles and adsorbed/bound analyte in the sample are concentrated as they flow into the channel; there is no need for additional active components in the device to concentrate the sample. This device is simpler and more robust to create, as nanofabrication is not required. The use of an on-chip micromixer, an on-chip bio-reaction zone, and integrated fiber optics highly improves automation and portability of the device. The examples of detected analytes in the work are evident of the device's high potential for real world applications.

Additionally, to the best of our knowledge, the competitive displacement assay for biological sample detection using SERS was reported for the first time utilizing our optofluidic SERS microsystem. Using packed surface-modified silica beads as the bio-reaction matrix improves bimolecular interaction and results in faster and more efficient performance. Moreover, preparing batches of devices can be performed much easier by loading functionalized beads into the channel rather than modifying the surface of channel sidewalls for each device separately.

Competitive displacement is advantageous as compared to previous SERS assays for DNA sequence detection because it requires only a single step, saving the user multiple steps as compared to the typical DNA hybridization sandwich assay.

Additionally, it does not require target labeling which makes this assay practical for real-world applications.

7.3 Future Work

In this work, we have shown sensitive and multiplexed detection of a variety of samples. However, additional microfluidic functions can be added to further enhance its functions.

One future direction for the device is to detect proteins and enzymes through competitive displacement assays. Similar to the DNA detection concept, for protein and enzyme detection, labeled nucleic acids or peptides could be used as SERS reporters. A target protein with higher affinity to the immobilized probe would displace the labeled nucleic acid, resulting in a SERRS signal. In the case of protease detection (including prostate specific antigen, botulinum neurotoxin, and thrombin), the protease can cleave the labeled peptides, and the labeled peptide segment can be detected via SERRS.

Another possible future work is to add on-chip chromatography for complicated mixed samples. In some real word applications, samples can contain highly fluorescent contaminants or analytes with extremely high SERS intensities as compared to the other analytes within the sample. In this case, by adding on-chip chromatography to the device utilizing another column of packed silica beads, the analytes can be detected separately and accurately.

Additionally, our device can be easily integrated with other functions for better automation and performance. The reagents required for SERS detection can be stored inside the on-chip reservoirs and released into the microchannels using micro-

valves. This can be followed by on-chip synthesis of metal nanoparticles. While improving the device's automation by reducing the required manual preparation steps, it might lead to an improved sensitivity due to the use of freshly synthesized metal nanoparticles.

Finally, integration of the highly automated and sensitive optofluidic SERS microsystem with hand-held Raman spectrometer/laser could result in a sensing platform suitable for real-world applications.

Bibliography

(1) Chin, C. D.; Linder, V.; Sia, S. K. Lab-on-a-chip Devices for Global Health: Past Studies and Future Opportunities. *Lab on a Chip* **2007**, *7*, 41–57.

(2) Yager, P.; Edwards, T.; Fu, E.; Helton, K.; Nelson, K.; Tam, M. R.; Weigl, B. H. Microfluidic Diagnostic Technologies for Global Public Health. *Nature* **2006**, *442*, 412–418.

(3) Popp, J.; Kiefer, W. *Raman Scattering, Fundamentals*; Wiley, **2006**).

(4) Dietzek, B.; Cialla, D.; Schmitt, M.; Popp, J. Introduction to the Fundamentals of Raman Spectroscopy, *Confocal Raman Microscopy*; *Springer series in Optical Sciences* **2011**, *158*, 21–42.

(5) Kneipp, K.; Kneipp, H.; Itzkan, I.; Dasari, R. R.; Feld, M. S. Ultrasensitive Chemical Analysis by Raman Spectroscopy. *Chemical Reviews* **1999**, *99*, 2957–2976.

(6) Nie, S.; Emory, S. Probing Single Molecules and Single Nanoparticles by Surface-Enhanced Raman Scattering. *Science* **1997**, *275*, 1102–1106.

(7) Fleischmann, M.; Hendra, P. J.; McQuillan, A. J. Raman Spectra of Pyridine Adsorbed at a Silver Electrode. *Chemical Physics Letters* **1974**, *26*, 163–166.

(8) Jeanmaire, D. L.; Van Duyne, R. P. Surface Raman spectroelectrochemistryPart I. Heterocyclic, Aromatic, and Aliphatic Amines Adsorbed on the Anodized Silver Electrode. *Journal of Electroanalytical Chemistry and Interfacial Electrochemistry* **1977**, *84*, 1–20.

(9) Albrecht, M. G.; Creighton, J. A. Anomalously Intense Raman Spectra of Pyridine at a Silver Electrode. *Journal of the American Chemical Society* **1977**, *99*, 5215–5217.

(10) Kneipp, K.; Wang, Y.; Kneipp, H.; Perelman, L. T.; Itzkan, I.; Dasari, R. R.; Feld, M. S. Single Molecule Detection Using Surface-enhanced Raman Scattering (SERS). *Physical Review Letters* **1997**, *78*, 1667–1670.

(11) Campion, A.; Kambhampati, P. Surface-enhanced Raman Scattering. *Chemical Society Reviews* **1998**, *27*, 241–250.

(12) Hutter, E.; Fendler, J. H. Exploitation of Localized Surface Plasmon Resonance. *Advanced Materials* **2004**, *16*, 1685–1706.

(13) Moskovits, M. Surface-enhanced Spectroscopy. *Reviews of Modern Physics* **1985**, *57*, 783.

(14) Michaels, A. M.; Nirmal, M.; Brus, L. Surface Enhanced Raman Spectroscopy of Individual Rhodamine 6G Molecules on Large Ag Nanocrystals. *Journal of the American Chemical Society* **1999**, *121*, 9932–9939.

(15) Faulds, K.; Hernandez-santana, A.; Smith, W. E. The Inorganic Chemistry of Surface Enhanced Raman Scattering (SERS). *Spectrosc. Prop. Inorg. Organomet. Compd* **2010**, *41*, 1–21.

(16) Stiles, P. L.; Dieringer, J. a.; Shah, N. C.; Van Duyne, R. P. Surface-enhanced Raman Spectroscopy. *Annual Review of Analytical Chemistry* **2008**, *1*, 601–626.

(17) Le Ru, E.; Etchegoin, P. *Principles of Surface-Enhanced Raman Spectroscopy: And Related Plasmonic Effects*; Elsevier, **2008**.

(18) Dhawan, A.; Norton, S. J.; Gerhold, M. D. Comparison of FDTD Numerical Computations and Analytical Multipole Expansion Method for Plasmonics-active Nanosphere Dimers. *Optics Express* **2009**, *17*, 1536–1540.

(19) Liao, P. F. Lightning Rod Effect in Surface Enhanced Raman Scattering. *The Journal of Chemical Physics* **1982**, *76*, 751.

(20) Baker, G. a; Moore, D. S. Progress in Plasmonic Engineering of Surface-enhanced Raman-scattering Substrates Toward Ultra-trace Analysis. *Analytical and Bioanalytical Chemistry* **2005**, *382*, 1751–70.

(21) Lee, D.; Lee, S.; Seong, G. H.; Choo, J.; Lee, E. K.; Gweon, D.-G.; Lee, S. Quantitative Analysis of Methyl Parathion Pesticides in a Polydimethylsiloxane Microfluidic Channel Using Confocal Surface-enhanced Raman Spectroscopy. *Applied Spectroscopy* **2006**, *60*, 373–377.

(22) Li, J.-M.; Ma, W.-F.; Wei, C.; You, L.-J.; Guo, J.; Hu, J.; Wang, C.-C. Detecting Trace Melamine in Solution by SERS Using Ag Nanoparticle Coated Poly(styrene-co-acrylic Acid) Nanospheres as Novel Active Substrates. *Langmuir : the ACS journal of surfaces and colloids* **2011**, *27*, 14539–14544.

(23) Mukherjee, K.; Sanchez-Cortes, S.; García-Ramos, J. V. Raman and Surface-enhanced Raman Study of Insecticide Cyromazine. *Vibrational Spectroscopy* **2001**, *25*, 91–99.

(24) Sanchez-Cortes, S.; Domingo, C.; Garcia-Ramos, J. Surface-enhanced Vibrational Study (SEIR and SERS) of Dithiocarbamate Pesticides on Gold

Films. *Langmuir : the ACS journal of surfaces and colloids* **2001**, *17*, 1157–1162.

(25) Saute, B.; Narayanan, R. Solution-based Direct Readout Surface Enhanced Raman Spectroscopic (SERS) Detection of Ultra-low Levels of Thiram with Dogbone Shaped Gold Nanoparticles. *The Analyst* **2011**, *136*, 527–532.

(26) Khaing Oo, M. K.; Chang, C.-F.; Sun, Y.; Fan, X. Rapid, Sensitive DNT Vapor Detection with UV-assisted Photo-chemically Synthesized Gold Nanoparticle SERS Substrates. *The Analyst* **2011**, *136*, 2811–7.

(27) Kneipp, K.; Wang, Y.; Dasari, R. R.; Feld, M. S.; Gilbert, B. D.; Janni, J.; Steinfeld, J. I. Near-infrared Surface-enhanced Raman Scattering of Trinitrotoluene on Colloidal Gold and Silver. *Spectrochimica Acta Part a Molecular and Biomolecular Spectroscopy* **1995**, *51*, 2171–2175.

(28) Ko, H.; Chang, S.; Tsukruk, V. V Porous Substrates for Label-free Molecular Level Detection of Nonresonant Organic Molecules. *ACS nano* **2009**, *3*, 181–8.

(29) Meinhart, C.; Piorek, B.; Seung, J. L.; Moskovits, M.; Cummings, C. Microfluidic/SERS Detection of Trace Explosives. **2008**, 1–6.

(30) Yea, K.; Lee, S.; Kyong, J. B.; Choo, J.; Lee, E. K.; Joo, S.-W.; Lee, S. Ultra-sensitive Trace Analysis of Cyanide Water Pollutant in a PDMS Microfluidic Channel Using Surface-enhanced Raman Spectroscopy. *The Analyst* **2005**, *130*, 1009–1011.

(31) Wang, G.; Lim, C.; Chen, L.; Chon, H.; Choo, J.; Hong, J.; deMello, A. J. Surface-enhanced Raman Scattering in Nanoliter Droplets: Towards High-sensitivity Detection of Mercury (II) Ions. *Analytical and Bioanalytical Chemistry* **2009**, *394*, 1827–32.

(32) Ackermann, K. R.; Henkel, T.; Popp, J. Quantitative Online Detection of Low-concentrated Drugs via a SERS Microfluidic System. *Chemphyschem : a European Journal of Chemical Physics and Physical Chemistry* **2007**, *8*, 2665–70.

(33) Clarke, S. J.; Littleford, R. E.; Smith, W. E.; Goodacre, R. Rapid Monitoring of Antibiotics Using Raman and Surface Enhanced Raman Spectroscopy. *The Analyst* **2005**, *130*, 1019–26.

(34) Jarvis, R.; Clarke, S.; Goodacre, R. Rapid Analysis of Microbiological Systems Using SERS. *Surface-Enhanced Raman Scattering* **2006**, *408*, 397–408.

(35) Lyandres, O.; Glucksberg, M. R.; T. Walsh, J.; C. Shah, N.; R. Yonzon, C.; Zhang, X.; Van Duyne, R. P. *Surface-Enhanced Raman Sensors for Metabolic*

Analytes; Lasch, P.; Kneipp, J., Eds.; John Wiley & Sons, Inc.: Hoboken, NJ, USA, 2008; pp. 221–241.

(36) Seballos, L.; Zhang, J. Z.; Sutphen, R. Surface-enhanced Raman Scattering Detection of Lysophosphatidic Acid. *Analytical and Bioanalytical Chemistry* **2005**, *383*, 763–767.

(37) Cao, Y. C.; Jin, R.; Mirkin, C. Nanoparticles with Raman Spectroscopic Fingerprints for DNA and RNA Detection. *Science* **2002**, *297*, 1536–1540.

(38) Driskell, J. D.; Seto, a G.; Jones, L. P.; Jokela, S.; Dluhy, R. a; Zhao, Y.-P.; Tripp, R. a Rapid microRNA (miRNA) Detection and Classification via Surface-enhanced Raman Spectroscopy (SERS). *Biosensors & Bioelectronics* **2008**, *24*, 923–928.

(39) Isola, N. R.; Stokes, D. L.; Vo-Dinh, T. Surface-enhanced Raman Gene Probe for HIV Detection. *Analytical Chemistry* **1998**, *70*, 1352–1356.

(40) Strelau, K. K.; Kretschmer, R.; Möller, R.; Fritzsche, W.; Popp, J. SERS as Tool for the Analysis of DNA-chips in a Microfluidic Platform. *Analytical and Bioanalytical Chemistry* **2010**, *396*, 1381–4.

(41) Park, T.; Lee, S.; Seong, G. H.; Choo, J.; Lee, E. K.; Kim, Y. S.; Ji, W. H.; Hwang, S. Y.; Gweon, D.-G.; Lee, S. Highly Sensitive Signal Detection of Duplex Dye-labelled DNA Oligonucleotides in a PDMS Microfluidic Chip: Confocal Surface-enhanced Raman Spectroscopic Study. *Lab on a Chip* **2005**, *5*, 437–42.

(42) Fabris, L.; Dante, M.; Braun, G.; Lee, S. J.; Reich, N. O.; Moskovits, M.; Nguyen, T.-Q.; Bazan, G. C. A Heterogeneous PNA-based SERS Method for DNA Detection. *Journal of the American Chemical Society* **2007**, *129*, 6086–6087.

(43) Li, T.; Guo, L.; Wang, Z. Gold Nanoparticle-based Surface Enhanced Raman Scattering Spectroscopic Assay for the Detection of Protein-protein Interactions. *Analytical Sciences* **2008**, *24*, 907–910.

(44) Wang, M.; Benford, M.; Jing, N.; Coté, G.; Kameoka, J. Optofluidic Device for Ultra-sensitive Detection of Proteins Using Surface-enhanced Raman Spectroscopy. *Microfluidics and Nanofluidics* **2009**, *6*, 411–417.

(45) Han, X. X.; Zhao, B.; Ozaki, Y. Surface-enhanced Raman Scattering for Protein Detection. *Analytical and Bioanalytical Chemistry* **2009**, *394*, 1719–1727.

(46) Grubisha, D. S.; Lipert, R. J.; Park, H. Y.; Driskell, J.; Porter, M. D. Femtomolar Detection of Prostate-specific Antigen: An Immunoassay Based on Surface-enhanced Raman Scattering and Immunogold Labels. *Analytical Chemistry* **2003**, *75*, 5936–5943.

(47) Choi, I.; Huh, Y. S.; Erickson, D. Size-selective Concentration and Label-free Characterization of Protein Aggregates Using a Raman Active Nanofluidic Device. *Lab on a Chip* **2011**, *11*, 632–688.

(48) Driskell, J. D.; Kwarta, K. M.; Lipert, R. J.; Porter, M. D.; Neill, J. D.; Ridpath, J. F. Low-level Detection of Viral Pathogens by a Surface-enhanced Raman Scattering Based Immunoassay. *Analytical Chemistry* **2005**, *77*, 6147–54.

(49) Grow, A. New Biochip Technology for Label-free Detection of Pathogens and Their Toxins. *Journal of Microbiological Methods* **2003**, *53*, 221–233.

(50) Jarvis, R. M.; Goodacre, R. Characterisation and Identification of Bacteria Using SERS. *Chemical Society Reviews* **2008**, *37*, 931–6.

(51) Shanmukh, S.; Jones, L.; Zhao, Y.-P.; Driskell, J. D.; Tripp, R. a; Dluhy, R. a Identification and Classification of Respiratory Syncytial Virus (RSV) Strains by Surface-enhanced Raman Spectroscopy and Multivariate Statistical Techniques. *Analytical and Bioanalytical Chemistry* **2008**, *390*, 1551–5.

(52) Shanmukh, S.; Jones, L.; Driskell, J.; Zhao, Y.; Dluhy, R.; Tripp, R. a Rapid and Sensitive Detection of Respiratory Virus Molecular Signatures Using a Silver Nanorod Array SERS Substrate. *Nano Letters* **2006**, *6*, 2630–6.

(53) Wabuyele, M. B.; Vo-Dinh, T. Detection of Human Immunodeficiency Virus Type 1 DNA Sequence Using Plasmonics Nanoprobes. *Analytical Chemistry* **2005**, *77*, 7810–7815.

(54) Stacy, A. A.; Van Duyne, R. P. Surface Enhanced Raman and Resonance Raman Spectroscopy in a Non-aqueous Electrochemical Environment: Tris(2,2′-bipyridine)ruthenium(II) Adsorbed on Silver from Acetonitrile. *Chemical Physics Letters* **1983**, *102*, 365–370.

(55) McNay, G.; Eustace, D.; Smith, W. E.; Faulds, K.; Graham, D. Surface-enhanced Raman Scattering (SERS) and Surface-enhanced Resonance Raman Scattering (SERRS): a Review of Applications. *Applied Spectroscopy* **2011**, *65*, 825–37.

(56) Faulds, K.; Fruk, L.; Robson, D. C.; Thompson, D. G.; Enright, A.; Ewen Smith, W.; Graham, D. A New Approach for DNA Detection by SERRS. *Faraday Discussions* **2006**, *132*, 261–268.

(57) Huh, Y. S.; Chung, A. J.; Erickson, D. Surface Enhanced Raman Spectroscopy and Its Application to Molecular and Cellular Analysis. *Microfluidics and Nanofluidics* **2009**, *6*, 285–297.

(58) Mahajan, S.; Richardson, J.; Brown, T.; Bartlett, P. N. SERS-melting: a New Method for Discriminating Mutations in DNA Sequences. *Journal of the American Chemical Society* **2008**, *130*, 15589–15601.

(59) Park, T.; Lee, S.; Seong, G. H.; Choo, J.; Lee, E. K.; Kim, Y. S.; Ji, W. H.; Hwang, S. Y.; Gweon, D.-G.; Lee, S. Highly Sensitive Signal Detection of Duplex Dye-labelled DNA Oligonucleotides in a PDMS Microfluidic Chip: Confocal Surface-enhanced Raman Spectroscopic Study. *Lab on a Chip* **2005**, *5*, 437–442.

(60) Erickson, D.; Sinton, D.; Psaltis, D. Optofluidics for Energy Applications. *Nature Photonics* **2011**, *5*, 583–590.

(61) Fan, X.; White, I. M. Optofluidic Microsystems for Chemical and Biological Analysis. *Nature Photonics* **2011**, *5*, 591–597.

(62) Y. Fainman, L. Lee, D. Psaltis, and C. Y. *Optofluidics: Fundamentals, Devices, and Applications*; McGraw-Hill, **2010**.

(63) Schmidt, H.; Hawkins, A. R. *Handbook of Optofluidics*; CRC, Boca Raton, **2010**.

(64) Psaltis, D.; Quake, S. R.; Yang, C. Developing Optofluidic Technology Through the Fusion of Microfluidics and Optics. *Nature* **2006**, *442*, 381–6.

(65) Monat, C.; Domachuk, P.; Eggleton, B. Integrated Optofluidics: A New River of Light. *Nature Photonics* **2007**, *1*, 106–114.

(66) Unger, M. a. Monolithic Microfabricated Valves and Pumps by Multilayer Soft Lithography. *Science* **2000**, *288*, 113–116.

(67) Husband, B.; Bu, M.; Evans, a G. R.; Melvin, T. Investigation for the Operation of an Integrated Peristaltic Micropump. *Journal of Micromechanics and Microengineering* **2004**, *14*, S64–S69.

(68) Gambin, Y.; Simonnet, C.; VanDelinder, V.; Deniz, A.; Groisman, A. Ultrafast Microfluidic Mixer with Three-dimensional Flow Focusing for Studies of Bioechemical Kinetics. *Lab on a Chip*, **2010**, 10, 598-609

(69) Escobedo, C.; Brolo, A. G.; Gordon, R.; Sinton, D. Flow-through Vs Flow-over: Analysis of Transport and Binding in Nanohole Array Plasmonic Biosensors. *Analytical Chemistry* **2010**, *82*, 10015–10020.

(70) Yang, J. C.; Ji, J.; M., H.; Larson, D. N. Metallic Nanohole Arrays on Fluoropolymer Substrates as Small Label-free Real-time Bioprobes. *Nano Letters* **2008**, *8*, 2718–2724.

(71) Yanik, A. A.; Huang, M.; Artar, A.; Chang, T.-Y.; Altug, H. Integrated Nanoplasmonic-nanofluidic Biosensors with Targeted Delivery of Analytes. *Applied Physics Letters* **2010**, *96*, 021101(1)–021101(3).

(72) Im, H.; Lesuffleur, A.; Lindquist, N. C.; Oh, S. . Plasmonic Nanoholes in a Multichannel Microarray Format for Parallel Kinetic Assays and Differential Sensing. *Analatical Chememistry* **2009**, *81*, 2854–2859.

(73) Pang, L.; Hwang, G. M.; Slutsky, B.; Fainman, Y. Spectral Sensitivity of Two-dimensional Nanohole Array Surface Plasmon Polariton Resonance Sensor. *Applied Physics Letters* **2007**, *91*, 123112-123115.

(74) Chow, E.; Grot, a; Mirkarimi, L. W.; Sigalas, M.; Girolami, G. Ultracompact Biochemical Sensor Built with Two-dimensional Photonic Crystal Microcavity. *Optics Letters* **2004**, *29*, 1093–1095.

(75) Rindorf, L.; Jensen, J. B.; Dufva, M.; Pedersen, L. H.; Høiby, P. E.; Bang, O. Photonic Crystal Fiber Long-period Gratings for Biochemical Sensing. *Optics Express* **2006**, *14*, 8224–31.

(76) Nunes, P. S.; Mortensen, N. a; Kutter, J. P.; Mogensen, K. B. Photonic Crystal Resonator Integrated in a Microfluidic System. *Optics Letters* **2008**, *33*, 1623–5.

(77) Lee, M. R.; Fauchet, P. M. Nanoscale Microcavity Sensor for Single Particle Detection. *Optics Letters* **2007**, *32*, 3284–6.

(78) Barrios, C. a.; Bañuls, M. J.; González-Pedro, V.; Gylfason, K. B.; Sánchez, B.; Griol, A.; Maquieira, a.; Sohlström, H.; Holgado, M.; Casquel, R. Label-free Optical Biosensing with Slot-waveguides. *Optics Letters* **2008**, *33*, 708.

(79) Bernardi, a.; Kiravittaya, S.; Rastelli, a.; Songmuang, R.; Thurmer, D. J.; Benyoucef, M.; Schmidt, O. G. On-chip Si/SiO_2 Microtube Refractometer. *Applied Physics Letters* **2008**, *93*, 094106.

(80) Li, H.; Fan, X. Characterization of Sensing Capability of Optofluidic Ring Resonator Biosensors. *Applied Physics Letters* **2010**, *97*, 011105.

(81) Sumetsky, M.; Dulashko, Y.; Windeler, R. S. Optical Microbubble Resonator. *Optics Letters* **2010**, *35*, 898–900.

(82) White, I. M.; Oveys, H.; Fan, X. Liquid-core Optical Ring-resonator Sensors. *Optics Letters* **2006**, *31*, 1319–21.

(83) Song, W. Z.; Zhang, X. M.; Liu, a. Q.; Lim, C. S.; Yap, P. H.; Hosseini, H. M. M. Refractive Index Measurement of Single Living Cells Using On-chip Fabry-Pérot Cavity. *Applied Physics Letters* **2006**, *89*, 203901.

(84) Shao, H.; Member, S.; Wang, W.; Lana, S. E.; Lear, K. L. Optofluidic Intracavity Spectroscopy of Canine Lymphoma and Lymphocytes. *Photonics Technology Letters* **2008**, *20*, 493–495.

(85) St-Gelais, R.; Masson, J.; Peter, Y. -a. All-silicon Integrated Fabry–Pérot Cavity for Volume Refractive Index Measurement in Microfluidic Systems. *Applied Physics Letters* **2009**, *94*, 243905-243908.

(86) Grillet, C.; Domachuk, P.; Ta'eed, V.; Mägi, E.; Bolger, J.; Eggleton, B.; Rodd, L.; Cooper-White, J. Compact Tunable Microfluidic Interferometer. *Optics Express* **2004**, *12*, 5440–7.

(87) Cho, S. H.; Godin, J.; Lo, Y.-H. Optofluidic Waveguides in Teflon AF-Coated PDMS Microfluidic Channels. *IEEE photonics technology letters : a publication of the IEEE Laser and Electro-optics Society* **2009**, *21*, 1057–1059.

(88) Manor, R.; Datta, a.; Ahmad, I.; Holtz, M.; Gangopadhyay, S.; Dallas, T. Microfabrication and Characterization of Liquid Core Waveguide Glass Channels Coated with Teflon Af. *IEEE Sensors Journal* **2003**, *3*, 687–692.

(89) Fink, Y. A Dielectric Omnidirectional Reflector. *Science* **1998**, *282*, 1679–1682.

(90) Ganesh, N.; Zhang, W.; Mathias, P. C.; Chow, E.; Soares, J. a N. T.; Malyarchuk, V.; Smith, A. D.; Cunningham, B. T. Enhanced Fluorescence Emission from Quantum Dots on a Photonic Crystal Surface. *Nature Nanotechnology* **2007**, *2*, 515–20.

(91) Smolka, S.; Barth, M.; Benson, O. Highly Efficient Fluorescence Sensing with Hollow Core Photonic Crystal Fibers. *Optics Express* **2007**, *15*, 12783–91.

(92) Coscelli, E.; Sozzi, M.; Poli, F.; Passaro, D.; Cucinotta, A.; Selleri, S.; Member, S.; Corradini, R.; Marchelli, R. Toward A Highly Specific DNA Biosensor : Photonic Crystal Fibers. *Journal of Selected Topics in Quantum Electronics* **2010**, *16*, 967–972.

(93) Liu, Y.; Wang, S.; Park, Y.-S.; Yin, X.; Zhang, X. Fluorescence Enhancement by a Two-dimensional Dielectric Annular Bragg Resonant Cavity. *Optics Express* **2010**, *18*, 25029–34.

(94) Rudenko, M. I.; Kühn, S.; Lunt, E. J.; Deamer, D. W.; Hawkins, a R.; Schmidt, H. Ultrasensitive Qbeta Phage Analysis Using Fluorescence Correlation Spectroscopy on an Optofluidic Chip. *Biosensors & Bioelectronics* **2009**, *24*, 3258–63.

(95) Kühn, S.; Phillips, B. S.; Lunt, E. J.; Hawkins, a R.; Schmidt, H. Ultralow Power Trapping and Fluorescence Detection of Single Particles on an Optofluidic Chip. *Lab on a Chip* **2010**, *10*, 189–94.

(96) Chen, a; Eberle, M. M.; Lunt, E. J.; Liu, S.; Leake, K.; Rudenko, M. I.; Hawkins, a R.; Schmidt, H. Dual-color Fluorescence Cross-correlation Spectroscopy on a Planar Optofluidic Chip. *Lab on a Chip* **2011**, *11*, 1502–6.

(97) Moskovits, M. Surface Roughness and the Enhanced Intensity of Raman Scattering by Molecules Adsorbed on Metals. *The Journal of Chemical Physics* **1978**, *69*, 4159–4161.

(98) Kneipp, K.; Kneipp, H.; Kartha, V. B.; Manoharan, R.; Deinum, G.; Itzkan, I.; Dasari, R. R.; Feld, M. S. Detection and Identification of a Single DNA Base Molecule Using Surface-enhanced Raman Scattering (SERS). *Physical Review E* **1998**, *57*, 6281–6284.

(99) Huh, Y. S.; Erickson, D. Aptamer Based Surface Enhanced Raman Scattering Detection of Vasopressin Using Multilayer Nanotube Arrays. *Biosensors & Bioelectronics* **2010**, *25*, 1240–1243.

(100) Fang, Ch.; Agarwal, A.; Buddharaju, K.; Khalid, N.; Salim, M.; Widjaja, E.; Garaland, M.; Balasubramanian, N.; and Kwong, D. DNA Detection using Nanostructured SERS Substrates with Rhodamine B as Raman Label, *Biosensors and Bioelectronics* **2008**, 24, 216-221

(101) Culha, M.; Stokes, D.; Allain, L. R.; Vo-Dinh, T. Surface-enhanced Raman Scattering Substrate Based on a Self-assembled Monolayer for Use in Gene Diagnostics. *Analytical Chemistry* **2003**, *75*, 6196–6201.

(102) Lowe, A. J.; Huh, Y. S.; Strickland, A. D.; Erickson, D.; Batt, C. A. Multiplex Singel Nucleotide Polymorphism Genotyping Utilizing Ligase Detection Reaction Coupled Surface Enhanced Raman Spectroscopy. *Analatical Chemistry* **2010**, *82*, 5810–5814.

(103) Faulds, K.; Smith, W. E.; Graham, D. Evaluation of Surface-enhanced Resonance Raman Scattering for Quantitative DNA Analysis. *Analytical Chemistry* **2004**, *76*, 412–417.

(104) Lee, S.; Choi, J.; Chen, L.; Park, B.; Kyong, J. B.; Seong, G. H.; Choo, J.; Lee, Y.; Shin, K.-H.; Lee, E. K. et al. Fast and Sensitive Trace Analysis of

Malachite Green Using a Surface-enhanced Raman Microfluidic Sensor. *Analytica Chimica Acta* **2007**, *590*, 139–144.

(105) Quang, L. X.; Lim, C.; Seong, G. H.; Choo, J.; Do, K. J.; Yoo, S.-K. A Portable Surface-enhanced Raman Scattering Sensor Integrated with a Lab-on-a-chip for Field Analysis. *Lab on a Chip* **2008**, *8*, 2214–2219.

(106) Wilson, R.; Bowden, S. a; Parnell, J.; Cooper, J. M. Signal Enhancement of Surface Enhanced Raman Scattering and Surface Enhanced Resonance Raman Scattering Using in Situ Colloidal Synthesis in Microfluidics. *Analytical Chemistry* **2010**, *82*, 2119–2123.

(107) Tong, L.; Righini, M.; Gonzalez, M. U.; Quidant, R.; Käll, M. Optical Aggregation of Metal Nanoparticles in a Microfluidic Channel for Surface-enhanced Raman Scattering Analysis. *Lab on a Chip* **2009**, *9*, 193–195.

(108) Psaltis, D.; Quake, S. R.; Yang, C. Developing Optofluidic Technology Through the Fusion of Microfluidics and Optics. *Nature* **2006**, *442*, 381–386.

(109) Guo, Y.; Li, H.; Reddy, K.; Shelar, H. S.; Nittoor, V. R.; Fan, X. Optofluidic Fabry–Pérot Cavity Biosensor with Integrated Flow-through Micro-/nanochannels. *Applied Physics Letters* **2011**, *98*, 041104(1)–041104(3).

(110) Sun, Y.; Shopova, S. I.; Wu, C.-S.; Arnold, S.; Fan, X. Bioinspired Optofluidic FRET Lasers via DNA Scaffolds. *Proceedings of the National Academy of Sciences of the United States of America* **2010**, *107*, 16039–42.

(111) Yan, H.; Gu, C.; Yang, C.; Liu, J.; Jin, G.; Zhang, J.; Hou, L.; Yao, Y. Hollow Core Photonic Crystal Fiber Surface-enhanced Raman Probe. *Applied Physics Letters* **2006**, *89*, 204101.

(112) Yang, X.; Shi, C.; Wheeler, D.; Newhouse, R.; Chen, B.; Zhang, J. Z.; Gu, C. High-sensitivity Molecular Sensing Using Hollow-core Photonic Crystal Fiber and Surface-enhanced Raman Scattering. *Journal of the Optical Society of America. A, Optics, image science, and vision* **2010**, *27*, 977–984.

(113) Khaing Oo, M. K.; Han, Y.; Kanka, J.; Sukhishvili, S.; Du, H. Structure Fits the Purpose: Photonic Crystal Fibers for Evanescent-field Surface-enhanced Raman Spectroscopy. *Optics Letters* **2010**, *35*, 466–468.

(114) Measor, P.; Seballos, L.; Yin, D.; Zhang, J. Z.; Lunt, E. J.; Hawkins, A. R.; Schmidt, H. On-chip Surface-enhanced Raman Scattering Detection Using Integrated Liquid-core Waveguides. *Applied Physics Letters* **2007**, *90*, 211107(1)–211107(3).

(115) Cho, H.; Lee, B.; Liu, G. L.; Agarwal, A.; Lee, L. P. Label-free and Highly Sensitive Biomolecular Detection Using SERS and Electrokinetic Preconcentration. *Lab on a Chip* **2009**, *9*, 3360–3363.

(116) Hwang, H.; Han, D.; Oh, Y.-J.; Cho, Y.-K.; Jeong, K.-H.; Park, J.-K. In Situ Dynamic Measurements of the Enhanced SERS Signal Using an Optoelectrofluidic SERS Platform. *Lab on a Chip* **2011**, *11*, 2518–2525.

(117) Han, B.; Choi, N.; Kim, K. H.; Lim, D. W.; Choo, J. Application of Silver-Coated Magnetic Microspheres to a SERS-Based Optofluidic Sensor. *The Journal of Physical Chemistry C* **2011**, *115*, 6290–6296.

(118) Wang, M.; Jing, N.; Chou, I.-H.; Cote, G. L.; Kameoka, J. An Optofluidic Device for Surface Enhanced Raman Spectroscopy. *Lab on a Chip* **2007**, *7*, 630–632.

(119) Chou, I.-H.; Benford, M.; Beier, H. T.; Coté, G. L.; Wang, M.; Jing, N.; Kameoka, J.; Good, T. a Nanofluidic Biosensing for Beta-amyloid Detection Using Surface Enhanced Raman Spectroscopy. *Nano Letters* **2008**, *8*, 1729–35.

(120) Park, S.; Huh, Y. S.; Craighead, H. G.; Erickson, D. A Method for Nanofluidic Device Prototyping Using Elastomeric Collapse. *Proceedings of the National Academy of Sciences of the United States of America* **2009**, *106*, 15549–15554.

(121) Liu, J.; White, I.; DeVoe, D. L. Nanoparticle-functionalized Porous Polymer Monolith Detection Elements for Surface-enhanced Raman Scattering. *Analytical Chemistry* **2011**, *83*, 2119–2124.

(122) Guo, Y.; Khiang, M.; Reddy, K.; Fan, X. Ultrasensitive Optofluidic Surface-Enhanced Raman Scattering Detection. *ACS Nano* **2012**, *6*, 381–388.

(123) Baehr-Jones, T.; Hochberg, M.; Walker, C.; Scherer, A. High-Q Optical Resonators in Silicon-on-insulator-based Slot Waveguides. *Applied Physics Letters* **2005**, *86*, 081101.

(124) Bog, U.; Smith, C. L. C.; Lee, M. W.; Tomljenovic-Hanic, S.; Grillet, C.; Monat, C.; O'Faolain, L.; Karnutsch, C.; Krauss, T. F.; McPhedran, R. C. et al. High-Q Microfluidic Cavities in Silicon-based Two-dimensional Photonic Crystal Structures. *Optics Letters* **2008**, *33*, 2206–8.

(125) Gorodetsky, M. L.; Ilchenko, V. S. Optical Microsphere Resonators: Optimal Coupling to high-Q Whispering-gallery Modes. *Journal of the Optical Society of America B* **1999**, *16*, 147.

(126) Hossein-Zadeh, M.; Vahala, K. J. Free ultra-high-Q Microtoroid: a Tool for Designing Photonic Devices. *Optics Express* **2007**, *15*, 166–75.

(127) Vollmer, F.; Arnold, S.; Keng, D. Single Virus Detection from the Reactive Shift of a Whispering-gallery Mode. *Proceedings of the National Academy of Sciences of the United States of America* **2008**, *105*, 20701–4.

(128) White, I. M.; Gohring, J.; Fan, X. SERS-based Detection in an Optofluidic Ring Resonator Platform. *Optics Express* **2007**, *15*, 17433–42.

(129) Cai, M.; Painter, O.; Vahala, K. Observation of Critical Coupling in a Fiber Taper to a Silica-microsphere Whispering-gallery Mode System. *Physical Review Letters* **2000**, *85*, 74–7.

(130) Zhao, Y.; Zhang, X.-J.; Chen, L.-M.; Lau, S.; Zhang, W.; Lee, S. Metallo-Dielectric Photonic Crystals for Surface-Enhanced Raman Scattering. *ACS Nano* **2011**, *5*, 3027–3033.

(131) Kim, S.; Zhang, W.; Cunningham, B. T. Photonic Crystals with SiO2–Ag "post-cap" Nanostructure Coatings for Surface Enhanced Raman Spectroscopy. *Applied Physics Letters* **2008**, *93*, 143112.

(132) Kim, S.; Zhang, W.; Cunningham, B. T. Coupling Discrete Metal Nanoparticles to Photonic Crystal Surface Resonant Modes and Application to Raman Spectroscopy. *Optics Express* **2010**, *18*, 4300–9.

(133) Lee, P.; Meisel, D. Adsorption and Surface-enhanced Raman of Dyes on Silver and Gold Sols. *The Journal of Physical Chemistry* **1982**, *86*, 3391–3395.

(134) McDonald, J. C.; Duffy, D. C.; Anderson, J. R.; Chiu, D. T.; Wu, H.; Schueller, O. J.; Whitesides, G. M. Fabrication of Microfluidic Systems in Poly(dimethylsiloxane). *Electrophoresis* **2000**, *21*, 27–40.

(135) Ng, J. M. K.; Stroock, A. D.; Whitesides, G. M. Review Components for Integrated Poly (Dimethylsiloxane) Microfluidic Systems. *Electrophoresis* **2002**, *23*, 3461–3473.

(136) Ashok, P. C.; Singh, G. P.; Rendall, H. a; Krauss, T. F.; Dholakia, K. Waveguide Confined Raman Spectroscopy for Microfluidic Interrogation. *Lab on a Chip* **2011**, *11*, 1262–1270.

(137) Monteiro, D. A.; Rantin, F. T.; Kalinin, A. L. The Effects of Selenium on Oxidative Stress Biomarkers in the Freshwater Characid Fish Matrinxã, Brycon Cephalus (Günther, 1869) Exposed to Organophosphate Insecticide Folisuper 600 BR (methyl Parathion). *Comparative Biochemistry and Physiology. Toxicology & Pharmacology* **2009**, *149*, 40–49.

(138) EPA *R.E.D. FACTS Thiram*.

(139) Srivastava, S.; Sinha, R.; Roy, D. Toxicological Effects of Malachite Green. *Aquatic Toxicology* **2004**, *66*, 319–329.

(140) Alak, a M.; Vo-Dinh, T. Surface-enhanced Raman Spectrometry of Organophosphorus Chemical Agents. *Analytical Chemistry* **1987**, *59*, 2149–2153.

(141) Yan, F.; Vo-Dinh, T. Surface-enhanced Raman Scattering Detection of Chemical and Biological Agents Using a Portable Raman Integrated Tunable Sensor. *Sensors and Actuators B: Chemical* **2007**, *121*, 61–66.

(142) Lee, C.; Lee, G.; Fu, L.; Lee, K.; Yang, R. Electrokinetically Driven Active Micro-mixers Utilizing Zeta Potential Variation Induced by Field Effect. *Journal of Micromechanics and Microengineering* **2004**, *14*, 1390–1398.

(143) Lin, J.; Lee, K.; Lee, G. Active Mixing Inside Microchannels Utilizing Dynamic Variation of Gradient Zeta Potentials. *Electrophoresis* **2005**, *26*, 4605–4615.

(144) Tsai, J.; Lin, L. Active Microfluidic Mixer and Gas Bubble Filter Driven by Thermal Bubble Micropump. *Sensors and Actuators A* **2002**, *97-98*, 665–671.

(145) Rida, A.; Gijs, M. A. M. Manipulation of Self-assembled Structures of Magnetic Beads for Microfluidic Mixing and Assaying. *Analytical Chemistry* **2004**, *76*, 6239–46.

(146) Tseng, W.-K.; Lin, J.-L.; Sung, W.-C.; Chen, S.-H.; Lee, G.-B. Active Micro-mixers Using Surface Acoustic Waves on Y-cut 128° LiNbO 3. *Journal of Micromechanics and Microengineering* **2006**, *16*, 539–548.

(147) Yaralioglu, G. G.; Wygant, I. O.; Marentis, T. C.; Khuri-Yakub, B. T. Ultrasonic Mixing in Microfluidic Channels Using Integrated Transducers. *Analytical Chemistry* **2004**, *76*, 3694–3698.

(148) Stroock, A. D.; Dertinger, S. K. W.; Ajdari, A.; Mezic, I.; Stone, H. a; Whitesides, G. M. Chaotic Mixer for Microchannels. *Science* **2002**, *295*, 647–651.

(149) Howell, P. B.; Mott, D. R.; Fertig, S.; Kaplan, C. R.; Golden, J. P.; Oran, E. S.; Ligler, F. S. A Microfluidic Mixer with Grooves Placed on the Top and Bottom of the Channel. *Lab on a Chip* **2005**, *5*, 524–530.

(150) Liu, R. H.; Stremler, M. a.; Sharp, K. V.; Olsen, M. G.; Santiago, J. G.; Adrian, R. J.; Aref, H.; Beebe, D. J. Passive Mixing in a Three-dimensional Serpentine Microchannel. *Journal of Microelectromechanical Systems* **2000**, *9*, 190–197.

(151) FDA *Interim Safety and Risk Assessment of Melamine and Its Analogues in Food for Humans*.

(152) Betz, J. F.; Cheng, Y.; Rubloff, G. W. Direct SERS Detection of Contaminants in a Complex Mixture : Rapid , Single Step Screening for Melamine in Liquid Infant Formula. The *Analyst* **2012**, *137*, 826–828.

(153) Lin, M.; He, L.; Awika, J.; Yang, L.; Ledoux, D. R.; Li, H.; Mustapha, A. Detection of Melamine in Gluten, Chicken Feed, and Processed Foods Using Surface Enhanced Raman Spectroscopy and HPLC. *Journal of Food Science* **2008**, *73*, 129–134.

(154) Chen, L.-M.; Liu, Y.-N. Surface-enhanced Raman Detection of Melamine on Silver-nanoparticle-decorated Silver/carbon Nanospheres: Effect of Metal Ions. *ACS Applied Materials & Interfaces* **2011**, *3*, 3091–3096.

(155) Zheng, X.; Chen, Y.; Chen, Y.; Bi, N.; Qi, H.; Qin, M.; Song, D.; Zhang, H.; Tian, Y. High Performance Au/Ag Core/shell Bipyramids for Determination of Thiram Based on Surface-enhanced Raman Scattering. *Journal of Raman Spectroscopy* **2012**, *43*, 1374–1380.

(156) Sánchez-Cortés, S.; Vasina, M.; Francioso, O.; García-Ramos, J. . Raman and Surface-enhanced Raman Spectroscopy of Dithiocarbamate Fungicides. *Vibrational Spectroscopy* **1998**, *17*, 133–144.

(157) Domingo, C.; Resta, V.; Sanchez-cortes, S.; Garcı, V. Pulsed Laser Deposited Au Nanoparticles as Substrates for Surface-Enhanced Vibrational. *Journal of Physical Chemistry C* **2007**, *111*, 8149–8152.

(158) Fournier, R. *Basic Transport Phenomena in Biomedical Engineering, 2nd Edition*; 2007.

(159) Huh, Y. S.; Chung, A. J.; Cordovez, B.; Erickson, D. Enhanced On-chip SERS Based Biomolecular Detection Using Electrokinetically Active Microwells. *Lab on a Chip* **2009**, *9*, 433–439.

(160) Park, T.; Lee, S.; Seong, G. H.; Choo, J.; Lee, E. K.; Kim, Y. S.; Ji, W. H.; Hwang, S. Y.; Gweon, D.-G.; Lee, S. Highly Sensitive Signal Detection of Duplex Dye-labelled DNA Oligonucleotides in a PDMS Microfluidic Chip: Confocal Surface-enhanced Raman Spectroscopic Study. *Lab on a Chip* **2005**, *5*, 437–42.

(161) Sun, L.; Irudayaraj, J. Quantitative Surface-enhanced Raman for Gene Expression Estimation. *Biophysical Journal* **2009**, *96*, 4709–4716.

(162) Li, J.-M.; Wei, C.; Ma, W.-F.; An, Q.; Guo, J.; Hu, J.; Wang, C.-C. Multiplexed SERS Detection of DNA Targets in a Sandwich-hybridization Assay Using SERS-encoded Core–shell Nanospheres. *Journal of Materials Chemistry* **2012**, *22*, 12100–12106.

(163) Zangmeister, R. A.; Tarlov, M. J. DNA Displacement Assay Integrated into Microfluidic Channels. *Analytical Chemistry* **2004**, *76*, 3655–3659.

(164) Zammatteo, N.; Alexandre, I.; Ernest, I.; Le, L.; Brancart, F.; Remacle, J. Comparison Between Microwell and Bead Supports for the Detection of Human Cytomegalovirus Amplicons by Sandwich Hybridization. *Analytical Biochemistry* **1997**, *253*, 180–189.

(165) Ng, J. K.-K.; Feng, H.; Liu, W.-T. Rapid Discrimination of Single-nucleotide Mismatches Using a Microfluidic Device with Monolayered Beads. *Analytica Chimica Acta* **2007**, *582*, 295–303.

(166) Kohara, Y. Hybridization Reaction Kinetics of DNA Probes on Beads Arrayed in a Capillary Enhanced by Turbulent Flow. *Analytical Chemistry* **2003**, *75*, 3079–3085.

(167) Kim, J.; Heo, J.; Crooks, R. M. Hybridization of DNA to Bead-immobilized Probes Confined Within a Microfluidic Channel. *Langmuir : the ACS Journal of surfaces and colloids* **2006**, *22*, 10130–10134.

(168) Faulds, K.; Jarvis, R.; Smith, W. E.; Graham, D.; Goodacre, R. Multiplexed Detection of Six Labelled Oligonucleotides Using Surface Enhanced Resonance Raman Scattering (SERRS). *The Analyst* **2008**, *133*, 1505–1512.

(169) Jarvis, R. M.; Goodacre, R. Discrimination of Bacteria Using Surface-enhanced Raman Spectroscopy. *Analytical Chemistry* **2004**, *76*, 40–7.

(170) Pearman, W. F.; Fountain, A. W. Classification of Chemical and Biological Warfare Agent Simulants by Surface-enhanced Raman Spectroscopy and Multivariate Statistical Techniques. *Applied Spectroscopy* **2006**, *60*, 356–65.